

DELFT UNIVERSITY OF TECHNOLOGY

# Methods of Improving the Post Shear-Buckled Stiffness of Glare

---

**Andrew Marshall**

5 July 2017

# Table of Contents

Table of Figures .....	IV
Table of Tables.....	VI
Nomenclature.....	VII
Abstract .....	1
CHAPTER 1:Introduction.....	2
CHAPTER 2: Background.....	5
History of Glare .....	5
Review of Glare Components.....	6
Aluminum .....	6
Fiber Type.....	7
Fiber Layup .....	8
Adhesive .....	8
Fiber Metal Laminates.....	9
Glare Design .....	10
Metal .....	10
Fibers .....	10
Adhesive .....	10
Current Glare designs.....	10
Shear Web Design .....	11
Metal Shear Webs .....	13
Composite Shear Webs .....	14
Modified Glare Design.....	15
Material Parameters.....	16
Design Criteria .....	16
Analytical Models .....	17
Research Scope.....	18
Research Question: .....	18
CHAPTER 3: Post Shear-Buckled Stiffness and Damage Tolerance of Off-Axis Glare3.....	20
Test Methods.....	20
Picture Frame Shear Test Method.....	20
Picture Frame Apparatus.....	20
Problems with the picture frame apparatus .....	22

Shear Specimen Specifications .....	22
Manufacturing .....	24
Digital Imaging Correlation.....	25
Test Rate.....	25
Analytical Methods.....	25
Classical Laminate Theory (CLT) .....	26
Rayleigh-Ritz .....	27
Kuhn Method.....	28
Rule of Mixtures .....	30
Metal Volume Fraction (MVF) .....	30
FMLGROW_V2.0.....	31
Stiffness Calculations.....	31
Results and Discussion .....	32
Manufacturing.....	32
Glare3 Shear Tests.....	33
Glare3 Fatigue Analysis .....	41
Conclusion1 .....	43
CHAPTER 4: Parametric Study of Glare3 Modifications for Improved Post Shear-Buckled Stiffness ...	45
Methodology.....	47
Adjusting the Metal Volume Fraction .....	47
Conclusion 2 .....	50
Adding Off-Axis Fibers to Glare3 .....	50
Conclusion 3 .....	56
CHAPTER 5: Post Shear-Buckled Stiffness and Damage Tolerance of Modified Glare3.....	58
Methodology.....	58
Manufacturing.....	58
Fatigue Test Method .....	60
Stiffness Results & Discussion .....	62
Fatigue Results & Discussion .....	64
Conclusion 4 .....	68
Conclusions.....	70
Conclusion 1 .....	70
Conclusion 2 .....	70
Conclusion 3 .....	70

Conclusion 4 .....	71
Recommendations .....	72
References.....	73
APPENDIX: A .....	2
Laminate Selection Criteria .....	3
Material Parameters.....	3
Design Criteria .....	3
APPENDIX: B .....	2
Analytical Models .....	2
Classical Laminate Theory (CLT) .....	2
Rayleigh-Ritz .....	2
Kuhn Method.....	3
Rule of Mixtures .....	4
Metal Volume Fraction (MVF) .....	5
FMLGROW_V2.0.....	5
Stiffness Calculations.....	8

## Table of Figures

Figure 1: Knowledge gap in improving post shear-buckled performance in FMLs. ....	2
Figure 2: Propagation curves in solid and laminated panels with a central crack [1].....	6
Figure 3: Radial plot of the elastic modulus of an S2 Glass prepreg ply at 0°.....	8
Figure 4: Radial plot of the elastic modulus of two S2 Glass prepreg plies at 0° and 90°.....	8
Figure 5: Principle of Incomplete Diagonal Tension.....	12
Figure 6: Diagonal tension beam. [21] .....	12
Figure 7: Shear-buckling-stress coefficient of plates as a function of a/b for clamped and hinged edges. [24] .....	13
Figure 8: "Yield and Ultimate strength of two variants of Glare3 (with 2024 alloy and 7475 alloy) under off-axis loading" [1].....	13
Figure 9: Possible modified Glare layup for improved shear performance [Al/0/45/90/Al]. ....	17
Figure 10: Diagonal-tension beam [NACA TN 2661] .....	20
Figure 11: Picture frame apparatus.....	21
Figure 12: Shear specimen corner cut-out and pivot centroid. ....	21
Figure 13: GD&T of shear specimen.....	23
Figure 14: Cure cycle for Glare at 6 bars of pressure. ....	24
Figure 15: Six panels of varying fiber angles cut from single Glare3-2/1-0.3 sheet.....	25
Figure 16: Theoretical buckling coefficients for plates with simply supported edges. [21] .....	30
Figure 17: Graphical representation of the Metal Volume Fraction approach. [1] .....	31
Figure 18: Mohr's circles depicting the pre and post shear-buckling stress states. ....	32
Figure 19: Force vs. deflection plots of five Glare3 specimens at different orientations. ....	34
Figure 20: Shear-stress vs. shear-strain plots for Glare3 specimens at different orientations.....	34
Figure 21: Shear-stress vs. shear-strain plots zoomed in to buckling stress levels.....	36
Figure 22: Out-of-plane displacement (W) at 1.9 MPa .....	37
Figure 23: Out-of-plane displacement (W) at 2.5 MPa .....	37
Figure 24: Glare3 shear stress-shear strain curves with labels. ....	38
Figure 25: Estimated and measured $G_{\alpha}$ values for Glare3 .....	40
Figure 26: Radial plot of Glare3 with fibers oriented at 0° and 90° . ....	41
Figure 27: Crack growth life curve for Glare3-2/1-0.3 no rotation. ....	43
Figure 28: Crack growth life curve for Glare3-2/1-0.3 rotated 45 deg. ....	43
Figure 29: Percent increase in properties based on $t_{Al} = 0.2$ mm. ....	48
Figure 30: Normalized $G_{\alpha}$ values w.r.t. the baseline value. ....	49
Figure 31: Crack growth life curve for Glare3-2/1-0.2. ....	49
Figure 32: Crack growth life curve for Glare3-2/1-0.5. ....	49
Figure 33: Normalized $G_{\alpha}$ for various potential modified Glare3 layups with off-axis S2 glass fibers..	53
Figure 34: Normalized $G_{\alpha}$ for various potential modified Glare3 layups with off-axis T700 carbon fibers.....	54
Figure 35: Normalized values of $K$ as a percentage of Glare3 values. ....	55
Figure 36: Fatigue specimen dimensions and tolerances. ....	59
Figure 37: Prepared fatigue specimen .....	60
Figure 38: Fatigue specimen loaded in a Zwick 810 100kN fatigue machine. ....	61
Figure 39: Force-deflection curves for standard and modified Glare3. ....	62

Figure 40: Shear stress-shear strain curves for standard and modified Glare3 layups.....	63
Figure 41: Crack growth life curve for Glare3-2/1-0.3 no rotation. ....	65
Figure 42: Crack growth life curve for Glare3s-2/1-0.3 (glass).....	65
Figure 43: Crack growth life curve for Glare3s-2/1-0.3 (carbon). ....	65
Figure 44: Fatigue crack growth curve for modified Glare3s-2/1-0.3 (carbon) .....	66
Figure 45: Fatigue crack growth curve for modified Glare3s-2/1-0.3 (glass).....	66
Figure 46: Fatigue crack turning in modified Glare3 (carbon). ....	67
Figure 47: Shear stress element and an equivalent rotated principal stress element. ....	4
Figure 48: Mohr's circles depicting the pre and post shear-buckling stress states. ....	4
Figure 49: $G_{\alpha}/G_{\alpha\text{-Glare3}}$ for possible 2/1 layups. ....	5
Figure 50: $G_{\alpha}/G_{\alpha\text{-Glare3}}$ for possible 3/2 layups. ....	5
Figure 51: $K/K_{\text{Glare3}}$ for possible 2/1 layups. ....	6
Figure 52: $K/K_{\text{Glare3}}$ for possible 3/2 layups. ....	7
Figure 53: Crack growth rate for Glare3-2/1-0.2 .....	9
Figure 54: Crack growth rate for Glare3-3/2-0.3 .....	9
Figure 55: Crack growth rate for $[Al_{0.2}/0/45/90/Al_{0.2}]$ .....	10
Figure 56: Crack growth rate for $[Al_{0.3}/0/45/90/Al_{0.3}/0/45/90/Al_{0.3}]$ .....	10
Figure 57: $G_{\alpha}/G_{\alpha\text{-Glare3}}$ for possible 2/1 layups. ....	11
Figure 58: $G_{\alpha}/G_{\alpha\text{-Glare3}}$ for possible 3/2 layups. ....	11
Figure 59: $K/K_{\text{Glare3}}$ for possible 2/1 layups. ....	12
Figure 60: $K/K_{\text{Glare3}}$ for possible 3/2 layups. ....	12
Figure 61: Crack growth life curve for Glare3-2/1-0.2 .....	6
Figure 62: Crack growth life curve for Glare3-2/1-0.3 .....	6
Figure 63: Crack growth life curve for Glare3-2/1-0.4 .....	6
Figure 64: Crack growth life curve for Glare3-2/1-0.5 .....	6
Figure 65: Crack growth life curve for Glare3-2/1-0.3 no rotation. ....	7
Figure 66: Crack growth life curve for Glare3-2/1-0.3 rotated 15 deg. ....	7
Figure 67: Crack growth life curve for Glare3-2/1-0.3 rotated 30 deg. ....	7
Figure 68: Crack growth life curve for Glare3-2/1-0.3 rotated 45 deg. ....	7
Figure 69: Crack growth life curve for Glare3s-2/1-0.3.....	7

## Table of Tables

Table 1: Standard Glare grades [1].....	11
Table 2: Analytical Models and Their Inputs and Outputs .....	26
Table 3: FMLGROW_V2.0 Parameters and Values.....	31
Table 4: Glare3 Elastic and Shear Moduli from CLT .....	36
Table 5: Critical Shear Stresses for Shear Buckling of Various Glare Layups.....	36
Table 6: $G_{\alpha}$ Results for Glare3 Test Specimens in the Range of 20 MPa – 100 MPa .....	39
Table 7: Estimated $G_{\alpha}$ values for Glare3.....	39
Table 8: MVF Method Results for $E_{\alpha}$ and $G_{\alpha}$ of Various Glare Layups.....	47
Table 9: Stiffness Data for Glare3, Modified with Off-Axis S2 Glass Fibers .....	52
Table 10: Stiffness Data for Glare3, Modified with Off-Axis T700 Carbon Fibers .....	52
Table 11: Normalized values of $G_{\alpha}$ and $K$ as a Percentage of Glare3 [carbon] .....	55
Table 12: Fatigue Test Matrix.....	60
Table 13: Measured $G_{\alpha}$ Values for Standard and Modified Glare3 Layups.....	63
Table 14: Predicted $G_{\alpha}$ Values for Standard and Modified Glare3 Layups.....	63
Table 15: Glare3 Elastic and Shear Moduli from CLT .....	2
Table 16: Modified Glare3 Elastic and Shear Moduli from CLT.....	2
Table 17: Critical Running Shear Loads for Shear Buckling of Various Glare Layups .....	3
Table 18: Critical Shear Stresses for Shear Buckling of Various Glare Layups.....	3
Table 19: Principal Stresses and Percentages of Applied Shear Stresses Resisted by Diagonal Tension and Shear.....	4
Table 20: Elastic Moduli for Aluminum and Fiber Glass Plies at Various Orientations .....	4
Table 21: Elastic Moduli for Glare3 in the Direction of the Buckling Angle .....	4
Table 22: MVF Method Results for $E_{\alpha}$ and $G_{\alpha}$ of Various Glare Layups .....	5
Table 23: $G_{\alpha}$ Results for Various Glare Layups with Glass Fiber Angle Plies .....	8
Table 24: Spring Constant, $K$ , Results for Various Glare Layups with Glass Fiber Angle Plies.....	8
Table 25: $G_{\alpha}$ and $K$ Results for Various Glare Layups with Carbon Fiber Angle Plies .....	9

## Nomenclature

ABD	- ABD matrix obtained from CLT for converting stresses to strains in laminates
CLT	- Classical Laminate Theory
DIC	- Digital Imaging Correlation
DT	- Diagonal Tension
FML	- Fiber Metal Laminate
IDT	- Incomplete Diagonal Tension
MVF	- Metal Volume Fraction
ROM	- Rule of Mixtures
UD	- Uni-directional
w.r.t.	- With respect to
$a$	- Crack length or panel width (depending on context)
$\alpha$	- Shear buckling angle (in this case, $\alpha = 45^\circ$ )
$d$	- Displacement
$E$	- Modulus of elasticity
$G_{xy}$	- Shear modulus
$G_\alpha$	- Post shear-buckled shear modulus
$\gamma$	- Shear strain
$K$	- Spring coefficient (Hooke's law)
$K$	- Stress intensity factor (fatigue)
$k$	- Diagonal-tension factor
$k_s$	- Shear-buckling-stress coefficient
$k_{ss}$	- Shear buckling stress coefficient
$N_{xycrit}$	- Critical shear force (onset of buckling)
$N_{xy}$	- Shear force
$\rho$	- Density
$\rho_{aerial}$	- Aerial density
$S_{max}$	- Maximum applied stress
$\sigma_1$	- Web tensile stresses parallel to $\alpha$
$\sigma_2$	- Web compressive stresses perpendicular to $\alpha$
$t_{Al}$	- Thickness of the aluminum layers in Glare
$\tau$	- Shear stress
$\tau_{app}$	- Applied shear stress
$\tau_{crit}$	- Critical shear stress (onset of buckling)
$\tau_{DT}$	- Shear stress resisted with diagonal tension action
$\tau_s$	- Shear stress resisted with shear action
$\tau_y$	- Shear yield stress
$\theta$	- Orientation of off-axis plies
$x$	- Direction parallel to the aluminum rolling direction, or $0^\circ$
$y$	- Direction perpendicular to the aluminum rolling direction, or $90^\circ$

## Abstract

Glare is a type of fiber metal laminate which was seen much of its development occur the Delft University of Technology. Created and optimized primarily for its high damage tolerance, this material has already seen entry into the aerospace industry and continues to find new applications. One such application could one day be as a skin panel for narrow bodied aircraft, which experience relatively high shear loads, particularly near the wings. High shear loads acting on thin skin panels often requires that the skin panels perform well in the post shear-buckled regime. Most Glare materials, by nature of their design, are less stiff in shear. As a result, it becomes important to investigate the possibility of restoring the lost shear stiffness of Glare, while attempting to maintain its excellent damage tolerance properties.

The Glare materials have undergone many years of design and optimization, and striving to adhere to those same design criteria is a priority when considering modifications. Thus, a thorough investigation into the how and why of the design of Glare materials is first presented. This investigation lead to the identification of four possible methods of increasing the post shear-buckled stiffness of Glare3: 1) re-orienting the direction of the fiber layers, 2) adjusting the thickness of the aluminum sheets, 3) adding off-axis fibers in the direction of the shear buckling angle, and 4) changing the off-axis fiber type.

Analytical methods were employed to first predict the properties and behaviors of the many possible layups, and certain shear and fatigue tests were conducted to substantiate the findings. It was discovered that adjusting the fiber orientation of standard Glare3 provided marginal improvement to the material's shear stiffness, while its damage tolerance rapidly decrease. This provides little benefit for even larger losses. Increasing the thickness of the metal layers yields large improvements in stiffness. However, damage tolerance decreases rapidly and weight amassed at a rate five times faster than the stiffness. It was shown that the metal layers should be as thin as possible. Off-axis fibers aligned with the shear buckling angle, may increase the shear stiffness provided they are stiffer than standard Glare3. Off-axis carbon fibers improve stiffness, while off-axis glass fibers do not. And lastly, a modified Glare3 material with the layup  $[Al_{0.3}/0/45_c/90/Al_{0.3}]$ , where the off-axis ply is made of carbon fiber, is an optimized layup which improves the material's post shear-buckled stiffness, while not sacrificing damage tolerance.

# CHAPTER 1: Introduction

Fiber metal laminates (FML) are in a class of materials composed of alternating layers of resin impregnated fibers and metal sheets. Glare (GLAss REinforced aluminum) belongs to the FML family, and is made up of high strength glass fibers and damage tolerant aluminum alloys. This combination of materials gives Glare its characteristic resistance to fatigue crack growth. This is an especially attractive property for fuselage skin panels because of the high cyclic loads they experience which cause cracking. Glare is currently being used as the skin panels of the Airbus A380 fuselage.

The different grades of Glare are designed to have the fibers aligned in either the 0° and/or 90° directions (such as Glare3), or aligned in the ±45° directions (Glare 6). This alignment increases the material’s strength and damage tolerance in those specific directions to improve its performance when loaded along its axes or in shear. However, not all skin panels fall nicely into one of those two load cases. This is especially true for skin panels near the wings, which experience high axial and shear loads. To date, no attempts have been made to develop a grade of Glare for this load case. For large aircraft, such as the A380, this is not an issue because the skin thickness is nearly proportional to the diameter of the fuselage and is thick enough to resist the shear loads. However, for narrow bodied aircraft, the thin skin panels may not be able to resist the shear loads and may buckle. In those cases, skin panels can be designed to carry loads through diagonal tension allowing shear buckling to occur, instead of being shear resistant. However, this is where current Glare grades do not perform well.

Although there already is quite a lot of research and development of Glare, it is still a relatively new material, and more research is needed to fully understand all aspects of Glare. Of particular interest for this thesis is improving the performance of Glare in the post shear-buckled regime for use on narrow bodied aircraft. To help illustrate the need for this type of research, Figure 1 gives a simple overview of the knowledge gap in FML research as pertaining to improving the material in the post shear-buckled regime.

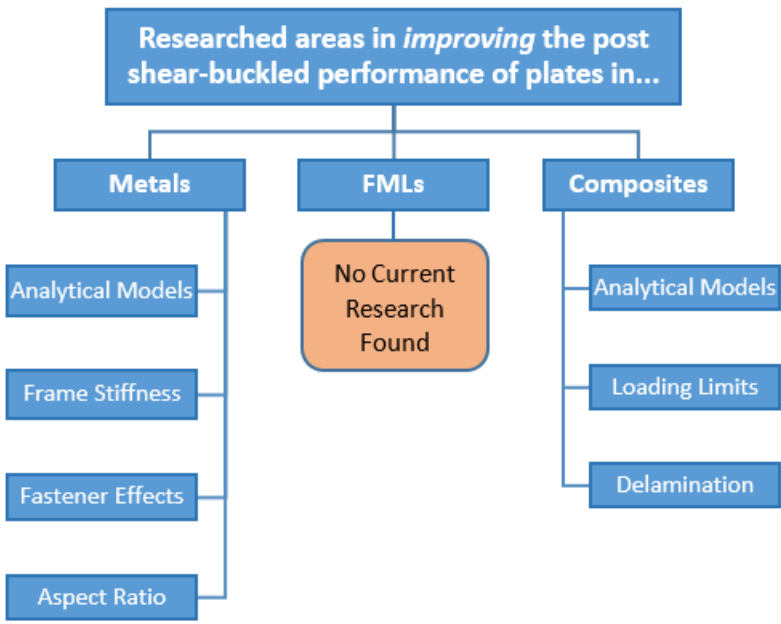


Figure 1: Knowledge gap in improving post shear-buckled performance in FMLs.

Simply stated, there is a knowledge gap created by the absence of research for *improving* the post shear-buckling performance of FMLs. A decent amount of research involving the post shear-buckled performance of standard grade FMLs already exists, along with some proposed analytical models – which don't always agree. However, no research aimed towards the redesign of FMLs that would yield *improved* post shear-buckling performance was found. An FML such as Glare, as discussed in later sections, requires straying away from common designs in search for a new or modified Glare material.

This thesis is aimed at filling in a piece of the knowledge gap shown in Figure 1 by investigating the post shear-buckled behavior of Glare3 and what improvements could be made it. Possible modifications to Glare3 include using different fiber materials, adjusting fiber angles, and changing metal layer thicknesses. The effects of each of these on the post shear-buckled stiffness and the damage tolerance of the modified Glare material are explored in the pages that follow. Yet, before making any changes to the Glare3 design, it is important to understand exactly why and how the material was designed to begin with.

In the pages that follow, an in-depth look into the history, original development, and final design choices of Glare are presented. Using this information, a modified Glare material, which is referred to as Glare3s, is proposed and an experimental approach outlined for testing the new material and evaluating how its stiffness changes. After the description of the manufacturing and testing methodologies, the results of the tests are given. This is followed by a discussion of the results and interpretation of the data. In the end, conclusions are drawn which identify the material design with an improved post shear-buckled stiffness.



# CHAPTER 2: Background

## History of Glare

In the 1970's considerable work was being done, mostly in the United States and Great Britain, to investigate the possibility of creating an intermediate material between metals and composites by bringing the two materials together. Early tests included bonding these materials together in rods, tubes, and beams and then studying them to determine their efficiency to reduce costs (and weight) for the Space Shuttle. Meanwhile, Rob Schliekelman, an engineer at Fokker, and graduate of Delft University, was studying the bonding of metal laminate structures. After visiting the US and becoming aware of the efforts being done to combine metals and composites together, Schliekelman realized that his bonded metal structures were very similar to those being tested by the Americans and the British. He also recognized that there could be an extra benefit to adding fibers to the resin layers in his metal laminates. He saw them as a way of further decreasing the fatigue crack growth rates of the metal laminates. Shortly thereafter, his group at Fokker came up with a material design and began testing.

The material Schliekelman and his group created proved to have fatigue crack growth rates some three times slower than in standard aluminum sheets. This discovery no doubt was encouraging, but the looming problems of resolving the issues with high cost, durability, and quality control caused them to lose interest in pursuing the material further [2]. However, in 1978, Schijve and Vogelesang at Delft University took hold of the idea and continued the research. They worked on optimizing the material and later developed an analytical model for predicting fatigue crack growth rates. In 1981, a partnership was formed between companies Akzo, Alcoa, and 3M to supply the fiber, metal, and adhesives respectively. A patent on the first Fiber Metal Laminate (FML) material was filed on January 9, 1981 [3].

The first FML was dubbed ARALL (Aramid Reinforced ALuminum Laminates) and went through extensive testing as it slowly worked its way through the technology readiness levels. It proved to be a very efficient material in many respects and showed a great deal of promise. However, the cost of producing the material was roughly ten times more per kilogram than aluminum. Regardless, Arall continued on for a while longer, but attentions started to shift when studies conducted by Aerospatiale in 1988 revealed that it was not suited for use in an aircraft fuselage shell, due to its disappointing performance in compression [4] and impact [5].

In 1987, a patent was filed for a new type of FML [6]. This FML, later dubbed GLARE, used glass fibers instead of aramid fibers and the result appeared to answer most of the problems Arall was facing. Interest in Glare quickly escalated and it was further optimized specifically for use as skin panels in aircraft fuselages. The results were Glare3 and Glare 4. These two grades of Glare performed wonderfully during studies and tests both small and large. In 1990, initial studies done by "Airbus Industrie and all its European partners... appeared to lead to a 25.9% weight reduction for 280 dollar per kilogram saved weight" [1] for an A320 fuselage using Glare skin panels. However, the price tag on Glare, just like Arall, was still five to ten times more expensive than aluminum.

Although the beneficial fatigue properties of Glare allowed for a simpler aircraft structure without crack stoppers or reinforcements to reduce stress and have fewer joints, these bonuses were never quantified when considering its total cost. What eventually brought down the cost was the

realization that the total cost of a finished skin panel was very close to the cost of a finished aluminum panel. This indicated that Glare should be produced as a component and not as a bulk material like aluminum [1]. After Glare was proven to reduce weight in a fuselage and be competitively priced against aluminum, it was then put on the fast track to completing its technology readiness with the financial backing of the Netherlands Agency for Aerospace Programmes (NIVR) and work being done by Structural Laminates Company (SLC), Delft University, and Netherlands Aerospace Centre (NLR). In 2007, the Airbus A380 was released with Glare skin panels on the upper, forward, and aft fuselage sections.

## Review of Glare Components

The three basic components of Glare are aluminum, glass fibers, and adhesive. Each one of these are addressed separately in this section to gain a clear understanding of the important role they play.

### Aluminum

In the mid 1900's, Rob Schliekelman optimized the process of bonding metal sheets together. Which originally had been developed at an English aircraft manufacturer called De Havilland. Schliekelman discovered that bonded metal structures exhibit good fatigue properties because cracks that developed in one metal layer did not easily propagate into the other layers that it was bonded to. In 1973 H. T. M. van Lipzig further investigated the fatigue crack growth in laminated structures and his research revealed that there was more going on than what Schliekelman had found.

With the knowledge that monolithic metal sheets exhibit slower fatigue crack growth rates than thicker sheets, van Lipzig laminated five 1mm thick aluminum sheets together and compared the fatigue crack growth rate with two monolithic 5mm and 1mm thick aluminum sheets. His research showed that the fatigue crack growth rate in the laminate was significantly slower than in the 5mm sheets. In fact, the laminate's crack growth rate very closely matched the crack growth rate of the 1mm sheets [7] (see Figure 2).

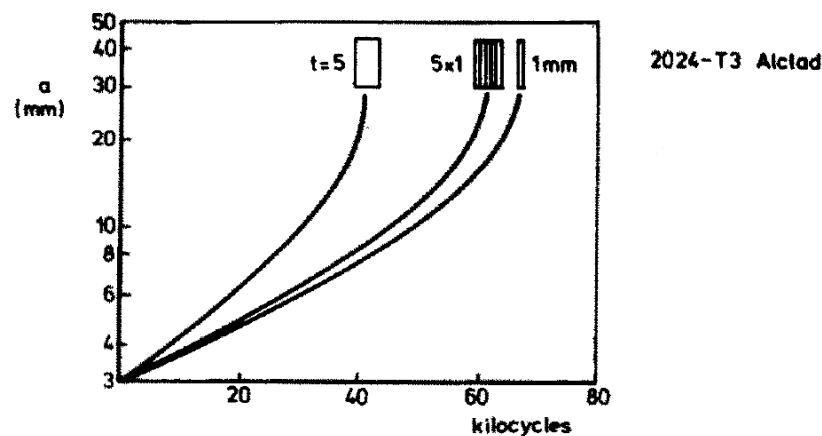


Figure 2: Propagation curves in solid and laminated panels with a central crack [1].

Other tests have been performed since Lipzig, with similar results demonstrating that fatigue crack growth rates of laminated metal structures are very close to the fatigue crack growth rates of the thin sheets of which the laminates are composed [8].

The reason for the difference in fatigue crack growth rates in the monolithic 5mm and 1mm metal sheets stems from the conditions of plane stress and plane strain. At a material's surface a crack tip is in a state of plane stress, which promotes larger crack tip plasticity zones. Further from the surface,

the crack tip is in a state of plane strain, which only allows for smaller crack tip plasticity zones. The size of the plastic zone around the crack tip has a large effect on the crack's " $K$ " factor, or how much stress is at the crack tip [9]. The larger the plastic zone is, the smaller the " $K$ " factor will be, and the fatigue crack growth rate decrease. Thus, by reducing the width of a sheet as much as possible, more of the crack tip will be in a plane stress condition and have a slower fatigue crack growth rate.

A lesser variable, which could have had some effect on the test results, lies in the crystal structure of the metal itself. The thinner aluminum sheets undergo a slightly different manufacturing process than the thicker sheets. This difference affects the crystal structure, which can change the fatigue crack growth rates.

Another important factor in fatigue crack growth rates is the type of metal being used. Stiff metals have higher fatigue crack growth rates because the plastic zone around the crack tips is smaller. This is not desirable in fatigue sensitive applications. On the other hand, ductile materials like Aluminum (which is also strong for its weight) are very attractive for fatigue sensitive applications due to their large plastic zones around the crack tips. In particular, the aluminum alloy 2024-T3 is frequently used in aerospace for its damage tolerant properties.

As a practical consideration, using a metal like Al2024-T3 (which is already used in aerospace) to form Glare has an advantage over other metals because it helps break down barriers to the material's entry. The various reasons for this are not included here but can be found in reference [10] on page 2, as well as reference [1] on page 4.

### Fiber Type

After applying Nylon weaves or unidirectional carbon fibers to the adhesive layers in metal laminates, Schliekelman observed that the fatigue crack growth rates of his structures were reduced by two or three times [9]. This occurred because the fibers in the cracks remained unbroken and were effectively bridging the gap in the crack. This phenomenon has become known as fiber bridging and it has some important characteristics that aid in slowing fatigue cracking. First, the fibers impede the crack from opening, and second, they help transmit part of the load through the crack. This results in a "most significant reduction on the stress intensity factor  $K$  in the Al-layers" [10]. Nonetheless, if a fiber's ability to transmit a load is reduced, then the " $K$ " factor will again increase. This happens to be one of the major problems with the FML called ARALL.

ARALL uses aramid fibers, which has a relatively poor adhesion to adhesives. Consequently, when high loads are applied over a crack, the fibers become loose inside the adhesive, and are prone to failure [10]. To prevent this from happening, other fibers that have a much better adhesion to the adhesives should be used. Glass fibers, as researched by Geert Roebroeks [11], avoid many of the problems faced by using aramid fibers (and do not cause Galvanic corrosion like carbon fibers). Glass has a stronger adhesion to the adhesive than the adhesive does to itself (cohesion). This means the fibers will not pull out or become loose. Also, "fiber failure does not occur in glass fibers" [10] like it does in aramid fibers. Roebroeks recommends using either an R or S2 type glass fiber for FMLs.

R and S2 glass are both high strength glass fibers. The high strength is important because "The combination of aluminum and glass fibers in Glare will result in a lower stiffness if compared to the stiffness of the monolithic aluminum. The reduced stiffness is a disadvantage of the new material, because it will increase the deformations of the aircraft structure under load. It might introduce problems, e.g. for the fuselage skin to frame connections, or by reduced buckling strength of compression loaded parts. For such reasons, the stiffness of the glass fibers in Glare should be as high as possible." [11]

## Fiber Layup

Fibers are similar to ropes in the way that they perform best in tension. When placed in a matrix, many types of fibers can also do reasonably well in compression. However, fibers carry loads along their length and they do not do well with off axis loadings. As the applied loads rotate off-axis, the ability of the fibers to carry those loads drops sharply (see Figure 3 and Figure 4 below). This limits the effectiveness of the fibers in many load cases. For this reason, fibers are aligned with the direction of the highest load paths, and because fatigue cracks grow perpendicular to the applied fatigue loads, this alignment of the fibers also allows for efficient fiber bridging. Figure 3 shows a radial plot of the elastic modulus of a single UD ply of S2 glass oriented at  $0^\circ$ . Figure 4 shows a radial plot of the elastic modulus of two UD plies of S2 glass oriented at  $0^\circ$  and  $90^\circ$ .

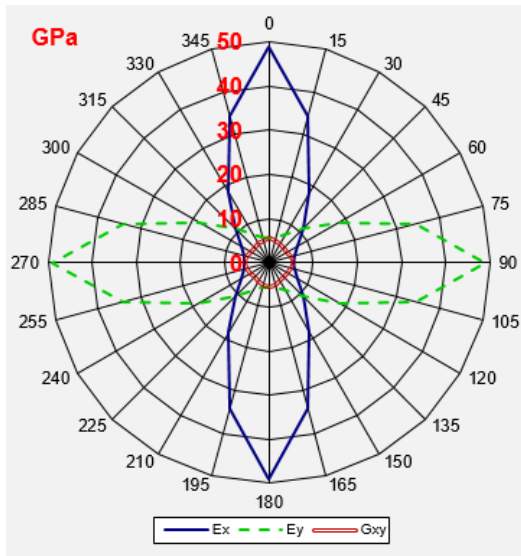


Figure 3: Radial plot of the elastic modulus of an S2 Glass prepreg ply at  $0^\circ$ .

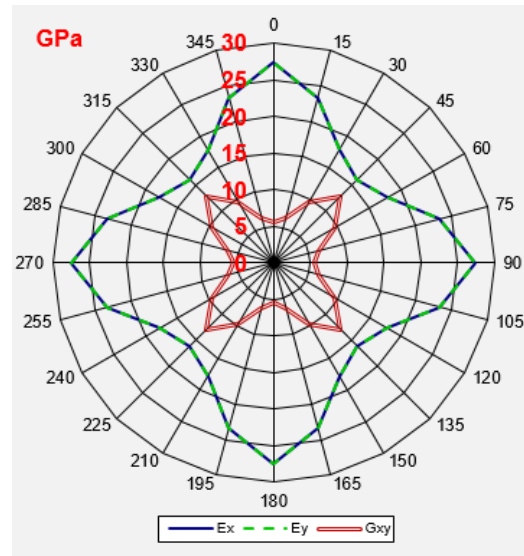


Figure 4: Radial plot of the elastic modulus of two S2 Glass prepreg plies at  $0^\circ$  and  $90^\circ$ .

Since the optimal fiber direction is known, the question now arises as to which method is better to use: two unidirectional plies at  $90^\circ$  to each other (cross ply), or weaves?

Cross ply layers have two plies placed at  $90^\circ$  to each other with each ply having straight fibers in just one direction. A weave has fibers woven together in two directions (also at  $90^\circ$  to each other). Tests conducted by Fokker in the late 1970's on FML's led them to the conclusion that cross plies using UD fiber layers were better than weaves [12]. Part of the reason for this is because in a weave the fibers are wavy instead of straight. The bends in the fibers cause a number of things to happen which reduce the stiffness and fatigue properties of FML's. This research is supported by Roebroeks, whose own tests revealed "a 9% advantage of the cross ply over the weave." [11]

## Adhesive

The adhesive in an FML is not only the glue that holds the layers together, but is also the matrix that supports the fibers. Compared to aluminum and glass fibers, the stiffness of the adhesive is quite small and it may seem that the adhesive, other than holding things together, does not contribute well to the performance of FMLs. Though it is true that the adhesive may not increase the strength or stiffness of a laminate, it does in fact play significant roles in fatigue crack growth. Two of these roles have been characterized as a crack arrestor and a crack divider.

As a crack divider, the adhesive separates the aluminum layers, which prevents cracks from one aluminum layer from propagating to the next due to the physical gap between them. This allows the cracks in each aluminum layer to grow independently at a rate based upon its own thickness. As a crack arrestor, the soft adhesive serves to reduce the stress concentration on the adjacent aluminum layer. In addition, with the presence of shear stresses between the aluminum and the adhesive, delamination, or “crack branching”, occurs which further reduces the stress concentrations [13].

Considering the material properties of an adhesive, there are two desirable properties in fatigue crack growth. The first is a high shear stiffness. Small fatigue cracks ( $a < 3 \text{ mm}$ ) often do not have delamination around them yet, and the adhesive is loaded in shear. A high shear stiffness helps prevent the crack from opening. The second is a resistance to delamination. Large delaminated areas allow cracks to open wider, which increases crack growth rates.

### Fiber Metal Laminates

FML's are composed of the three separate materials investigated above, and each one has a significant effect on the overall part. Research conducted by Fokker in the early 1970's [12] determined that an FML's properties and performance would increase with “much thinner metal sheets to raise the fiber/metal ratio, UD fibers instead of weaves with a metal adhesive as the matrix material for the fibers, and in increased number of fiber-layer/metal-sheet interfaces.” [10] During his Ph.D. dissertation at TU Delft, Roelof Marissen studied FML's, ARALL in particular, to find out what factors were involved in the fatigue crack growth rates. His findings supported the conclusions of Fokker from roughly ten years earlier. Marissen explains that thinner metal sheets and more fiber-layer/metal-sheet interfaces have a significant effect on reducing the crack opening displacement (a result of thinner layers) and increasing the fiber bridging efficiency (a result of having more layers of fibers). In addition, lower delamination rates due to better fiber bridging lowers the fatigue crack growth rates. He concludes that a well-balanced FML has thin metal layers with slightly thinner fiber layers, which have at least a 50% fiber volume fraction [14].

Roebroeks took the time to investigate which properties of an FML are most affected by the material's composition. This brief overview is given below and helps in gaining a quick, general understanding of FMLs.

- “Fatigue properties are affected by the aluminum thickness, type of fibers and type of adhesive.
- The tensile strength... depend[s] on the strength of the fiber layer, and also on the properties of the aluminum alloy layers and the delamination properties of the adhesive.
- The laminated stiffness depends on the fiber layer stiffness and the fiber layer thickness ratio.” [11]

These three properties are the main properties used in the Glare optimization process. Other factors which affect the “mechanical properties are the fiber volume fraction, fiber layer thickness ratio and the thickness of the aluminum alloy layers.” [11] The first two affect the strength, stiffness and fatigue properties, while the last affects mostly fatigue.

The manufacturing process of an FML uses hot bonding temperatures at or above  $120^{\circ}\text{C}$ . The coefficients of thermal expansion of the fibers and the aluminum are different, which means that after the curing and the material begins to cool, residual stresses will build. In the as-cured condition, the aluminum is in tension and the fibers are in compression. From a fatigue standpoint, this is not desirable since cracks would grow at lower fatigue loads and crack tips would be less prone to closing. To solve this issue, an FML can undergo a post-stretching process called “prestraining”, which

stretches the material to about 0.4% of plastic strain. Stretching reverses the signs of the residual stresses, putting the aluminum in compression and the fibers in tension [15]. However, the process is very expensive and limited to smaller panels. One of the benefits of FMLs is that they can be produced in wide panels, but it is practically impossible prestrain wide panels [11].

## Glare Design

The previous section covered the type of materials that should be used in a damage tolerant FML design as well as the reasoning behind it. Using this information, it should be relatively easy to come up with a good initial FML design. A summary of the design is given below.

### Metal

In section 0. it was shown that the metal Al2024-T3 is a good metal to use for a damage tolerant FML. This is because of its good fatigue properties, and partly due to its current use in aerospace (which helps break down barriers). Also, the aluminum sheets should be as thin as possible, while maintaining a proper metal volume fraction. Marissen suggests a sheet thickness between 0.3 *mm* and 0.5 *mm* [14], but with modern manufacturing techniques, this sheet thickness can be as low as 0.2 *mm* [1].

Conclusion: Al2024-T3 sheets, 0.2 *mm* – 0.5 *mm* thick.

### Fibers

Section 0. identified either R or S2 glass fibers as being good candidates. These are high strength fibers, which are not prone to compressive failure like Aramid fibers, and form a very strong bond with the adhesive. Their high strength and strong bond allow the fibers to transfer loads efficiently and reduce the fatigue crack growth rates.

Conclusion: R or S2 Glass fibers

### Adhesive

Adhesives were covered in section 0. There it was shown that an adhesive with a high shear stiffness and a low susceptibility to delamination was best. These two properties both have a large effect on decreasing fatigue crack growth rates. Section 0 also mentioned that the adhesive should be one that is used for metal bonding.

Conclusion: Metal adhesive with high shear stiffness and low susceptibility to delamination

### Current Glare designs

It is important to note that Glare grades are designed for damage tolerance with specific loading conditions. Unlike aluminum, it is not a monolithic or isotropic material, which means that no one grade is adequate for every application. Glare must be optimized for the loading conditions it will be experiencing, just like regular composite laminates. Up until the current date, only six grades of Glare have been developed. These are listed in Table 1.

Table 1: Standard Glare grades [1].

Glare grade	Sub	Metal sheet thickness [mm] & alloy	Prepreg orientation in each fiber layer	Main beneficial characteristics
Glare 1	-	0.3-0.4 7475-T761	0/0	Fatigue, strength, yield stress
Glare 2	Glare 2A	0.2-0.5 2024-T3	0/0	Fatigue, strength
	Glare 2B	0.2-0.5 2024-T3	90/90	Fatigue, strength
Glare3	-	0.2-0.5 2024-T3	0/90	Fatigue, impact
Glare 4	Glare 4A	0.2-0.5 2024-T3	0/90/0	Fatigue, strength in 0° direction
	Glare 4B	0.2-0.5 2024-T3	90/0/90	Fatigue, strength in 90° direction
Glare 5	-	0.2-0.5 2024-T3	0/90/90/0	Impact
Glare 6	Glare 6A	0.2-0.5 2024-T3	+45/-45	Shear, off-axis properties
	Glare 6B	0.2-0.5 2024-T3	-45/+45	Shear, off-axis properties

Grades 2-6 all use Al2024-T3 sheets which are 0.2 mm – 0.5 mm thick. Typically, the fibers are S2 glass and the adhesive is either FM 94 or FM 906, both of which are metal adhesives (see Table 1). The FM 94 adhesive also displays superior shear strength properties [16]. A comparison of these Glare designs show that the conclusions reached above are valid.

Taking a second look at the design of the Glare materials, while bearing in mind the loads that each carry, the design is both robust and relatively simple. Consider, for example, the fiber direction and quantity. Grade 2A can carry higher loads in the 0° direction and lower loads in the 90° direction. Grade 3 can carry moderate loads in both the 0° and 90° directions, and grade 4A can carry higher loads in the 0° direction and moderate loads in the 90° direction. As the number of fiber layers increases, the fiber/metal ratio changes. To balance this, a thicker aluminum sheet could be used to bring the fiber/metal ratio back to a desired range.

## Shear Web Design

Before the 1930's, shear webs were designed to be shear resistant. It was thought that “the load-bearing capacity of a shear web was exhausted when the web buckled” [21]. To prevent shear webs from buckling, additional stiffeners were added to effectively decrease the size of the web and thereby increase its load-bearing capacity without buckling. This caused shear web designs in aircraft to be very heavy. Then, in 1931, Herbert Wagner published Technical Memorandum No. 604 for the NACA in which he revealed that the load-bearing capacity of a buckled shear web is not exhausted upon initial buckling. Instead, the web begins to resist additional loads with the principle of pure diagonal tension. Wagner was the first to introduce the concept of pure diagonal tension [22]. He compared a shear-buckled web to the diagonal members of a truss, which resist shear loads through tension.

The theory of diagonal tension improved the design of shear webs and made them lighter because they could carry an additional load before they were considered to have failed. However, this theory was not complete, and as Paul Kuhn discovered, it was still too conservative. In 1952, Kuhn introduced the theory of incomplete diagonal tension (IDT). This took Wagner's theory to the next level. The IDT theory shows that “the state of pure diagonal tension is only a theoretical limiting case which is asymptotically approached but never reached in an actual structure.” [22] This is due to the fact that a buckled web still continues to resist some of the additional shear loads through shear action, while the rest was resisted through diagonal tension action. Figure 5 shows the principle of

IDT. This meant that a buckled shear web could safely carry loads beyond the failure load predicted by the pure diagonal tension theory. Shear web design was again improved and became even lighter. Figure 6 below shows one of the tests conducted by Kuhn.

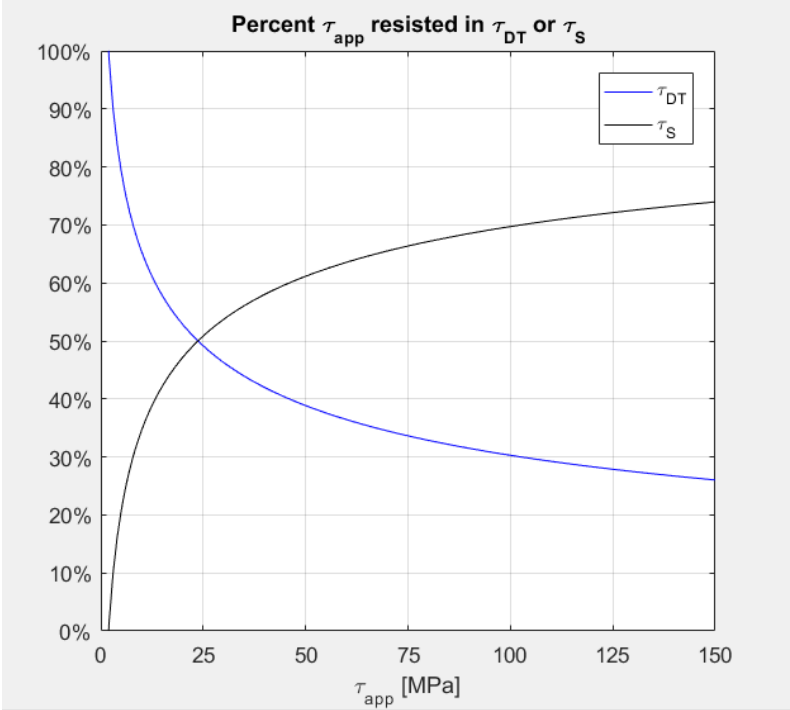


Figure 5: Principle of Incomplete Diagonal Tension

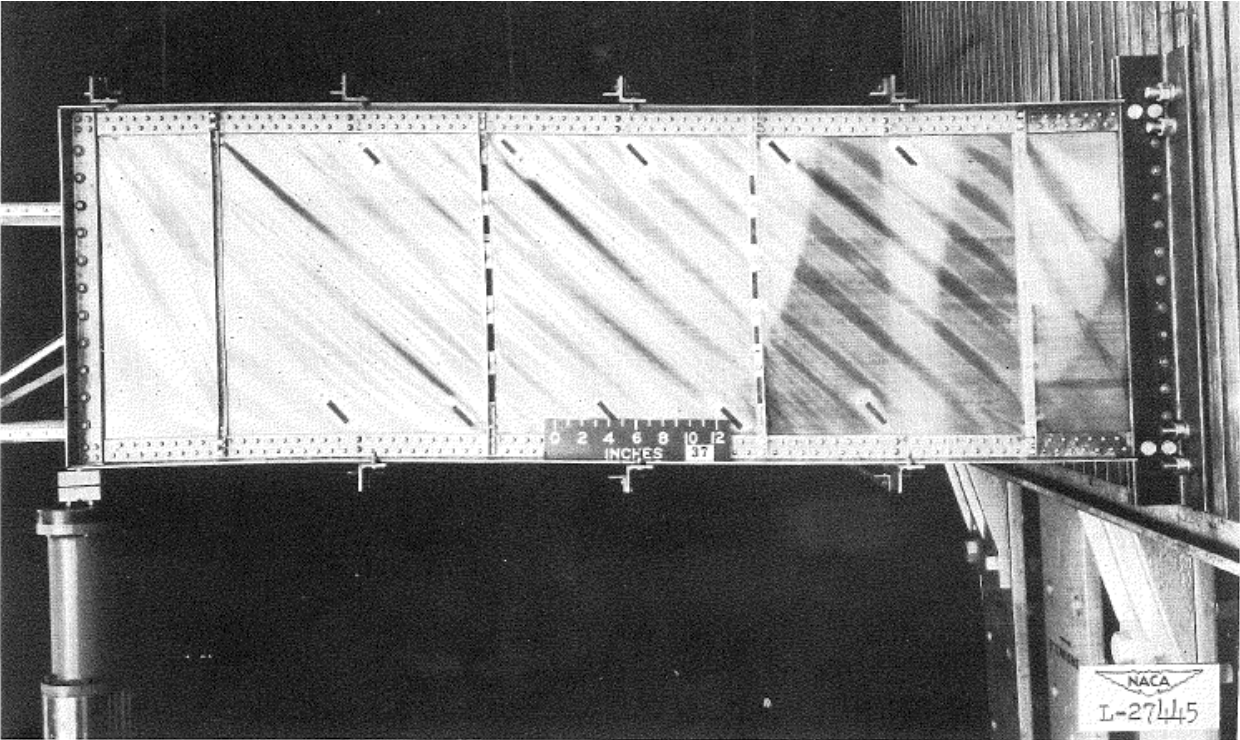


Figure 6: Diagonal tension beam. [21]

Over the years there have been many who have taken Kuhn’s IDT theory and modified it for special applications (including for FMLs), but the basic theory itself remains unchanged and is still used today. Other theories have been developed as well which attempt to analytically model the behavior

of post-buckled shear webs. However, IDT is still the method of choice in most cases and is also the method used in ESDU 71005: Buckling of Flat Plates in Shear [23].

The behavior of a shear web is dependent upon the material, its dimensions, and its boundary conditions. The web's aspect ratio and boundary conditions are used together to find a shear-buckling stress coefficient,  $k_s$ , which is empirically determined (see Figure 7).

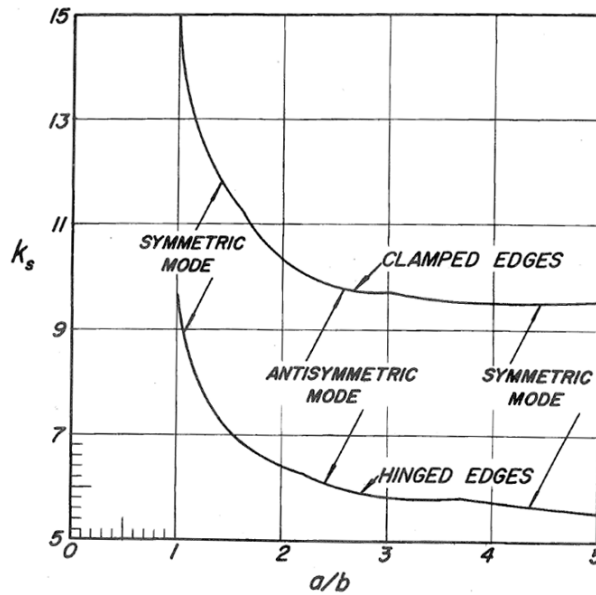


Figure 7: Shear-buckling-stress coefficient of plates as a function of  $a/b$  for clamped and hinged edges. [24]

The coefficient,  $k_s$ , is then used in calculations to find the buckling load. The IDT method takes these into account.

### Metal Shear Webs

To further improve the shear web design, the web material itself should be improved as well. Below, Figure 8 shows how the shear strengths of various aluminum alloys differ. “The influence of the aluminum layers on the behavior of Glare is huge” especially for those grades which feature fibers in only the  $0^\circ$  and  $90^\circ$  directions. This is because “under off-axis loading, the failure criterion is the aluminum shear strength”. [1]

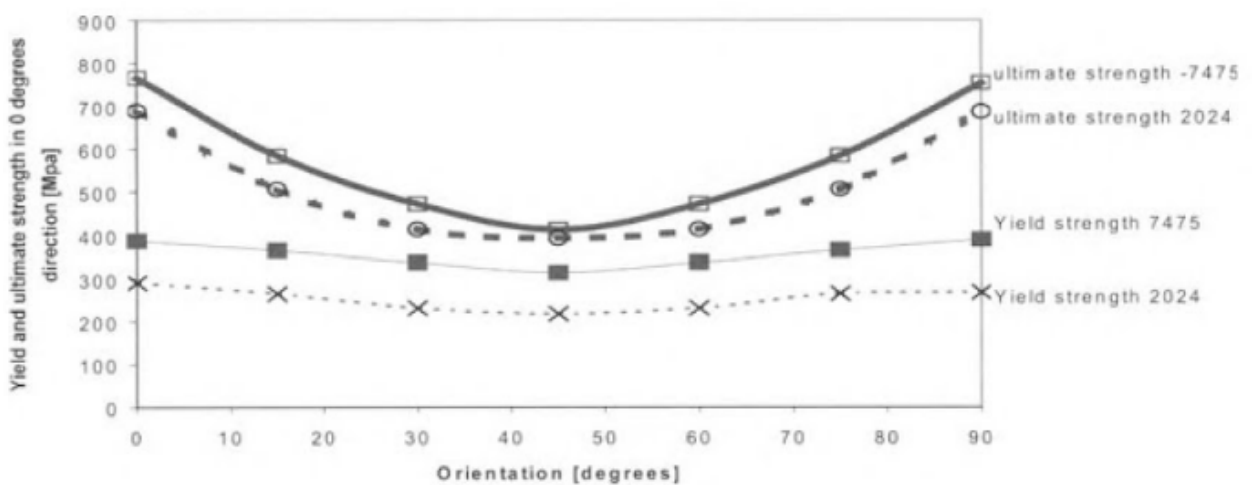


Figure 8: "Yield and Ultimate strength of two variants of Glare3 (with 2024 alloy and 7475 alloy) under off-axis loading" [1].

In Figure 8 “...the shear strength depends largely on the behavior of the aluminum alloys. An alloy with higher shear strength can improve the shear property of the laminate up to 15% with respect to the 2024 alloy.” [1]

In today’s practice, aluminum 2024-T3 is most frequently used in shear web designs. This is due to the alloy’s high shear modulus and its excellent resistance to fatigue cracking. Developed in the late 1960s, Al2024-T3 is one of the most common metals used in aerospace. Many other alloys have been developed since, but mostly with different purposes in mind. Al2024-T3 remains the preferred alloy for metal shear web design.

### Composite Shear Webs

Improving the shear performance of the fibers and matrix of FMLs was previously addressed. Many of the conclusions can be applied to composites as well with some exceptions. The principles in finding the right combination of fibers and matrix remains the same.

Many articles and books are readily available which address how to compute the buckling loads of composite webs in pure shear and combined loadings. Yet, most of the literature does not explore the performance of composites beyond the buckling load. One reason for this could be because buckling in composites is generally considered to be a failure mode. When composites buckle, they frequently experience delamination of their plies, which causes their performance to decrease rapidly. In a study investigating the post-buckling response of composite plates it was stated that “the presence of a delamination can significantly alter the post buckling response of composite plates.” However, since composite shear plates “can endure additional loads above the load causing the onset of buckling”, some have looked into just how far they can go in the hopes that delamination issues can be resolved [19].

In 1977, the Sirkorsky S-76 helicopter used shear resistant composite panels. Such shear resistant panels weigh more than panels designed for diagonal tension because of the extra material required. In an effort to save weight, U.S. Army Aerospace Engineers, G. Farley and D. Baker looked into the feasibility of using composite panels designed for diagonal tension. They published an article in 1982 which investigates the benefits of “thin-gage composite materials [for] helicopter fuselage structures... designed to operate at loads several times higher than initial buckling load.” During their research, they compared the performance of both thin aluminum and Kevlar panels and found that “*all* panels [emphasis added] ... continued to carry load well beyond 40 times initial buckling” [20].

The fibers in both composite panel designs were aligned in the  $\pm 45^\circ$  directions. The only difference between them was the thickness. The thin, four-ply shear panels buckled “at approximately 3.5 KN/m (20.0 lb/in.) and failed at about 101 KN/m (575 lb/in.)” Whereas the thicker, shear resistant panels failed (buckled) at “a shear load of 88 KN/m (500 lb/in.)” and “weigh 267 percent more than the buckled panel design.” In addition to this, it was stated that “after unloading, the aluminum panels had... deep permanent buckles, whereas the Kevlar panels returned to their original state.”

## Modified Glare Design

To make a new Glare material, one that is modified for improved shear strength, the same design criteria as the other Glare grades should also apply. Hence, it should use Al2024-T3 sheets, S2 Glass fibers, and the FM 94 adhesive. It will carry off-axis loads in addition to the axial loads, which means off-axis and axial fibers should be included. Also, to decrease the number of variables in testing and measurement, the material should be as simple and uniform as possible. This is interpreted as having the fewest layers possible.

Below are two sections labeled “Material Parameters” and “Design Criteria”. These identify the material and performance requirements for a modified Glare material, which adheres to the purpose and scope of this thesis. A full evaluation of these requirements and how a final laminate design was chosen is given in “Laminate Selection Criteria” in

APPENDIX: A. The two sections that follow are excerpts from that.

### Material Parameters

The following material parameters specify the modified Glare layup requirements.

1. Laminates must have a  $0^\circ$  and  $90^\circ$  glass fiber plies
2. Laminates must have an angle ply (otherwise there is no change in the material)
3. Angle plies may be either glass fiber or carbon fiber
4. Metal layers must have a thickness within the acceptable range of  $0.2 \text{ mm} \leq t_{Al} \leq 0.5 \text{ mm}$
5. Total laminate thickness must not exceed  $2 \text{ mm}$
6. Laminates must be within the valid range of  $0.45 < MVF < 0.85$

The inspiration for this thesis comes from the desire to use Glare materials on narrow bodied aircraft, which have thin skin panels. Often, the thickness of these skin panels does not exceed  $2 \text{ mm}$ . This is why the fifth parameter is listed above.

### Design Criteria

A laminate that matches the material parameters above must also show an improvement in shear performance. Below are the performance criteria for an acceptable modified Glare material.

1. Laminates should have an increase in post shear-buckled stiffness
2. Laminates should have an increase in geometric stiffness
3. Laminates should either maintain or increase the damage tolerance (for fatigue crack growth)
4. (For specific design requirements) Laminate should have a minimum stiffness value

In adherence to all the material parameters and design criteria, the layup [Al/0/45/90/Al] was selected with the Aluminum layers being  $0.3 \text{ mm}$  thick and unidirectional fiber layers, as seen in Figure 9.

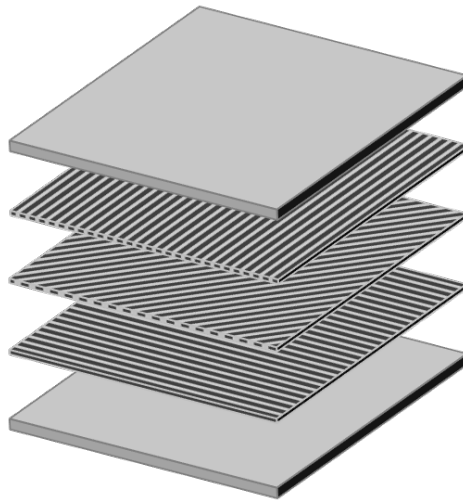


Figure 9: Possible modified Glare layup for improved shear performance [Al/0/45/90/Al].

## Analytical Models

Many models exist for analyzing metal shear webs and a few for analyzing FML shear webs. Many of the models for FMLs require complex computer software, take a considerable amount of time, or are not available. In addition, only one model for FMLs was found which accounted for off-axis fibers in FMLs (before buckling). However, the goal of this thesis is to use analytical methods that can quickly and accurately predict the behavior of modified Glare. Since most models do not account for off-axis fibers, the models will have to be compared with test data to see how similar they are.

The analytical methods used in this thesis were carefully selected for their versatility and applicability to FMLs. Each is mentioned briefly below, along with a description of what they are used for.

Classical Laminate Theory (CLT): This theory is widely used in composites and FMLs for analyzing material properties, calculating stresses and strains, and determining failure modes and ultimate strengths when combined with failure models such as Tsai-Wu. For this thesis, CLT is used to obtain the ABD matrix as well as the moduli of elasticity in the  $x$ ,  $y$ , and  $\alpha$  (buckling angle) directions. These are represented respectively as  $E_x$ ,  $E_y$ , and  $E_\alpha$ . The ABD matrix is then used in the Rayleigh-Ritz method, while one or two of the moduli are used in each of the subsequent models.

Rayleigh-Ritz: The Rayleigh-Ritz is also known simply as the Ritz method, and both names are commonly used. This method uses the ABD matrix obtained from CLT and provides the critical shear load,  $N_{xy_{crit}}$ , which causes initial shear buckling in webs.  $N_{xy_{crit}}$  is then used in the Kuhn method.

Kuhn: This method uses  $N_{xy_{crit}}$  to find the principle web stresses ( $\sigma_1$  and  $\sigma_2$ ) and how much of the applied shear stress ( $\tau_{app}$ ) is resisted through diagonal tension action ( $\tau_{DT}$ ) and how much is resisted through shear action ( $\tau_S$ ).

Rule of Mixtures (ROM): This method takes the moduli of elasticity of each ply and combines them to provide a modulus of elasticity for the laminate,  $E_{lam}$ .  $E_{lam}$  is compared with  $E_x$  from CLT.

Metal Volume Fraction (MVF): By assuming a linear relationship between the properties of the metal and composite layers this method will estimate the properties on the laminate. It has been approved for tensile strength, shear strength, and a few others. However, in this thesis it is used to find  $E_\alpha$  and then it is compared with the results from CLT and ROM. The metal volume fractions are also used for analysis of results.

FMLGROW\_V2.0: This is a model for analyzing the fatigue crack growth rates of FMLs. It is a complicated model, but necessarily so. It uses material properties obtained in CLT and produces crack growth life curves.

Hooke's Law: This law is used to obtain the spring constant,  $K$ , of a laminate using  $E_\alpha$  obtained from CLT.  $K$  is then used to compare the laminate's relative geometric stiffness with other laminates.

## Research Scope

From the information given in the previous chapter, it is clear that there exists a potential for an FML design optimized for post shear-buckled stiffness and fatigue crack growth performance. This need is echoed by Wittenberg (et al.), who researched shear buckling in Glare plates, when he said the following: "Most Glare grades were designed for applications in fuselage panels with the fibres aligned in the direction of the stringers and the frames (this configuration was driven by fatigue and damage tolerance considerations). This implies that in a case of pure shear loading the fibres are not stresses, so that almost the entire shear load is carried by the aluminium layers. Therefore, the reduction in stiffness and – even more pronounced – the yield properties is more severe for the case of pure shear loading than for compression or tension loading." [26]. In response to this need, the following research question was formulated.

### Research Question:

**What modifications to Glare3 will improve the material's post shear-buckled stiffness without sacrificing damage tolerance?**

To answer this question, three tests and a parametric study were designed that provide the key information necessary to discovering the effects of modification to the Glare3 material. These are explored in the chapter that follow next. First is a look into the effects of changing the fiber orientations of standard Glare3. Next is a parametric study where metal layer thickness and off-axis fibers are considered for their potential in optimizing a modified Glare3 material. Finally, the last chapter investigates the optimized material and evaluates its performance.



## CHAPTER 3: Post Shear-Buckled Stiffness and Damage Tolerance of Off-Axis Glare3

The performance of standard Glare3 under various orientations was investigated, as a first step to exploring possible modifications of Glare3 for improved post shear-buckled stiffness. This study was designed to provide information regarding the effects of fiber orientation on the post shear-buckled stiffness. In addition, it establishes a baseline data set that will be used to evaluate the effectiveness of the analytical models used to predict the relevant properties in Glare3 and in the modified Glare3s materials.

The approach taken to carry out this study is detailed in the two methodologies sections below. This is followed by a section on the results and discussion of the study.

### Test Methods

#### Picture Frame Shear Test Method

There are multiple methods of testing materials in shear, but very few are capable of testing the shear buckling responses of materials. The most common way of testing the shear buckling response of shear webs is by making a beam and applying shear loads to it. An example of this is shown in Figure 10.

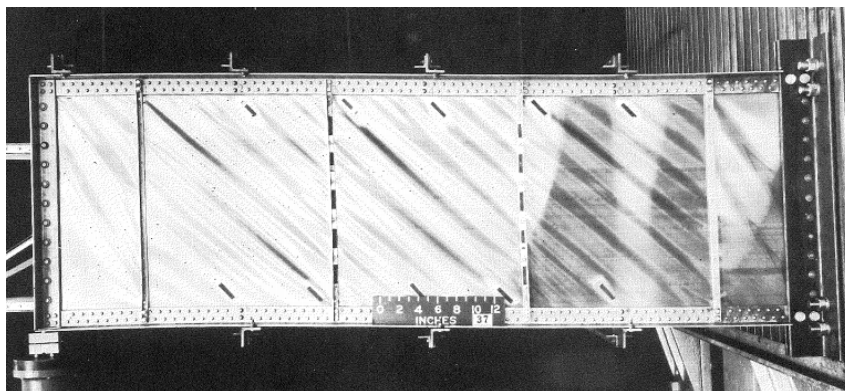


Figure 10: Diagonal-tension beam [NACA TN 2661]

Unfortunately, with this type of setup it is not possible to apply pure shear loads on a web and there are multiple other factors affecting the panels, which adds complication. Applying pure shear loads, with no secondary loading, is best achieved using a picture frame shear test. A specimen is clamped inside a square frame (picture frame) that pivots at the corners. When loaded uniaxially, the frame will apply a nearly uniform shear stress on the clamped material. This makes it possible to measure the post shear-buckled response of materials in a simple test.

#### Picture Frame Apparatus

The picture frame itself should be at least ten times stiffer than the specimen being tested. This helps ensure that the applied shear stresses are as uniform as possible. The picture frame shown in Figure 11 was used for the tests and is made of steel bars that are 360 mm long, 30 mm deep, and 15 mm

wide. Two bars are present on each side and the shear specimen is clamped between them with a single row of eleven evenly spaced bolts 25 mm apart.

Steel rods run through the bars at the pivot locations and their centroids are in-line with the outer edges of the shear specimen (see Figure 12). The location of the rods reduces stress concentrations at the corners of the specimen which helps to avoid premature failure. Two of the steel rods along the same diagonal have couplings attached to them, which allow a press to apply a compressive force on the frame.

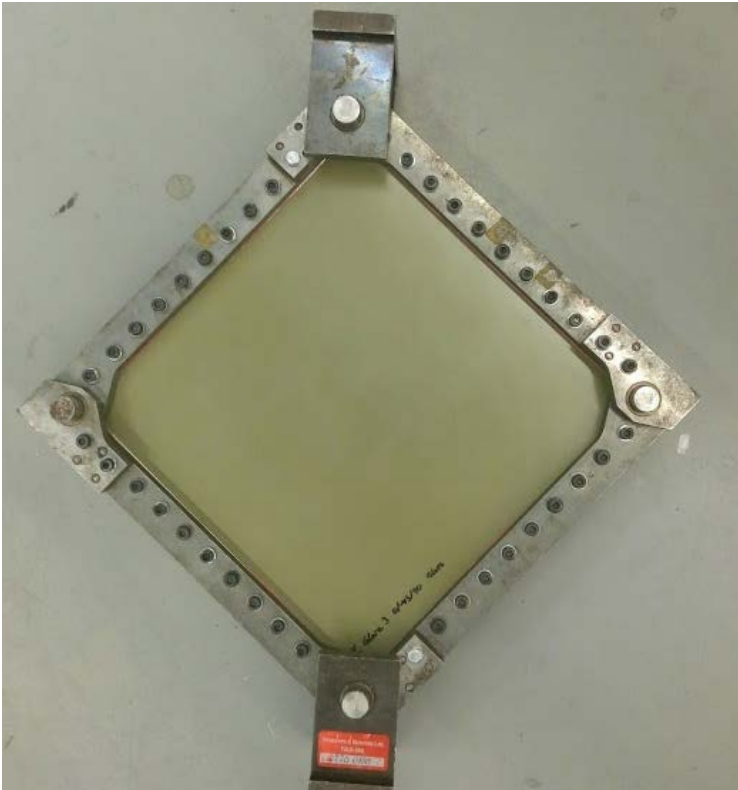


Figure 11: Picture frame apparatus.

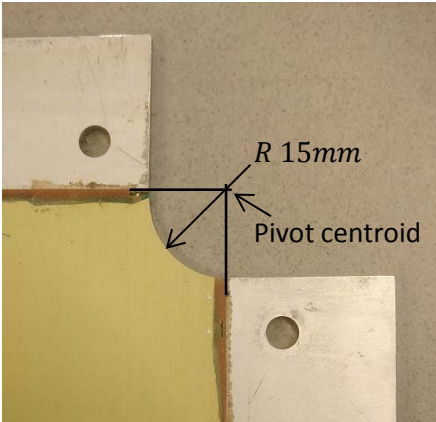


Figure 12: Shear specimen corner cut-out and pivot centroid.

Because the picture frame is loaded into a press and compressed, the data is collected in the form of force and deflection. These forces and displacements need to be converted into shear stresses and shear strains in the web. This is done with the following expressions:

Equation 1

$$q_0 = \frac{P}{2 \sin(\alpha) - \frac{\delta}{a}}$$

$$\tau = \frac{q_0}{a * t}$$

$$2\gamma = \frac{\cos\left(\sin^{-1}\left(\sin(\alpha) - \frac{\delta}{2a}\right)\right)}{\sin(\alpha)} - 1$$

where  $q_0$  is the shear force,

$P$  is the force exerted by the press,

$a$  is the laminate width,

$\delta$  is the displacement of the press,

$t$  is the laminate thickness,

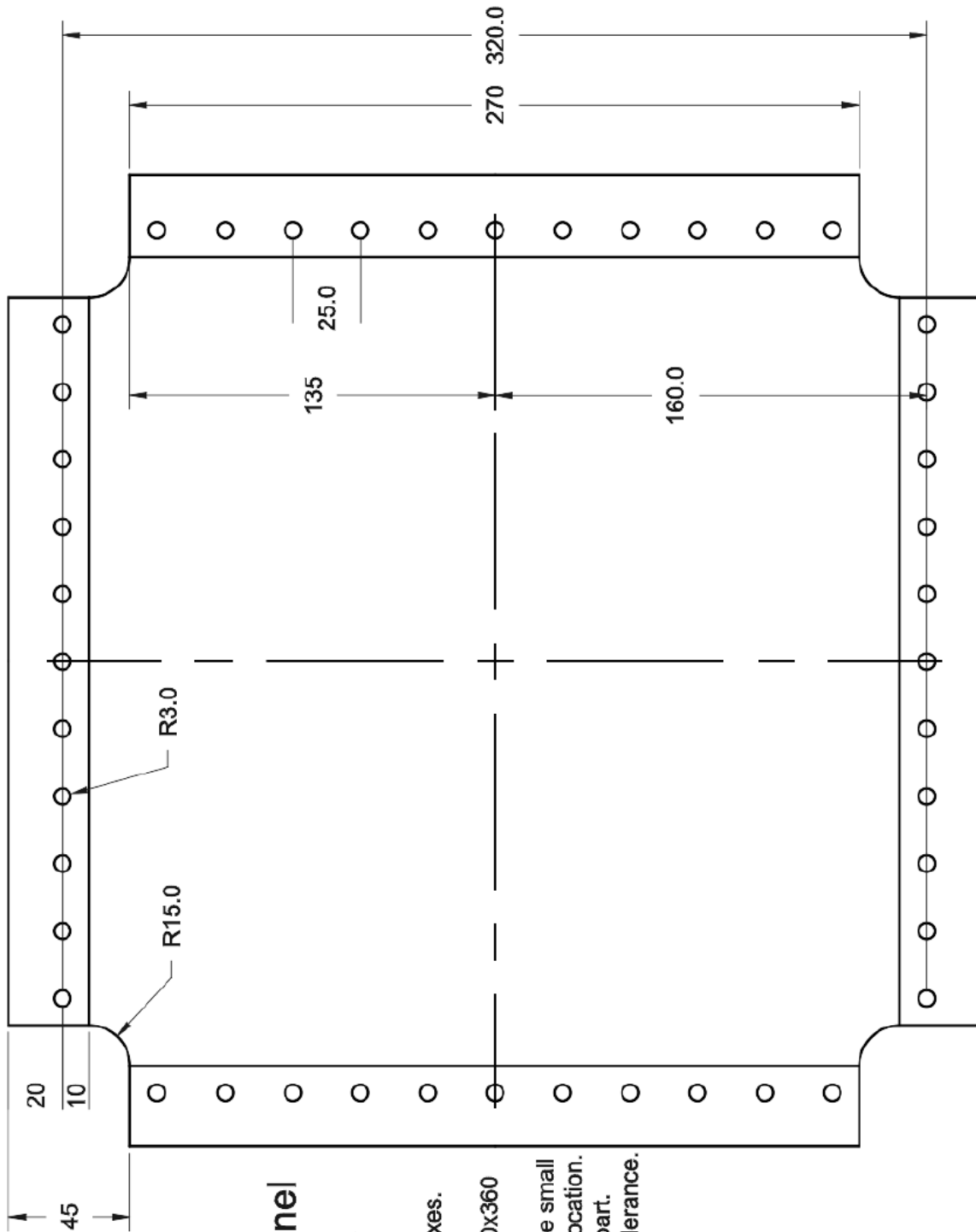
$\gamma$  is the engineering strain along angle  $\alpha$ .

### Problems with the picture frame apparatus

It must be noted that a picture frame test is not a perfect solution. It has a couple drawbacks which need to be accounted for. One is that the shear specimen is not *perfectly* loaded in pure shear, but it does come close. To achieve a perfectly pure shear loading scenario would require a hypothetical apparatus, but actions can be taken to get the loading as close as possible to an ideal pure shear scenario. These includes making the frame at least ten times stiffer than the test specimen and moving the centroids of the pivots to be directly over the corners of the shear specimen. The picture frame shown in Figure 11 is more than ten times as stiff as the specimens which were tested, and has the pivot centroids directly over the specimen's corners. As a result, the shear strains in the specimen are as uniform as possible which helps reduce the non-uniformity of the stress field that develops. The non-uniformity which remains may cause certain areas of the specimen to buckle/yield sooner than others, however, only average stresses can be calculated from the force-deflection data. This causes the transition in stiffness during the onset of buckling and the onset of yielding to appear smoother. Nevertheless, the area of most interest for this thesis is the post shear-buckled regime and not within the transition areas. Thus, it was assumed that the picture frame apparatus shown in Figure 11 would produce sufficiently accurate shear data of the specimens in the post shear-buckled regime to demonstrate confidence in the conclusions made.

### Shear Specimen Specifications

The shear specimen has an overall width and height of 360 mm as well, with 30 mm × 1.5 mm aluminum tabs on one side, giving an overall gauge area of 300 mm × 300 mm. Each specimen was 0.86 mm thick, and the cut-out corners allow room for the pivot rods of the picture frame and double as a way of reducing stress concentrations. On the next page, Figure 13 gives a drawing of the specimen dimensions which fit inside the picture frame described.



### FML Shear Panel

Symmetric about both axes.

Overall Dimensions: 360x360

Most important is that the small holes are in the proper location. They are each 25mm apart. The exterior has high tolerance.

All dimensions in mm

Figure 13: GD&T of shear specimen

## Manufacturing

For this first test, six shear panels were manufactured. The layups and manufacturing process of each is given below.

### Glare3 Shear Panels

- $[Al/0/90/Al]$  x2
- $[Al/15/-75/Al]$
- $[Al/30/-60/Al]$
- $[Al/45/-45/Al]$  x2

Each laminate was laid up in a clean room at TU Delft. The Glare3 panels were all created at the same time using a large sheet of aluminum 2024-T3 with unidirectional (UD) glass fiber ply laid down in the  $0^\circ$  direction, on in the  $90^\circ$  direction, followed by another sheet of aluminum 2024-T3. The FML was placed inside a vacuum bag and put into an autoclave where the autoclave ran through the curing cycle typical of Glare materials described in Figure 14.

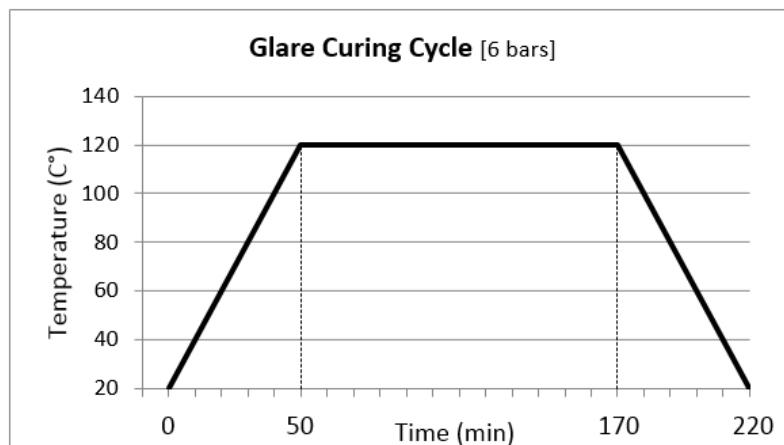


Figure 14: Cure cycle for Glare at 6 bars of pressure.

The large panel of Glare3-2/1-0.3 measured  $1\text{ m} \times 1.4\text{ m}$ . Out of this panel, six different panels measuring  $360\text{ mm} \times 360\text{ mm}$  were cut. By cutting them out at different angles it was possible to get all the different fiber angles shown in the list above. Figure 15 demonstrates how this was done. Cutting them all from the same sheet of Glare3 ensured that each of the panels were of the same manufacturing quality.

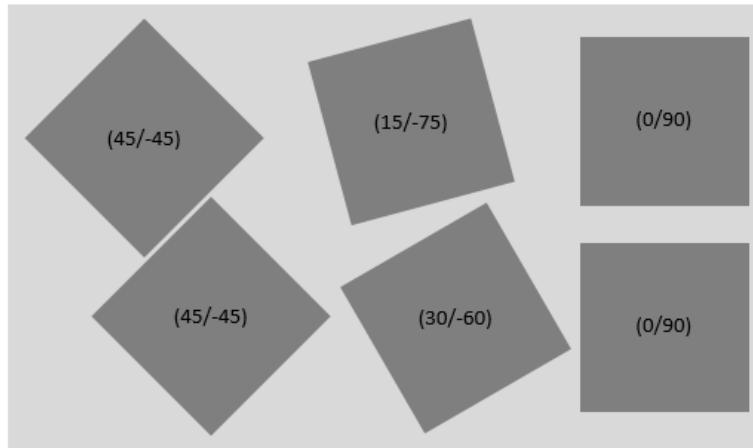


Figure 15: Six panels of varying fiber angles cut from single Glare3-2/1-0.3 sheet.

Aluminum tabs were adhered around the edges of the panels (see Figure 10) to increase the grip in the picture frame, reduce local stress concentrations, and guarantee a uniform distribution of shear forces. Once the adhesive had cured, the panels were submitted for final cutting and machining according to the dimensions shown in Figure 13.

### Digital Imaging Correlation

Digital Imaging Correlation (DIC) was used to measure the strain fields in the panels. DIC involves taking gray images and tracking the movement of locations on a panel relative to surrounding locations. To help the system identify points to track, the specimens are sprayed with a small speckle pattern of paint. The DIC system is calibrated to know its exact position and orientation relative to the panel, which allows it to accurately calculate the change in distances between certain points from image to image. From this, deformations, displacements, and strains throughout the entire panel can be obtained. This has an advantage over strain gauges, which can only measure strains in one place per gauge and assumptions are made as to what the strain field may look like between strain gauges. With DIC, the full strain field is obtained along with out-of-plane displacements.

In this test, two DIC cameras were set up about 2.5 m from the panels with images being taken every two seconds. After the full test, the images were analyzed to show the strain fields and out-of-plane displacements.

### Test Rate

The shear tests were conducted as described above, by loading a shear specimen into the picture frame, and installing the picture frame into a press. For Glare the maximum strain rate for quasi-static testing is 0.141 mm/sec. For these shear specimens, that strain rate translates to a mechanical displacement rate of 8.46 mm/min. Thus, during testing, the maximum mechanical displacement was set to 8 mm/min.

### Analytical Methods

The stiffness of a material can be determined by measuring the strain due to a given applied stress. This can be shown graphically in a stress-strain curve which shows the material's stiffness for all applied loads from start to failure. These curves have distinctive features that reveal different characteristics of the material, and each feature requires its own analytical model to be predicted.

Since a thorough analysis of the stiffness after the yielding point of the material is beyond the scope of this thesis, this section contains the analytical models that were used to analyze the stiffness of Glare materials up to, but not including, the yield point of the aluminum.

The analytical models presented here were carefully selected out of a wide variety of models for their applicability to FML shear webs. Table 2 gives a list of the analytical models, along with their inputs and outputs. A description of how these models are used is given after the table.

**Table 2: Analytical Models and Their Inputs and Outputs**

Model	Input	Output	Purpose
CLT	$E_x, E_y, \mu_{xy}, \mu_{yx}, G_{xy}, \theta$	$ABD, E_{lam}, Q$	Pre & post-buckling properties
Rayleigh-Ritz	$ABD$	$N_{xy_{crit}}, P_{crit}$	Buckling loads
Kuhn	$N_{xy}, N_{xy_{crit}}, E$	$\sigma_1, \sigma_2, \tau_{DT}, \tau_S$	Post-buckling web stresses
Rule of Mixtures	$E_{plies}$	$E_{lam}$	Pre-buckling stiffness
MVF	$E_{plies}$	$E_{lam}$	Tensile and shear strengths
FMLGROW_V2.0	$E_x, E_y, t$	Crack growth	Fatigue crack growth rates
Hooke's Law	$E$	$K$	Geometric stiffness

NOTE: Each of these models in Table 2 were written in MatLab scripts for analysis.

The goal of the shear tests was to determine the stiffness of the material before and after shear buckling, as well as determine the buckling load. Classical Laminate Theory (CLT) was used to obtain the ABD matrix, which is then used to calculate the shear stiffness ( $G_{xy}$ ) before buckling. The Rayleigh-Ritz method (which also uses the ABD matrix) was used to calculate the buckling load ( $N_{xy_{crit}}$ ). The the post shear-buckled stiffness ( $G_\alpha$ ) was calculated using three separate methods, CLT, Rule of Mixtures (ROM), and Metal Volume Fraction (MVF). The reason for the redundancy in calculating  $G_\alpha$  is because there is uncertainty as to whether the analytical models are robust enough to accurately predict a material's stiffness beyond shear buckling. As a second measure of the material's stiffness, Hooke's Law was used to calculate the spring constant,  $K$ . Together,  $G_\alpha$  and  $K$  provide a greater understanding of how the stiffness of the material changes.

Subsequent to the shear tests is an evaluation of the damage tolerance of the Glare3 material. This was done using FMLGROW\_V2.0. This model was specially created for Glare and is very accurate at determining the fatigue crack growth rates.

A detailed description of each of the models presented above is given in the following sections in the same order as in Table 2.

### Classical Laminate Theory (CLT)

Classical Laminate Theory is a common, yet powerful, analytical tool that can accurately predict many composite material properties as well as the stresses and strains due to applied loads. It does this by summing up the directional material properties of individual plies. For the purposes of this project, this tool is useful in obtaining material property predictions. These properties are used in one way or another in each of the other analytical models. The equations in CLT, which are used to calculate these properties, are shown below in Equation 2 to Equation 4. Because this well-known method can be readily found online and in many books, only relevant equations are shown here. It is assumed the reader is familiar with CLT.

Equation 2

$$Q = \begin{bmatrix} \frac{E_x}{1 - \mu_{xy}\mu_{yx}} & \frac{\mu_{xy}E_y}{1 - \mu_{xy}\mu_{yx}} & 0 \\ \frac{\mu_{xy}E_y}{1 - \mu_{xy}\mu_{yx}} & \frac{E_y}{1 - \mu_{xy}\mu_{yx}} & 0 \\ 0 & 0 & G_{xy} \end{bmatrix}$$

Equation 3

$$C = MQM^t$$

$$A = \sum_{i=1}^n C(z_i - z_{i-1})$$

$$B = \frac{1}{2} \sum_{i=1}^n C(z_i^2 - z_{i-1}^2)$$

$$D = \frac{1}{3} \sum_{i=1}^n C(z_i^3 - z_{i-1}^3)$$

$$ABD = \begin{bmatrix} A & B \\ B & D \end{bmatrix}$$

Where  $n$  is the number of plies in the laminate.

Equation 4

$$E_x = \frac{A_{11}A_{22} - A_{12}^2}{\frac{A_{22}}{a}}$$

The  $M$  matrix in Equation 3 is dependent upon an angle,  $\theta$ . Equation 4 will give the elastic modulus along of a laminate in the  $x$  direction. By setting  $\theta = 45^\circ$ , Equation 4 will still give the elastic modulus of a laminate in the  $x$  direction, but this is equal to the elastic modulus of the un-rotated laminate along a  $45^\circ$  angle, or  $\alpha$ . This rotated elastic modulus is referred to here as  $E_\alpha$ .

### Rayleigh-Ritz

The Rayleigh-Ritz method is specially designed to give “the buckling loads of rectangular composite panels with different boundary conditions and/or applied loads.” [25] Its versatility makes it a favorite in composite design. For this project, the Rayleigh-Ritz method is used to calculate the shear load that causes the initial shear buckling,  $N_{xy,crit}$ . It is an empirical approach that uses the  $ABD$  matrix from CLT, and is given in Equation 5.

$$N_{xy_{crit}} = K \left( \frac{4}{a^2} \right) (D_{11} D_{22}^3)^{\frac{1}{4}}$$

$$\beta = \left( \frac{D_{11}}{D_{22}} \right)^{\frac{1}{4}}$$

$$c = \frac{D_{12} + 2D_{66}}{\sqrt{D_{11} D_{22}}}$$

$$A = -0.27 + 0.185c$$

$$B = 0.82 + 0.46c - 0.2c^2$$

$$K = 8.2 + \frac{5c}{10^{\frac{A}{\beta} + B\beta}}$$

where  $N_{xy_{crit}}$ , is a running load with units [force/length].

Using  $N_{xy_{crit}}$ , the corresponding mechanical load,  $P_{crit}$ , applied on the picture frame can be calculated. This serves as a check to assess if the analytical results match the test results. This is done using Equation 6.

$$P_{crit} = 2a * N_{xy_{crit}} * \sin(\alpha)$$

### Kuhn Method

The Kuhn method, is based upon the earlier work of Wagner, who demonstrate that "...a thin web with transverse stiffeners does not "fail" when it buckles; it merely forms diagonal folds and functions as a series of tension diagonals, while the stiffeners act as compression posts." [21] Kuhn expanded upon this theory to show that post shear-buckled webs continue to resist some loads through shear and resist the rest through diagonal tension in a state referred to as "incomplete diagonal tension." The results of Kuhn's work are now known as the Kuhn method and it is still one of the most widely used analytical methods for stiffened shear panels today [1].

Central to the Kuhn method is the assumption that "...the nominal applied shear stress is split into a pure shear part,  $\tau_S$ , and a part carried by diagonal tension action of the skin,  $\tau_{DT}$ ..." [1]. Thus, the underlying expression (Equation 7) for the applied nominal shear stress,  $\tau$ , is

$$\begin{aligned}\tau &= \tau_S + \tau_{DT} \\ \tau_S &= (1 - k)\tau \\ \tau_{DT} &= k\tau \\ k &= \tanh\left(0.5 \operatorname{Log}\left(\frac{\tau}{\tau_{crit}}\right)\right) \quad (\tau \geq \tau_{crit}) \\ \tau_{crit} &= k_{ss}E_{1lam}\left(\frac{t_{lam}}{a}\right)^2\end{aligned}$$

where  $\tau_S$  = “shear stress carried by true shear action” [21],

$\tau_{DT}$  = “shear stress carried by diagonal-tension action” [21],

$k$  = “diagonal-tension factor” [21],

$\tau_{crit}$  = shear buckling stress,

$a$  = the width of the web,

$t_{lam}$  = web thickness,

$k_{ss}$  is the shear-buckling stress coefficient, which is obtained empirically through testing. An example of data obtained for  $k_{ss}$  is in Figure 16. Here,  $k_{ss}$  is chosen to be 8.5.

The stresses in the buckling direction,  $\alpha$ , and perpendicular to  $\alpha$ , are principle web stresses  $\sigma_1$  and  $\sigma_2$ . Equation 8 shows how they are obtained, using  $\alpha = 45^\circ$ .

$$\begin{aligned}\sigma_1 &= \frac{2k\tau}{\sin(2\alpha)} + \tau(1 - k) \sin(2\alpha) \\ \sigma_2 &= -\tau(1 - k) \sin(2\alpha)\end{aligned}$$

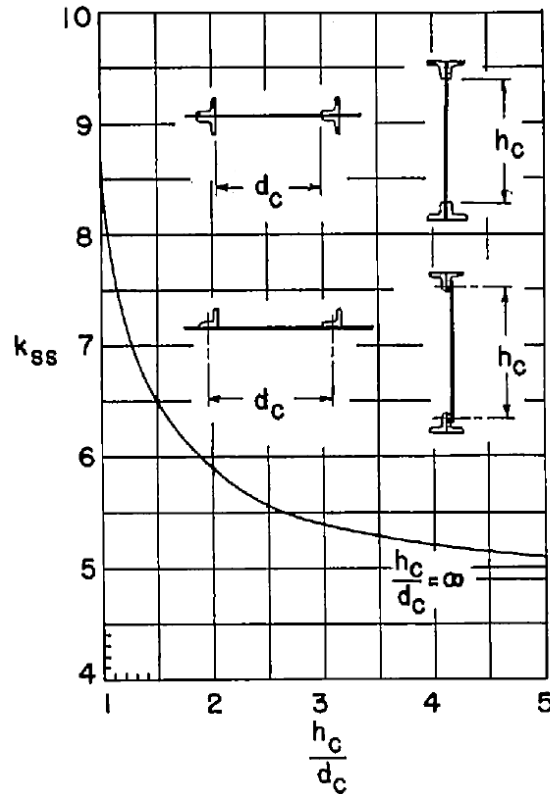


Figure 16: Theoretical buckling coefficients for plates with simply supported edges. [21]

### Rule of Mixtures

The Rule of Mixtures is a simple formula that multiplies a ply's properties by the volume fraction that ply occupies in a laminate. This is done for each ply and the summation of them all gives the values for the laminate's properties. This is shown in Equation 9

Equation 9

$$E_{lam} = \sum_{i=1}^n \frac{V_i}{V_{lam}} E_i$$

where  $n$  is the number of plies in the laminate,  
 $V$  is the volume.

### Metal Volume Fraction (MVF)

The Metal Volume Fraction method is an analytical model developed specifically for FMLs. As the name indicates, this model makes predictions based off of "the amount of metal present" within an FML [1]. It is very similar to the approach taken with the Rule of Mixtures. In this case, the MVF method assumes a linear relationship in the material's strengths and it has been validated within the range  $0.45 \leq MVF \leq 0.85$ . The nice thing about the MVF method, is that it can be applied to multiple material properties. "Authorities presently accept the MVF approach for the tensile strength, compression strength, shear strength, bearing strength and blunt notch strength." [1]

The formula used in the MVF method is as follows:

Equation 10

$$Property_{lam} = MVF * (Property_{metal}) + (1 - MVF) * (Property_{composite})$$

Figure 17 below shows a representation of how the MVF method works.

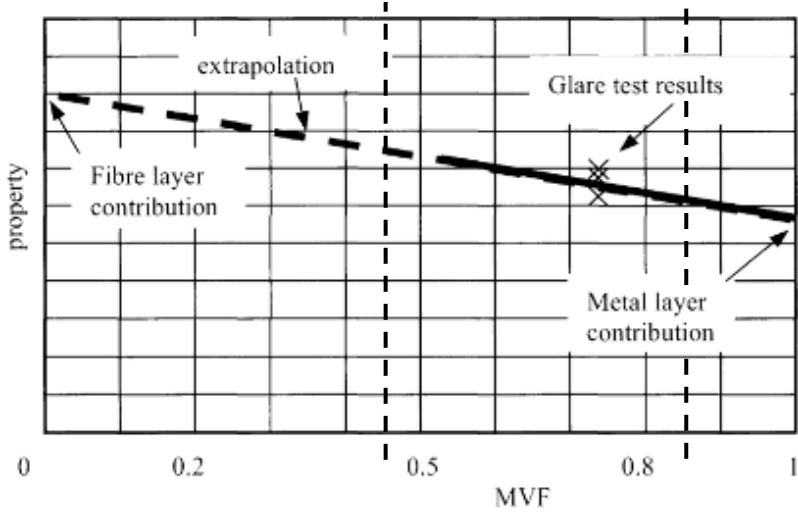


Figure 17: Graphical representation of the Metal Volume Fraction approach. [1]

Two dotted lines at the 0.45 and 0.85 points on the MVF axis have been added to show the valid range of the MVF method.

**FMLGROW\_V2.0**

This model was developed in-house at TU Delft and is designed specifically for predicting the fatigue crack growth rates in Glare panels [27]. Simply stated, this model is capable of calculating fatigue crack growth rates in all Glare materials as well as delamination growth in both single and multi-block analyses. An in-depth description of this model is beyond the scope of this thesis, but more details can be found in [27].

Glare materials were designed as an intermediate material between stiffness and fatigue resistance. As such, a modified Glare material’s performance cannot be complete using stiffness calculations alone. Instead, fatigue crack growth rates must also be considered in tandem with the stiffness. It is for this reason that the FMLGROW\_V2.0 model is used. Table 3 below gives the parameters that were used in calculating the Crack growth life curves for the various Glare layups.

Table 3: FMLGROW\_V2.0 Parameters and Values

Parameter	Value
Half-crack length (a)	3.5 [mm]
Half-saw cut length (s)	2 [mm]
Panel width (w)	140 [mm]
numloops	2700

**Stiffness Calculations**

The stiffness of a shear web can be calculated using its material properties as well as its geometry. The material properties are used to calculate the shear modulus, while geometry is used to calculate the spring constant. Both are necessary to understand how different webs behave in comparison to one another.

To find the post shear-buckled shear modulus, which is referred to here as  $G_\alpha$ , the web stresses in the direction of  $\alpha$  need to be found. With the help of Mohr's circle, the pre and post shear-buckling principal stresses in the web are easily calculated. An example of this can be seen in Figure 18.

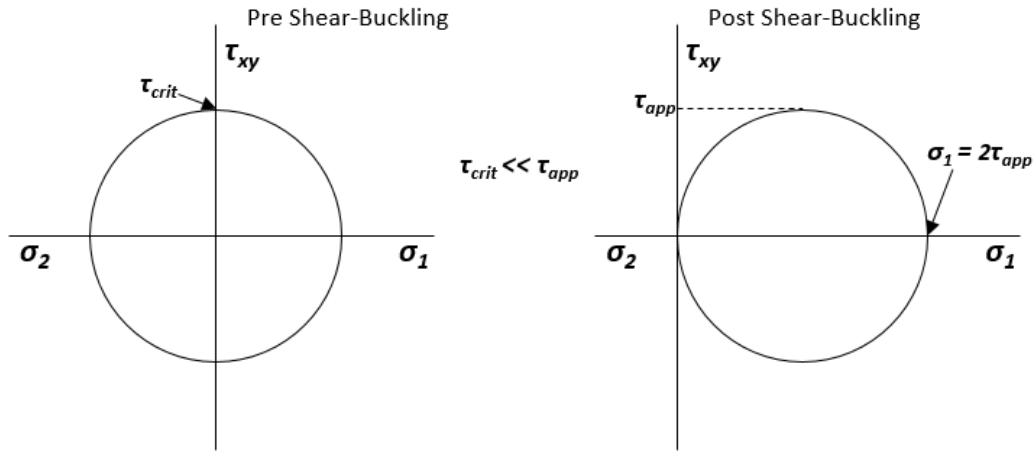


Figure 18: Mohr's circles depicting the pre and post shear-buckling stress states.

Mohr's circle shows that the principal stress,  $\sigma_1$ , is twice the value of the applied shear stress,  $\tau_{app}$ , after shear buckling has occurred. Since  $\tau_{app}$  can be much greater than the shear buckling load,  $\tau_{crit}$ , the compressive stresses in  $\sigma_2$  are negligible. Thus, by using  $\tau_{app}$  the expression to find  $G_\alpha$  is:

Equation 11

$$G_\alpha = \frac{2\tau_{app}}{\gamma} = \frac{E_x}{2}$$

The geometric stiffness of the laminates is calculated using Hooke's Law, as shown in Equation 12

Equation 12

$$K = \frac{F_\tau}{d}$$

$$F_\tau = \tau_{app} * t * a$$

where  $K$  is the spring constant,

$F_\tau$  is the applied shear force,

$d$  is the deformation of the laminate,

$a$  is the laminate width,

$t$  is the laminate thickness.

## Results and Discussion

### Manufacturing

The shear panels were manufactured well and without problems. The final product was uniform and a visual inspection showed that the tabs were properly bonded. It was noted, that during testing a tab on one panel became detached at the same time that the panel itself failed. However, it is believed that this detachment was a secondary failure and not the cause of initial failure.

### Glare3 Shear Tests

The first shear tests included six shear panels. However, due to technical difficulties while testing one of the panels with fibers oriented at  $0^\circ$  and  $90^\circ$ , the results were not included. Also, results for the two specimens with fiber angles at  $45^\circ$  and  $-45^\circ$  are nearly identical (see Figure 19), so further plots and discussions will only address one of them. Thus, the results for the remaining four panels listed below are discussed in this section.

Glare3 Shear Specimens:

- [Al/0/90/Al]
- [Al/15/-75/Al]
- [Al/30/-60/Al]
- [Al/45/-45/Al]

The purpose of these tests was to identify the change in shear stiffness of Glare3 at various fiber orientation. This was achieved by rotating Glare3 panels at different angles and testing them in a picture frame shear test apparatus. The press used for the tests gave force and deflection outputs. Calculations using the expressions shown below convert the force and deflection data from the press into the desired shear-stress and shear-strain data of the panel. Figure 19 and Figure 20 show plots of the test data obtained from each panel.

Equation 13

$$\tau = \frac{F}{\left(\frac{b}{\cos(\alpha)} - d\right) * t}$$
$$\gamma = \frac{\cos\left(\sin^{-1}\left(\frac{L_d - \frac{F}{2}}{b}\right)\right)}{b} - \frac{1}{2}$$
$$L_d = \frac{b}{\cos(\alpha)}$$

Where F = Force

b = specimen width

d = deflection

t = specimen thickness

$\alpha$  = buckling angle ( $45^\circ$ )

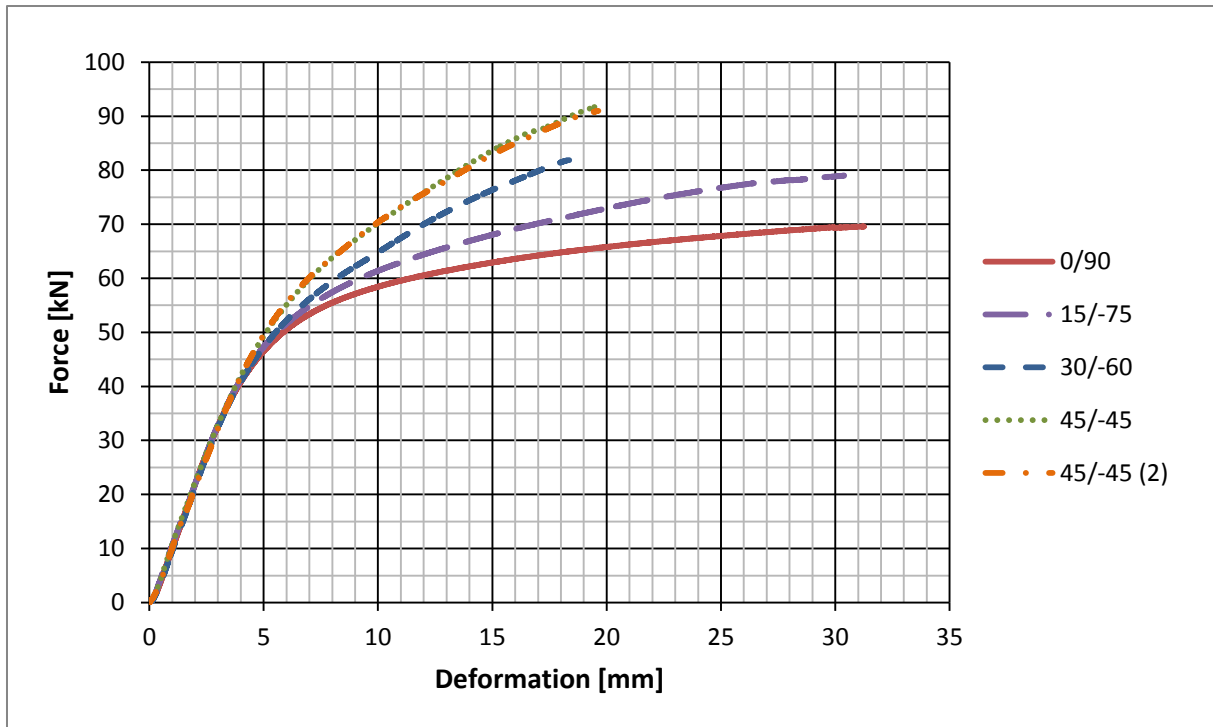


Figure 19: Force vs. deflection plots of five Glare3 specimens at different orientations.

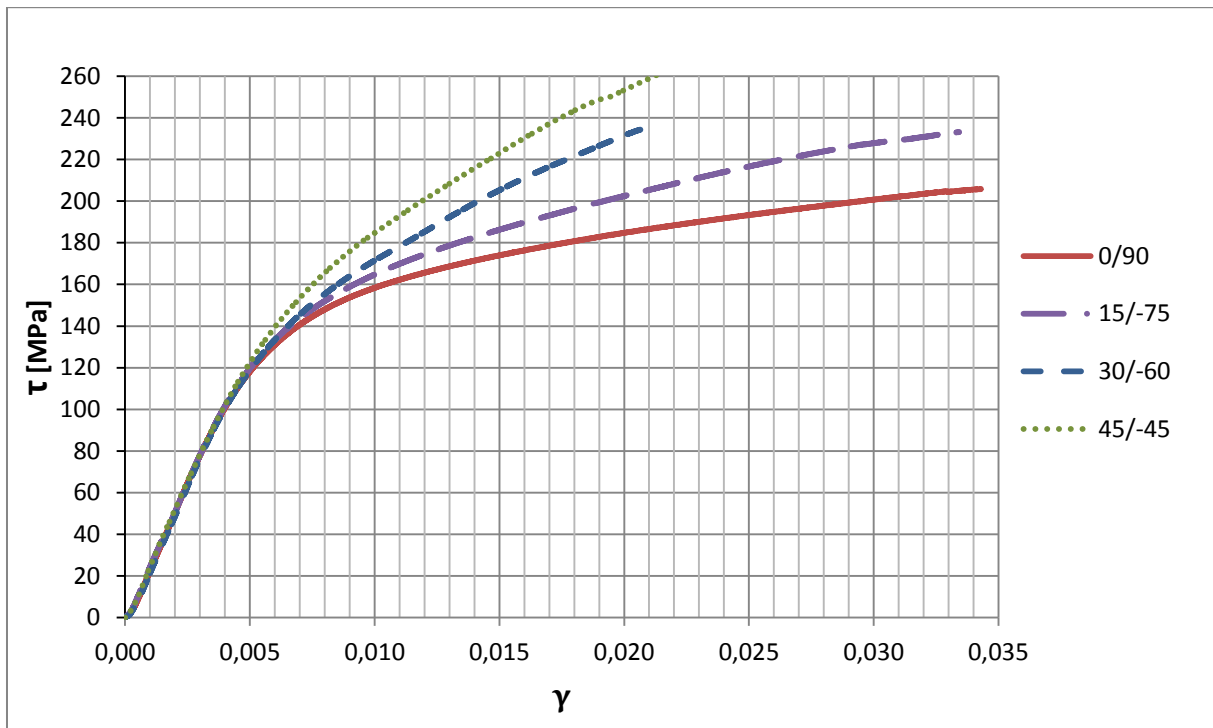


Figure 20: Shear-stress vs. shear-strain plots for Glare3 specimens at different orientations.

There are four important features in stress-strains curves that are of interest for this project: shear stiffness ( $G_{xy}$ ), buckling stress ( $\tau_{crit}$ ), post shear-buckled stiffness ( $G_{\alpha}$ ), and the stiffness after the yield stress ( $\tau_y$ ). However, Figure 20 only shows the latter two for reasons that will be explained shortly. Since  $G_{xy}$  and  $\tau_{crit}$  could not be obtained from the tests,  $G_{xy}$  was calculated using the CLT, ROM, and MVF models, while  $\tau_{crit}$  was calculated using the Rayleigh-Ritz model. The CLT, ROM, and MVF models each produced values that were within less than 1% of each other. These can be seen in

APPENDIX: B. The results from the CLT and Rayleigh-Ritz models are given in Table 4 and Table 5 respectively.

Table 4: Glare3 Elastic and Shear Moduli from CLT

Laminate	Fiber Orientation	$E_x$ [MPa]	$G_{xy}$ [MPa]	$E_\alpha$ [MPa]
Glare3-2/1-0.3	0/90	59024	20547	55158
Glare3-2/1-0.3	15/-75	58052	21103	56150
Glare3-2/1-0.3	30/-60	56150	22214	58052
Glare3-2/1-0.3	45/-45	55158	22769	59024

Table 5: Critical Shear Stresses for Shear Buckling of Various Glare Layups

Laminate	Fiber Orientation	$\tau_{crit}$ [MPa]			
		t=0.2 [mm]	t=0.3 [mm]	t=0.4 [mm]	t=0.5 [mm]
Glare3-2/1	0/90	1.089	1.892	2.899	4.112
	15/-75	1.087	1.890	2.898	4.111
	30/-60	1.085	1.888	2.896	4.110
	45/-45	1.083	1.887	2.895	4.109

Table 4 shows that the shear modulus for each of the Glare3 specimens should be somewhere between 20 GPa – 23 GPa. Table 5 shows that the specimens should all buckle at about 1.9 MPa. This is too small to see in Figure 20, so Figure 21 shows a zoomed in section of Figure 20.

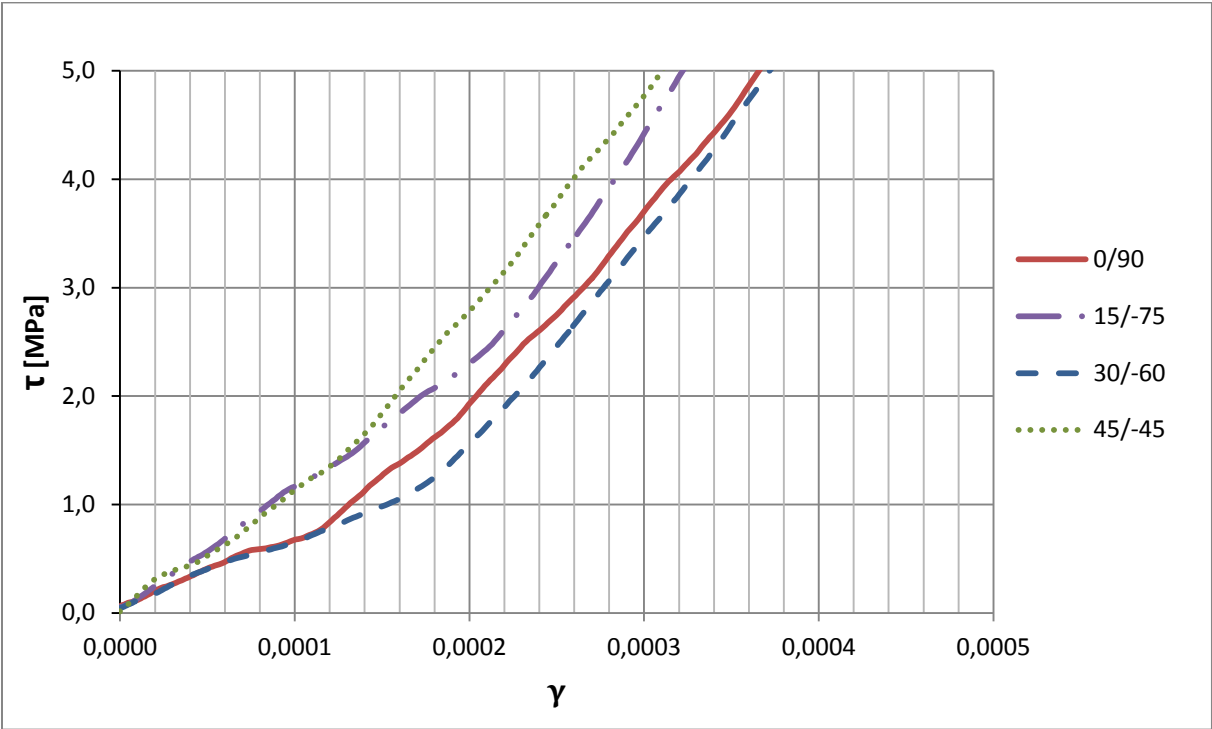


Figure 21: Shear-stress vs. shear-strain plots zoomed in to buckling stress levels.

In Figure 21 it can be seen is that the plots are at first somewhat erratic and then begin to stabilize between 2 MPa – 2.5 MPa. Below the estimated buckling stress of 1.9 MPa, the slope of the curves are less than half of the estimated shear modulus. Above 2.5 MPa, the slope of the plots have already reached the post shear-buckled stiffness shown later in Table 6. Thus, the pre-buckling shear modulus,  $G_{xy}$ , and the critical buckling shear stress,  $\tau_{crit}$ , are still not identifiable from Figure 21. However, since DIC cameras were used for the purpose of identifying  $\tau_{crit}$ , DIC images within the range of 0 MPa – 3 MPa were reviewed to try to identify the onset of buckling. Out of these images Figure 22 and Figure 23 were selected which show the out-of-plane displacements (W) for applied shear stresses of 1.9 MPa and 2.5 MPa respectively.

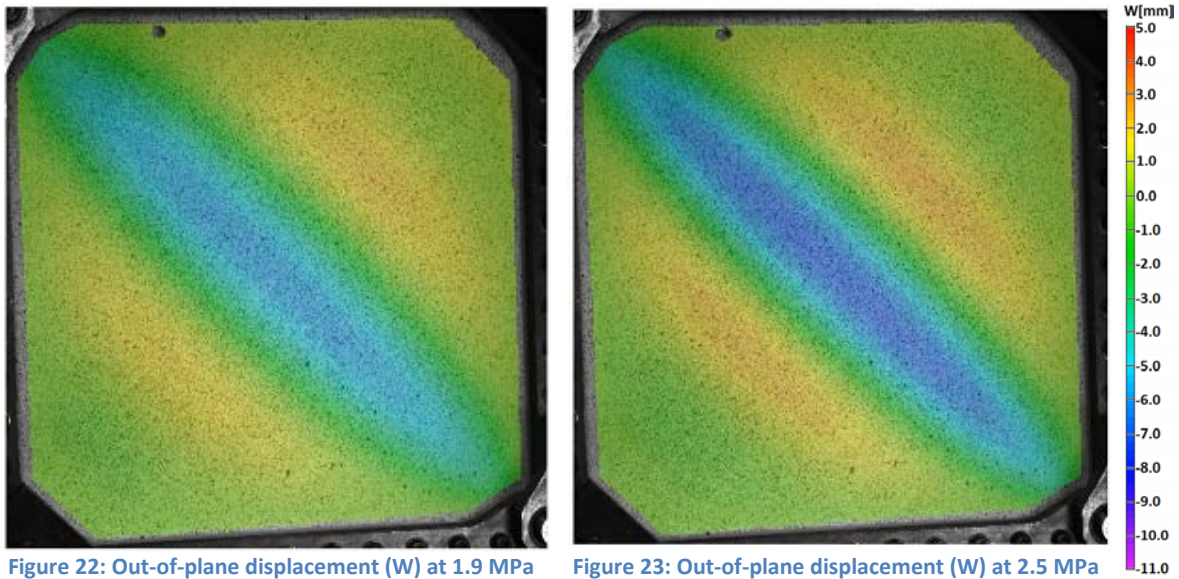


Figure 22: Out-of-plane displacement (W) at 1.9 MPa      Figure 23: Out-of-plane displacement (W) at 2.5 MPa

NOTE: The scale to the right of the figures ranges from 5 mm to –11 mm in whole number increments.

The two figures above show that at the given applied stresses the specimen has already buckled. From this it is confirmed that  $\tau_{crit}$  for the specimens tested is at most 1.9 MPa. However, at applied stresses below 1.9 MPa the DIC images show that no stable stress field had yet developed. This is because with each mechanical system, there is always a small amount of system play involved before every part begins working together. Take a set of meshing gears as an example. There is a small amount of wiggle room between the gears in which one gear will rotate slightly before it contacts the other. This causes the initial movements at the front of a system to not be in sync with the back of the system until all the wiggle room, or system play, has been removed.

In the shear tests for Glare3, the system play can be seen in Figure 21 between 0 MPa – 2.5 MPa. At 2.5 MPa, or a deformation of 0.2 mm, the system play for all the specimens has been removed and the data has stabilized. However, since the Glare3 panels should have buckled at about 1.9 MPa, this means that before the system play was removed, the panels had already buckled, which explains why the shear stress-shear strain curves in Figure 20 do not show the shear modulus, or the telltale signs of buckling.

Figure 24, which is a slightly zoomed in section of Figure 20, gives a visual summary of the shear test data.

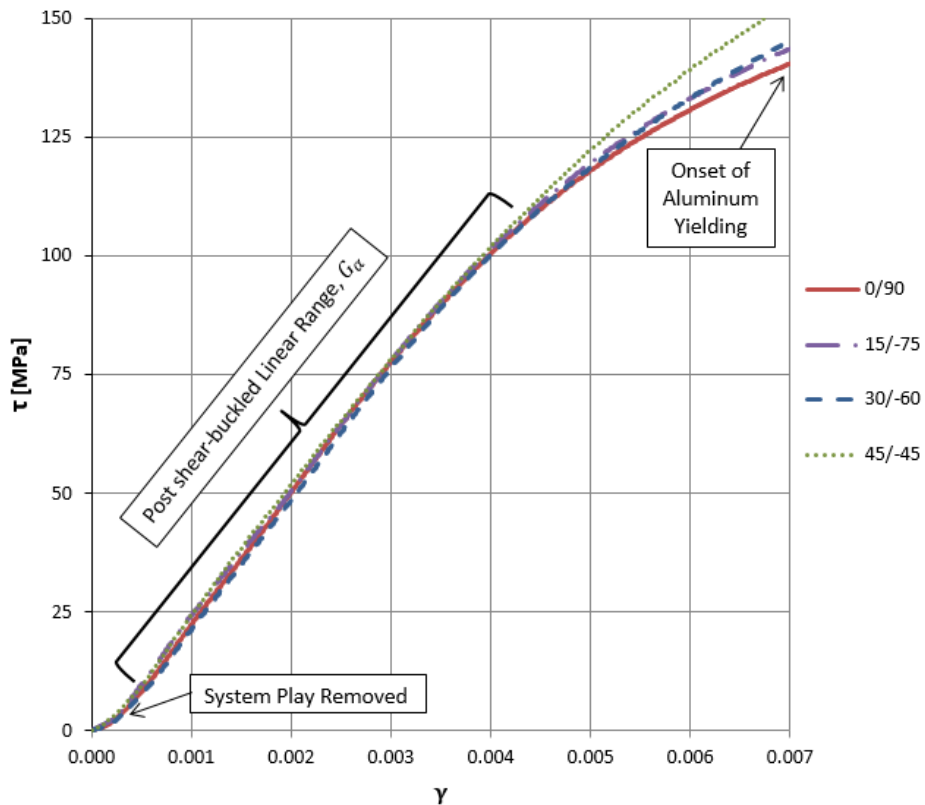


Figure 24: Glare3 shear stress-shear strain curves with labels.

The third and most important feature for this project, is the post shear-buckled stiffness,  $G_{\alpha}$ . The post shear-buckled stiffness has been represented by the notation  $G_{\alpha}$ , which is similar to the notation for the shear modulus,  $G$ . However, to refer to  $G_{\alpha}$  as a modulus would not be entirely accurate and it is important at this point that the reader understand the nature of  $G_{\alpha}$ .

One of the uses for the Kuhn method is to determine the degree to which a web, buckled in shear, resists the applied loads with either diagonal tension action,  $\tau_{DT}$ , or shear action,  $\tau_S$ . A description is available in the section labeled Shear Web Design in the

CHAPTER 2: B chapter. Figure 5 on page 12 shows a graph of how much of an applied shear stress is resisted in diagonal tension action or shear action. Once a web is in incomplete diagonal tension, the stresses and strains measured from a picture frame shear test are due to the combination of diagonal tension action and shear action. Knowing how to separate these two actions allows the engineer to predict when the material will begin to yield or fail due to tensile stresses, shear stresses, or a combination of the two depending on the application and specific loading conditions.

In materials, a modulus refers to the ratio of stresses to strains in a given direction. Thus, a tensile modulus is the ratio of tensile stresses to tensile strains when the material is under tension, and a shear modulus is the ratio of shear stresses to shear strains when the material is loaded in shear. So, according to Kuhn, even though the picture frame test apparatus only applies shear loads, in the post shear-buckled regime,  $G_\alpha$  is in fact the manifestation of two moduli working together to give a single set of data. For the purpose of this thesis, it is unnecessary to separate the two moduli since, in the post shear-buckled regime, both will always be working together. Thus,  $G_\alpha$  is simply a way of measuring the stiffness of the specimens, and it is this stiffness that this project aims to improve.

Also important to note is that the Kuhn method was developed for monolithic, isotropic metal webs. Using a non-monolithic, non-isotropic material may be outside the limitations for the Kuhn method. Therefore, the  $\tau_{DT}$  and  $\tau_S$  data presented in Table 19 on page 4 may not be accurate for FMLs. As such, it is not appropriate to attempt to calculate the values of  $\tau_{DT}$  and  $\tau_S$  since there can be no confidence as to its accuracy. The data given in Table 19 is merely intended to give the reader a better understanding of what occurs within post shear-buckled webs.

For these first shear tests, the values of  $G_\alpha$  that were measured and calculated are given below. Table 6 shows the average values of  $G_\alpha$  from the shear test data for the shear stresses between 20 MPa – 100 MPa. Table 7 shows the values calculated from Equation 11.

**Table 6:  $G_\alpha$  Results for Glare3 Test Specimens in the Range of 20 MPa – 100 MPa**

Laminate	$t_{Al}$ [mm]	Fiber Orientation	$G_\alpha$ [MPa] (Measured)
Glare3-2/1	0.3	0/90	27881
	0.3	15/-75	26869
	0.3	30/-60	27622
	0.3	45/-45	26980

**Table 7: Estimated  $G_\alpha$  values for Glare3**

Laminate	$t_{Al}$ [mm]	Fiber Orientation	$G_\alpha$ [MPa] (Estimated)
Glare3-2/1	0.3	0/90	27579
	0.3	15/-75	28075
	0.3	30/-60	29041
	0.3	45/-45	29512

Before conducting the shear tests, it was expected that the results would demonstrate that as the fibers in the material were rotated towards the shear buckling angle there would be a clear increase in  $G_{\alpha}$ . However, the trends in the estimated  $G_{\alpha}$  values were not reflected in the measured  $G_{\alpha}$  values. These values are represented graphically in Figure 25.

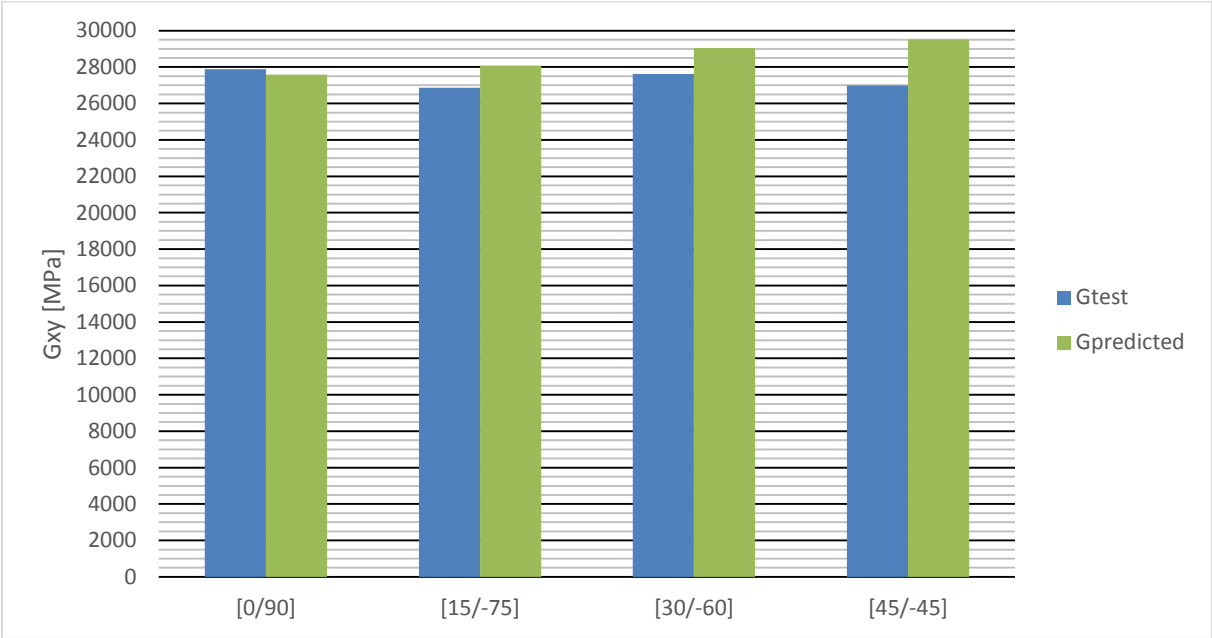


Figure 25: Estimated and measured  $G_{\alpha}$  values for Glare3

As seen in Figure 25, as the fiber angles in Glare3 are rotated from  $0^{\circ}/90^{\circ}$  to  $45^{\circ}/-45^{\circ}$ , the estimated  $G_{\alpha}$  values increased from  $27.6\text{ GPa}$  to  $29.5\text{ GPa}$ , a growth of seven percent. The measured  $G_{\alpha}$  values, on the other hand, show no definite trend and seem to simply vary between about  $27\text{ GPa}$  and  $28\text{ GPa}$ . These test results are somewhat disappointing because no definite conclusion as to the effects of off-axis fibers in Glare3 can be drawn based solely on the test results. However, as depicted in Figure 4, it is known that the modulus of elasticity ( $E$ ) is highest in the fiber direction. Thus, if Glare3 is loaded in tension in the direction of the buckling angle ( $\alpha$ ), the modulus of elasticity along  $\alpha$  ( $E_{\alpha}$ ) is highest when the fibers are also aligned with  $\alpha$ .  $\alpha$  in this case is  $45^{\circ}$ . A radial plot similar to Figure 4 is shown below as Figure 26 and depicts how  $E$  for Glare3-2/1-0.3 changes at different angles.

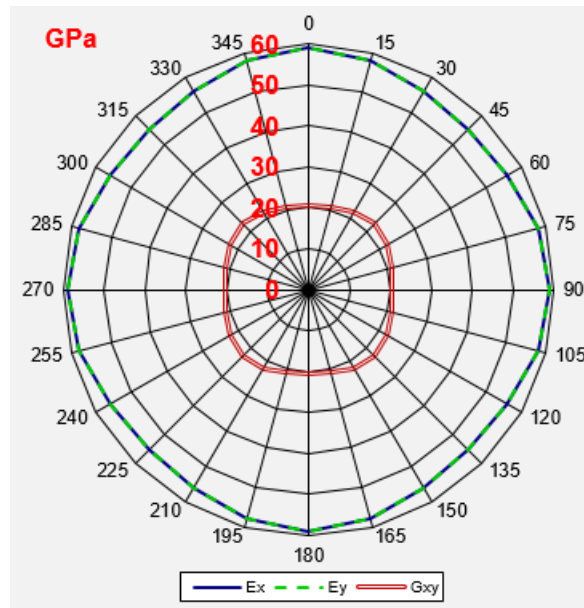


Figure 26: Radial plot of Glare3 with fibers oriented at 0° and 90°.

Figure 26 shows that the  $E$  of Glare3-2/1-0.3 is greatest in the directions of the fibers. It also shows that the shear modulus ( $G_{xy}$ ) is greatest when the fibers are rotated by 45°. The Kuhn method, declares that a web that has buckled in shear resists the loads with both diagonal tension action and shear action, and that the diagonal tension acts in the direction of the buckling angle. Thus, an increase in stiffness in either  $G_{xy}$  or  $E_{\alpha}$  should also increase  $G_{\alpha}$ . Combining the Kuhn method with the information presented in Figure 26, it is apparent that orienting the fibers in Glare3 to 45°/−45° will increase both  $G_{xy}$  and  $E_{\alpha}$ . Therefore, the stiffness of Glare3 in the post shear-buckled regime should benefit from the increase in  $G_{xy}$  and  $E_{\alpha}$  when the fibers are rotated 45°, which will cause  $G_{\alpha}$  to increase as well. However, since  $E_{\alpha}$  is inversely proportional to  $E_x$  and  $E_y$ , any increase in  $E_{\alpha}$  results in an equal decrease in  $E_x$  and  $E_y$ . For this project, decreasing  $E_x$  and  $E_y$  is not desirable because the application for this material likely involves high axial loads.

Even though it is unfortunate that the shear test results did not display the expected changes in  $G_{\alpha}$  and are inconclusive, the theory behind rotating the fibers to be aligned with  $\alpha$  is strong. Consequently, the analytical results for the changes in  $G_{\alpha}$  are relied upon for further analysis.

The final feature is the stiffness of the material after the onset of yielding. Even though a thorough analysis of the post-yielding regime is beyond the scope of this thesis, but it is important to note what is happening in that region. Yielding in the aluminum begins at about 125 MPa and it can be seen in Figure 20 that this is where the specimens really begin to differ. As the fiber angle in the specimens increased, the post-yielding stiffness increased dramatically. This is because the aluminum yields before the glass fibers, causing the fibers to begin carrying more of the applied loads. With the fibers carrying more load, the effects of fiber orientation on the shear stiffness of the material is augmented. The change in the stiffness in this regime suggests that orienting the fibers to  $\pm 45^\circ$  does in fact improve the shear stiffness of the material.

### Glare3 Fatigue Analysis

**Another important consideration to rotating fiber angles is how the fatigue crack growth rates are affected. An analysis of the fatigue crack growth rates for Glare3 at various orientations was completed using FMLGROW\_V2.0. Figure 65 through Figure 68 in**

APPENDIX: B show the fatigue crack growth rates for Glare3-2/1-0.3 as the fiber angles rotate. For convenience, two of these figures are repeated below as Figure 27 and Figure 28.

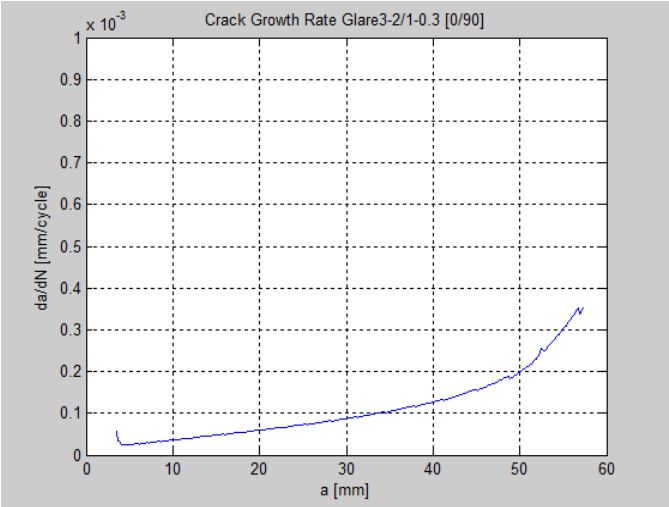


Figure 27: Crack growth life curve for Glare3-2/1-0.3 no rotation.

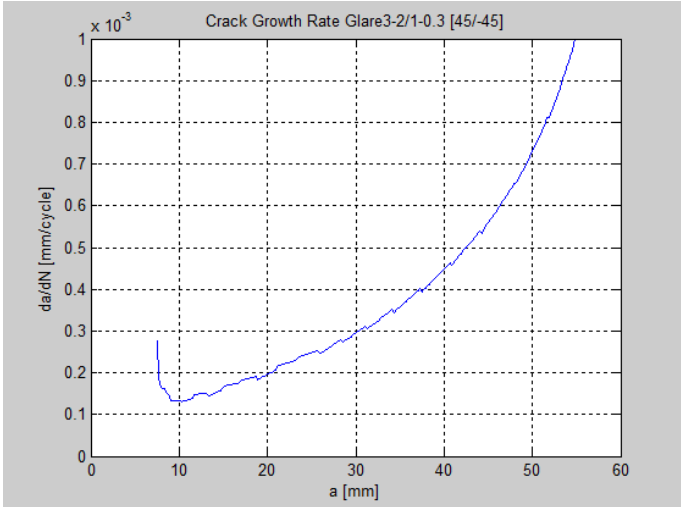


Figure 28: Crack growth life curve for Glare3-2/1-0.3 rotated 45 deg.

As can be seen in Figure 27 and Figure 28, the fatigue crack growth rate between Glare3 with no rotation and Glare3 rotated at 45° has a significant increase. An increase in the fatigue crack growth rate lowers the material’s damage tolerance. This is an undesirable effect of rotating the fibers in Glare3.

It is resolved that the effects of rotating the fibers in Glare3 to align with the shear buckling angle will cause an increase in  $G_{\alpha}$ , a decrease in  $E_x$  and  $E_y$ , and a decrease in the material’s damage tolerance. Thus, for application as a skin panel in narrow bodied aircraft where shear loads are high, simply rotating the fiber angles in Glare3 is not recommended.

**Conclusion1**

The post shear-buckled stiffness of standard Glare3 oriented at various angles, was tested in a picture frame shear apparatus, and compared against analytical models. The shear test results were inconclusive, but the analytical models predicted the post shear-buckled stiffness of Glare3 oriented at ±45° would be seven percent higher than the un-rotated standard Glare3. They also demonstrated that in the axial directions, an increase in the fiber angles resulted in a steady decrease in the axial stiffness, while the fatigue crack growth rates increased. This leads to the conclusion that simply rotating Glare3 will have more disadvantages than benefits and attempts at improving the post shear-buckled stiffness of Glare3 should involve more than a simple rotation of the existing fiber layers.



## **CHAPTER 4: Parametric Study of Glare3 Modifications for Improved Post Shear-Buckled Stiffness**

Based on the results of the previous chapter, a parametric study was designed to assess the effectiveness of modifying the Glare3-2/1 configuration for improved post shear-buckled stiffness. The goal of this study is to optimize the layup configuration that will most likely yield the greatest improvements to the post shear-buckled stiffness. The modifications investigated are: adjusting the thickness and number of the metal layers, and adding either off-axis glass or carbon fiber layers.

**This section closely resembles the analysis for the Laminate Selection Criteria found in**

## Methodology

In this study, the Metal Volume Fraction method was used to calculate  $G_\alpha$  for Glare3 laminates with varying Aluminum thickness layers in the section below, and CLT was used in the Adding Off-Axis Fibers to Glare3 section. Both methods were scripted in MatLab and looped through various parameters to find the predicted material properties of each possible layup. The MVF method looped through the used in accordance to their specifications described in the Analytical Methods section of the previous chapter.

## Adjusting the Metal Volume Fraction

Aside from changing the orientation of Glare3, the other option to improve the post shear-buckled stiffness without changing the design of Glare3 is to adjust the metal volume fraction. This adjustment can be accomplished by simply changing the thickness and/or number of the aluminum layers. Since current grades of Glare are limited to an aluminum layer thickness between  $0.2\text{ mm}$  –  $0.5\text{ mm}$ , this study investigates aluminum layer thickness within that range.

The Metal Volume Fraction (MVF) method was used to estimate the  $G_\alpha$  values given in Table 22 and was expanded to also include the corresponding values for the material's aerial density ( $\rho_{aerial}$ ). For convenience, a part of this table is shown here as Table 8.

**Table 8: MVF Method Results for  $E_\alpha$  and  $G_\alpha$  of Various Glare Layups**

Laminate	$t_{Al}$ [mm]	Fiber Orientation	$\rho_{aerial}$ [kg/m <sup>2</sup> ]	MVF [%]	$G_\alpha$ [MPa]
Glare3-2/1	0.2	0/90	1.619	60.6%	24971
	0.3	0/90	2.175	69.8%	27536
	0.4	0/90	2.731	75.5%	29133
	0.5	0/90	3.287	79.4%	30223

Table 8 shows that an increase in the thickness of the aluminum layers ( $t_{Al}$ ) causes a clear increase in each of the three material properties listed in the three columns on the right. Noting the extent to which each of them increase in relation to each other is important for evaluating the benefits and disadvantages of changing the metal thickness. Using the data in Table 8 and setting the values for  $t_{Al} = 0.2\text{ mm}$  as the baseline, Figure 29 compares the properties for  $t_{Al} = 0.3\text{ mm} - 0.5\text{ mm}$  as a percent of the baseline values.

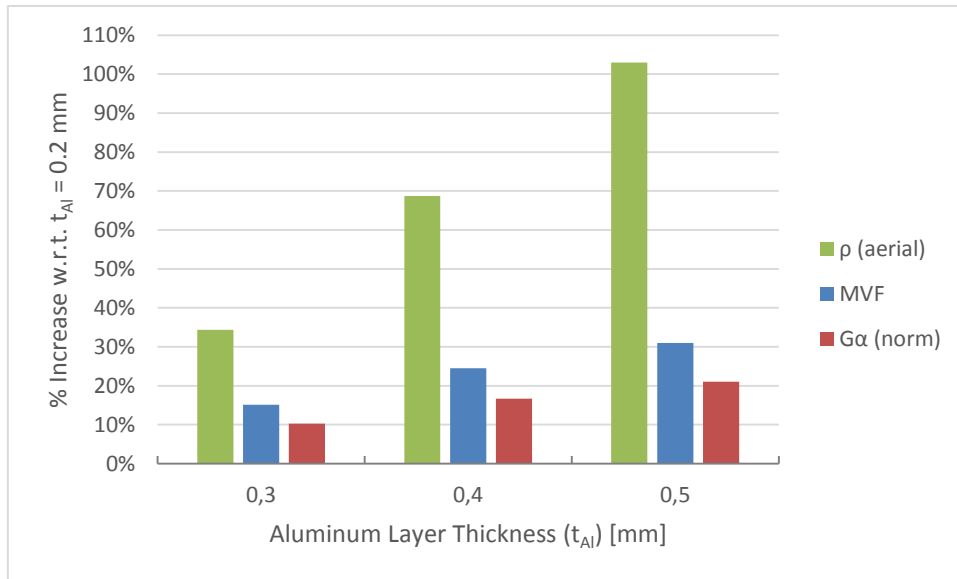


Figure 29: Percent increase in properties based on  $t_{Al} = 0.2$  mm.

The graphical representation in Figure 29 of how the properties in Glare3 change as  $t_{Al}$  increases shows that  $\rho_{aerial}$  increases very rapidly (up to 103%), while  $G_\alpha$  increases more slowly (up to 21%). Even though a 21% increase in  $G_\alpha$  is significant, the benefits of this increase are lost in the disadvantage of the high  $\rho_{aerial}$ . This can be demonstrated by normalizing the  $G_\alpha$  values with their respective  $\rho_{aerial}$  values, and then looking at how it compares as a percentage of the baseline values. Equation 14 demonstrates how this is done.

Equation 14

$$\frac{\left(\frac{G_{\alpha 0.3}}{\rho_{aerial 0.3}}\right)}{\left(\frac{G_{\alpha 0.2}}{\rho_{aerial 0.2}}\right)}$$

Figure 30 shows the results of Equation 14 for  $t_{Al} = 0.3$  mm – 0.5 mm.

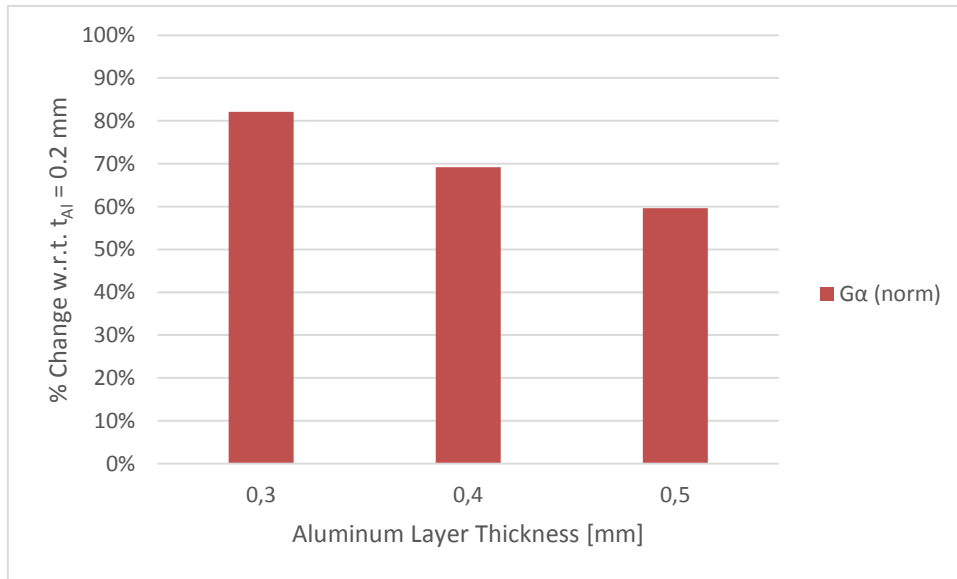


Figure 30: Normalized  $G_\alpha$  values w.r.t. the baseline value.

The normalized  $G_\alpha$  values in Figure 30 clearly show that any increase in  $t_{Al}$  will not yield any benefits for the increase in  $G_\alpha$  because  $\rho_{aerial}$  increases too rapidly. From this perspective, attempts at improving  $G_\alpha$  should not come from increasing the MVF, but from some other modification.

Because stiffness and damage tolerance should always be considered together when dealing with Glare, the fatigue crack growth rates were also calculated. The Crack growth life curves for these can be seen in Figure 61 through Figure 64. Figure 61 and Figure 64 are repeated here as Figure 31 and Figure 32 for convenience.

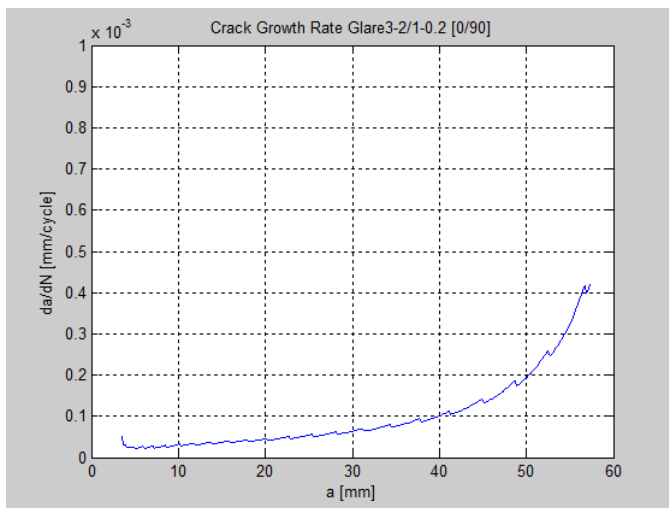


Figure 31: Crack growth life curve for Glare3-2/1-0.2.

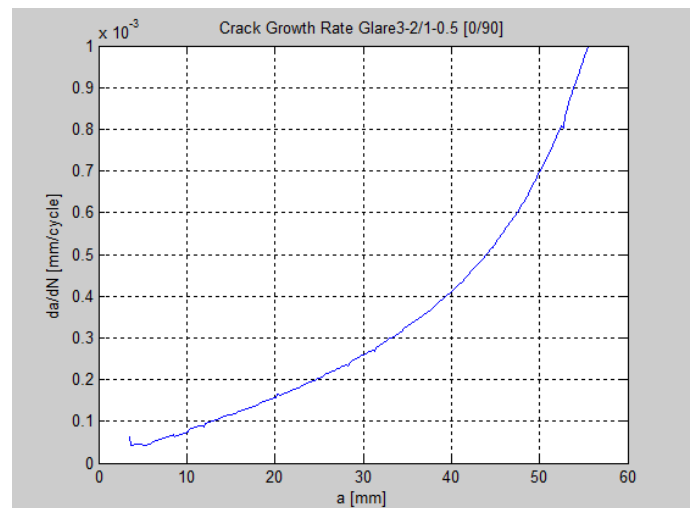


Figure 32: Crack growth life curve for Glare3-2/1-0.5.

Figure 31 and Figure 32 show that the fatigue crack growth rates increase quickly with thicker aluminum layers. This was previously discussed in the Review of Glare Components section in the

CHAPTER 2: B chapter. In addition to this, it was also determined that simply increasing the number of aluminum layers had a negligible effect on the fatigue crack growth rates and caused a slight decrease in stiffness due to the decrease in the MVF.

From the analysis of the effects of increasing the MVF in Glare3, it was shown that  $G_{\alpha}$  will increase, but it is not beneficial in terms of weight gain and damage tolerance. Also, simply increasing the number of metal layers has very little to no effect on the stiffness and damage tolerance.

## **Conclusion 2**

The aluminum in Glare materials is responsible for most of the material's stiffness, and is the main driving factor. Thus, increasing the metal volume fraction (MVF) of Glare3 will rapidly increase the post shear-buckled stiffness. However, a sharp increase in the MVF only yields a small increase in stiffness, and the aerial density goes up five times faster than the stiffness does. Also, the increased thickness of the aluminum layers decreases the damage tolerance. Thus, it is concluded that for purposes of this thesis, increasing the material's MVF will not yield desirable results and should be avoided.

## **Adding Off-Axis Fibers to Glare3**

The last option considered to improve the post shear-buckled stiffness is by adding off-axis fiber layers. In the previous two chapters, it was shown that fibers oriented at  $\pm 45^\circ$  are best for improving the shear stiffness, and that in the post shear-buckled regime, fibers aligned with the buckling angle,  $\alpha$  (which in this case is  $45^\circ$ ) are best for improving the stiffness in the  $\alpha$  direction. Based off this, an initial layup of  $[Al/0/45/90/Al]$  was proposed as a possible solution. This section contains a brief discussion of how the modified Glare3 design was optimized for post shear-buckled stiffness by adding off-axis fiber layers. A more in-depth discussion how the final optimized layup configuration was chosen can be found in the Laminate Selection Criteria section in

APPENDIX: A.

Glare materials are a compromise between stiffness and damage tolerance. The glass fibers in Glare are less stiff than the aluminum, and the result of combining the glass fibers with the aluminum is a material with an intermediate stiffness. However, the fibers also decrease the fatigue crack growth rate in the aluminum through fiber bridging. Thus, it can be expected that by adding an additional glass fiber layer, regardless of orientation, the stiffness of the modified Glare material as well as its fatigue crack growth rates should decrease. Since the additional fibers in this case are oriented at 45°, the stiffness in that direction will not decrease as much as in the other directions, and fatigue crack growth perpendicular to the fibers should be significantly reduced.

While there may be applications for such a modified Glare material, the goal of this thesis is to identify a modified Glare material with improved post shear-buckled performance. To achieve this, any added off-axis fiber layers should have a higher stiffness than Glare3 does in the buckling direction ( $E_\alpha$ ). Carbon fibers are significantly stiffer than Glare3 and should cause a modified Glare3 material to be stiffer than Glare3 as well as decrease the fatigue crack growth rate. However, because adding fiber layers will also change the material's density, to make a fair comparison of Glare3 with a modified Glare3, the stiffness of the materials should be normalized with respect to density. Table 9 and Table 10 gives the aerial density, MVF, and stiffness data obtained through CLT for laminates with  $t_{Al} = 0.2 \text{ mm} - 0.5 \text{ mm}$  and the number of off-axis plies ranging from one to three for glass and carbon fibers respectively. Figure 33 and Figure 34 plot the normalized  $G_\alpha$  values.

Table 9: Stiffness Data for Glare3, Modified with Off-Axis S2 Glass Fibers

Laminate	$t_{Al}$ [mm]	Layup (45=glass)	$\rho_{aerial}$ [kg/m <sup>2</sup> ]	MVF [%]	$E_\alpha$ [MPa]	$G_\alpha$ [MPa]	$(G_\alpha/\rho) / (G_{0.3}/\rho_{0.3})$
Glare3-2/1	0.3	0/90	2.175	69.8%	55158	27579	100.0%
Glare3S-2/1	0.2	0/45/90	1.873	50.6%	49860	24930	105.0%
Glare3S-2/1	0.3	0/45/90	2.429	60.6%	54336	27168	88.2%
Glare3S-2/1	0.4	0/45/90	2.985	67.2%	57306	28653	75.7%
Glare3S-2/1	0.5	0/45/90	3.541	71.9%	59422	29711	66.2%
Glare3S-2/1	0.3	0/45 <sub>2</sub> /90	2.682	53.6%	53705	26852.5	79.0%
Glare3S-2/1	0.4	0/45 <sub>2</sub> /90	3.238	60.6%	56479	28239.5	68.8%
Glare3S-2/1	0.5	0/45 <sub>2</sub> /90	3.794	65.8%	58522	29261	60.8%
Glare3S-2/1	0.3	0/45 <sub>3</sub> /90	2.936	48.0%	53206	26603	71.5%
Glare3S-2/1	0.4	0/45 <sub>3</sub> /90	3.492	55.2%	55799	27899.5	63.0%
Glare3S-2/1	0.5	0/45 <sub>3</sub> /90	4.048	60.6%	57764	28882	56.3%

Table 10: Stiffness Data for Glare3, Modified with Off-Axis T700 Carbon Fibers

Laminate	$t_{Al}$ [mm]	Layup (45=carbon)	$\rho_{aerial}$ [kg/m <sup>2</sup> ]	MVF [%]	$E_\alpha$ [MPa]	$G_\alpha$ [MPa]	$(G_\alpha/\rho) / (G_{0.3}/\rho_{0.3})$
Glare3S-2/1	0.2	0/45/90	1.853	50.6%	63700	31850	135.6%
Glare3S-2/1	0.3	0/45/90	2.409	60.6%	65380	32690	107.0%
Glare3S-2/1	0.4	0/45/90	2.965	67.2%	66494	33247	88.4%

Glare3S-2/1	0.5	0/45/90	3.521	71.9%	67288	33644	75.4%
Glare3S-2/1	0.3	0/45 <sub>2</sub> /90	2.643	53.6%	73228	36614	109.3%
Glare3S-2/1	0.4	0/45 <sub>2</sub> /90	3.199	60.6%	73044	36522	90.0%
Glare3S-2/1	0.5	0/45 <sub>2</sub> /90	3.755	65.8%	72907	36453.5	76.6%
Glare3S-2/1	0.3	0/45 <sub>3</sub> /90	2.877	48.0%	79445	39722.5	108.9%
Glare3S-2/1	0.4	0/45 <sub>3</sub> /90	3.433	55.2%	78419	39209.5	90.1%
Glare3S-2/1	0.5	0/45 <sub>3</sub> /90	3.989	60.6%	77642	38821	76.8%

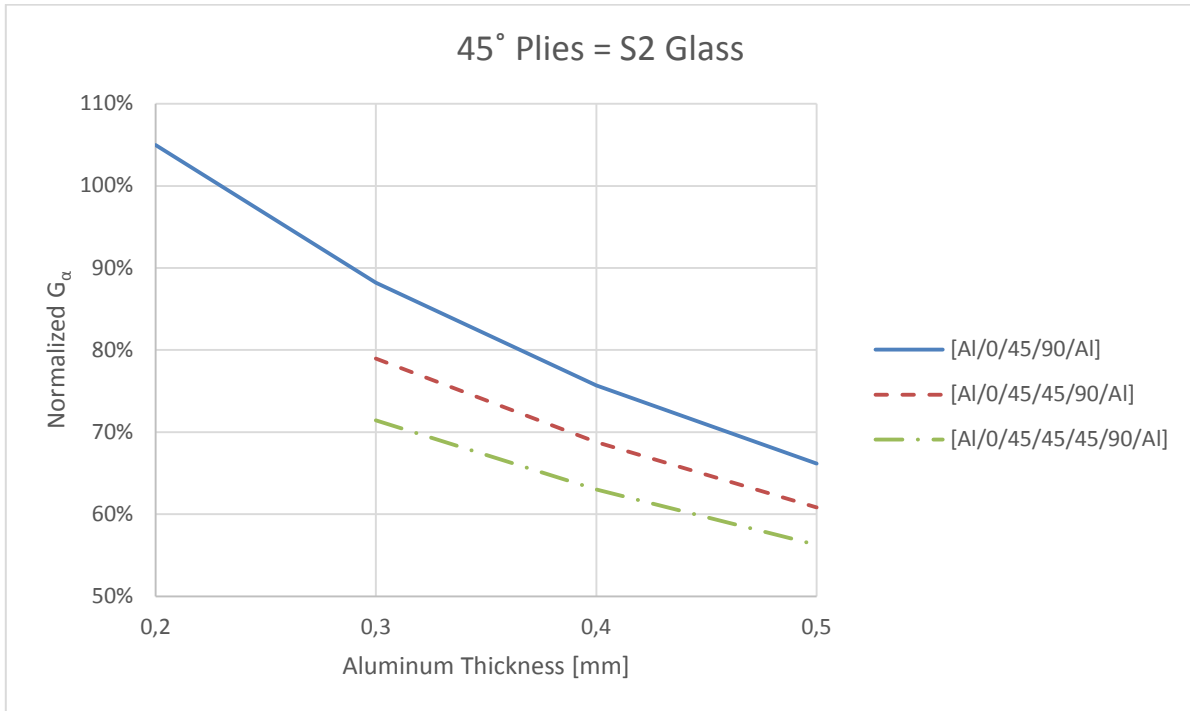


Figure 33: Normalized  $G_{\alpha}$  for various potential modified Glare3 layups with off-axis S2 glass fibers.

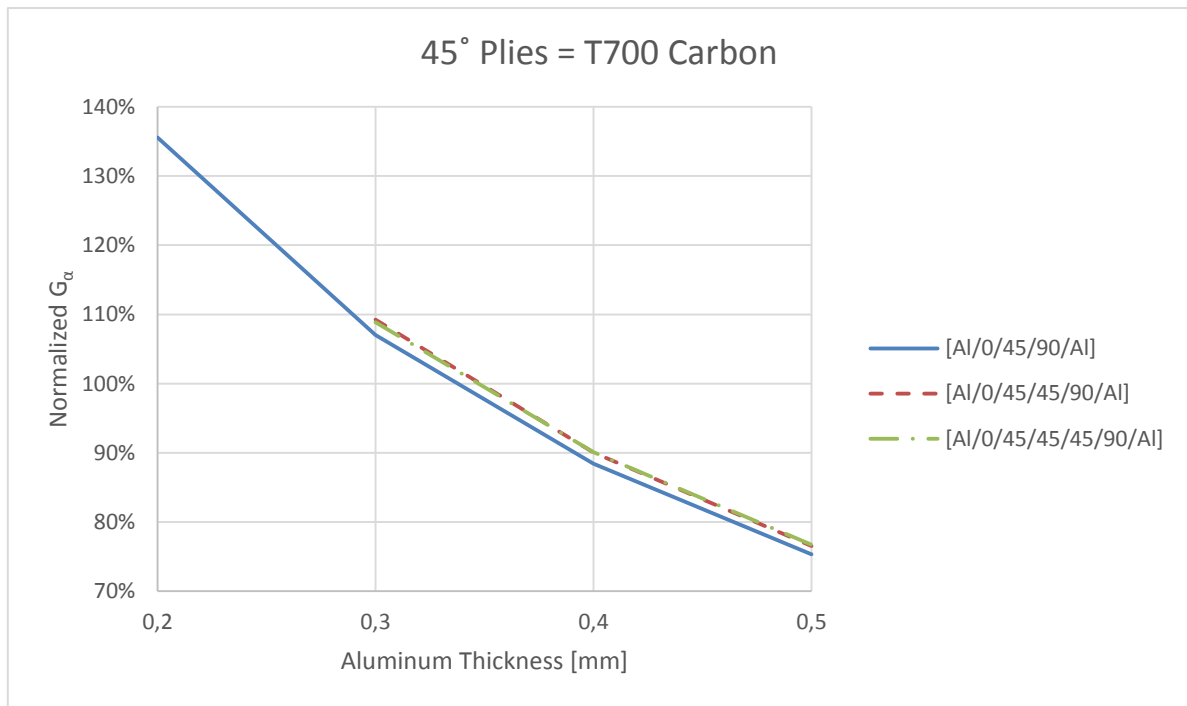


Figure 34: Normalized  $G_{\alpha}$  for various potential modified Glare3 layups with off-axis T700 carbon fibers.

Note: Only layups that have an MVF content within the valid range of 0.45% - 0.85% are included in the figures and tables above.

Figure 33 and **Error! Reference source not found.** show how the relative stiffness of a modified Glare3 changes with respect to the standard Glare3-2/1-0.3 material, which is serving as the baseline material for comparisons. These figures, both show a downward trend in the normalized  $G_{\alpha}$  as the thickness of the aluminum layers increases. This is because the aluminum is not only stiffer than Glare3, but it is also denser. Which means that any increase in its thickness has a significant effect on the Glare material and quickly diminishes the effectiveness of added off-axis fibers. Figure 33 also shows that each additional off-axis glass fiber layer only decreases the normalized  $G_{\alpha}$  values. As mentioned previously, this effect was anticipated. In fact, the only way to increase the normalized  $G_{\alpha}$  values of Glare3 by adding off-axis glass fibers, is to decrease the thickness of the aluminum layers. Otherwise, the glass off-axis fibers do not improve the normalized  $G_{\alpha}$ .

**Error! Reference source not found.** shows that there is very little difference in the normalized  $G_{\alpha}$  values for each added off-axis carbon fiber layer. It also shows rapid diminishing returns as the thickness of the aluminum layers increases. This means that, if Glare3-2/1-0.3 were only modified with a single off-axis carbon layer, the normalized  $G_{\alpha}$  value would be higher. This is a good result, but  $G_{\alpha}$  is just one way of measuring material stiffness. Another way to measure stiffness is geometrically, using the spring constant,  $K$ .

As with  $G_{\alpha}$ , after  $K$  has been calculated it should be normalized with the aerial density before comparing the different materials. Table 11 shows the normalized  $K$  values as a percentage of standard Glare3. The data presented in Table 11 is shown graphically in Figure 35.

Table 11: Normalized values of  $G_\alpha$  and  $K$  as a Percentage of Glare3 [carbon]

Laminate	$t_{Al}$ [mm]	Fiber Orientation	$(K/\rho) / (K_{0.3}/\rho_{0.3})$
Glare3s-2/1	0.2	0/45 <sub>g</sub> /90	96.3%
Glare3s-2/1	0.3	0/45 <sub>g</sub> /90	101.5%
Glare3s-2/1	0.4	0/45 <sub>g</sub> /90	104.8%
Glare3s-2/1	0.5	0/45 <sub>g</sub> /90	107.1%
Glare3s-2/1	0.2	0/45 <sub>c</sub> /90	124.6%
Glare3s-2/1	0.3	0/45 <sub>c</sub> /90	123.3%
Glare3s-2/1	0.4	0/45 <sub>c</sub> /90	122.5%
Glare3s-2/1	0.5	0/45 <sub>c</sub> /90	122.0%

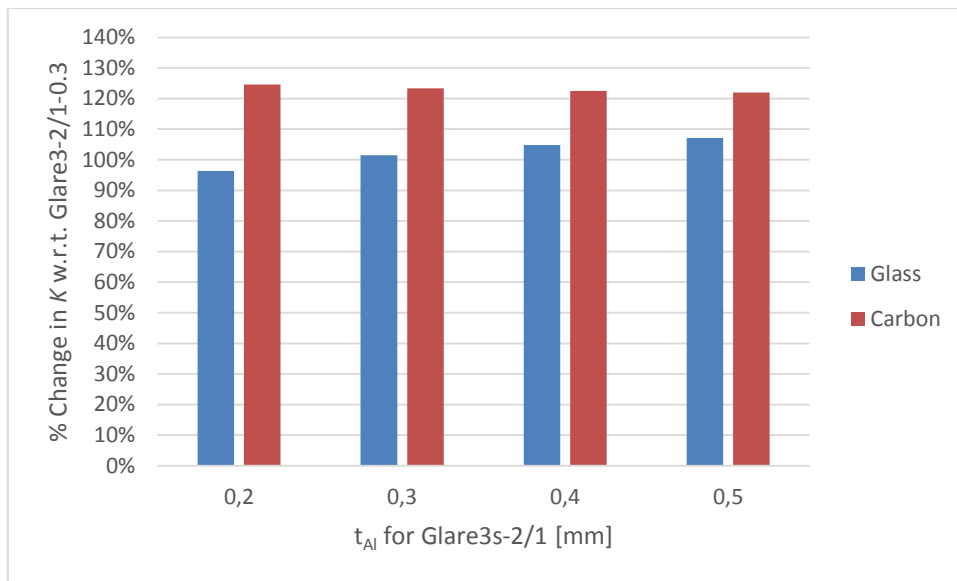


Figure 35: Normalized values of  $K$  as a percentage of Glare3 values.

Figure 35 shows a steady increase as  $t_{Al}$  gets bigger. This is because  $K$  uses forces instead of stresses, and any added material will always cause  $K$  to rise regardless of its  $G_\alpha$ , which means  $K$  gives another perspective on stiffness that can be very helpful. In this case, the glass fibers begin to increase  $K$  after  $t_{Al} = 0.3 \text{ mm}$ , but only just slightly, while the carbon fibers yield about a 22% increase for all  $t_{Al}$  thicknesses. From the perspective of  $K$ , adding off-axis glass fibers only show benefit for  $t_{Al} \leq 0.4 \text{ mm}$ , while off-axis carbon fibers will be beneficial for all  $t_{Al}$  values. However, there are other factors to consider before using carbon fibers.

When carbon fiber and aluminum come into contact, galvanic corrosion can occur unless they are well insulated. This is a serious disadvantage. Careful precautions need to be taken to prevent this from happening. These precautions such as insulating fasteners can add weight to a structure quickly, and increase the cost of manufacturing. Although using off-axis carbon fibers in the buckling direction should accomplish the goal of discovering how to improve the post-shear buckled stiffness of Glare3, it is important to analyze how the modified Glare3 will affect the design of the structure it is used in.

### Conclusion 3

Modifying Glare3 to include off-axis fibers which are in-line with the shear buckling angle may increase or decrease the material's post shear-buckled stiffness depending upon the type of fibers used. Glass fibers are less stiff than Glare3 and using them as off-axis fibers will decrease the material's post shear-buckled stiffness. Carbon fibers are much stiffer than Glare3 and using them as off-axis fibers will increase the material's geometric stiffness and should also increase its post shear-buckled stiffness. However, the addition of a carbon fiber layer comes with the potential for galvanic corrosion, which requires additional measures to mitigate. In terms of increasing the post shear-buckled stiffness of Glare3-2/1-0.3, adding a single off-axis fiber layer appears to produce the largest benefits. This results in an optimized layup of  $[Al/0/45/90/Al]$ , when the off-axis layer is carbon fiber.



## CHAPTER 5: Post Shear-Buckled Stiffness and Damage Tolerance of Modified Glare3

Chapter 3 and chapter 4 addressed the effects of rotating Glare3, adjusting the thickness of the aluminum layers, and adding off-axis layers of either glass or carbon fibers. At the end of chapter 4, the optimized layup  $[Al/0/45/90/Al]$  was given. This layup should show the most improvement to the post shear-buckled stiffness. To validate the conclusions of chapter 4, two shear specimens were made with the optimized layup: one with an off-axis glass fiber ply, and the other with a carbon fiber off-axis ply. Two fatigue specimens with the same layups were also made. This chapter evaluates these layups analytically and mechanically through shear and fatigue tests to discover its post shear-buckled behavior and its damage tolerance.

### Methodology

#### Manufacturing

The shear specimens for these tests were manufactured in accordance with the manufacturing process described in Chapter 3. The fatigue specimens were laid up and cured in a similar manner to the shear specimens, but were cut to different dimension. The materials this chapter investigates are listed below. The two specimens of each material made, one for shear and one for fatigue are given below.

Shear specimens:

- $[Al_{0.3}/0/-45_g/90/Al_{0.3}] \times 1$
- $[Al_{0.3}/0/-45_c/90/Al_{0.3}] \times 1$

Fatigue specimens:

- $[Al_{0.3}/0/-45_g/90/Al_{0.3}] \times 1$
- $[Al_{0.3}/0/-45_c/90/Al_{0.3}] \times 1$

*Note: The off-axis plies are at  $-45^\circ$  instead of at  $45^\circ$  due to an error during the layup process. However, either orientation can be used and will give the same results if the loads are correctly applied. Care was taken during testing to make sure this was the case.*

The fatigue specimens were cut to have a width of 140 mm wide and a height of 340 mm. For the mechanical grips, 30 mm tabs were placed on top and bottom the of specimens. This gave them a total gauge area of 140 mm  $\times$  280 mm. Fatigue specimens which are longer along the fatigue axis allow the far field stresses in the specimen to even out and become more uniform surrounding the crack area. The uniformity helps the fatigue crack to grow steadily without sudden changes due to higher or lower stress areas.

In the center of the fatigue specimens a 3 mm hole was drilled and a fine saw was used to cut a 2 mm slit on either side of the hole. This gave an initial crack length ( $a$ ) of 3.5 mm. Figure 36 is a drawing of the fatigue specimen dimensioning and tolerances.

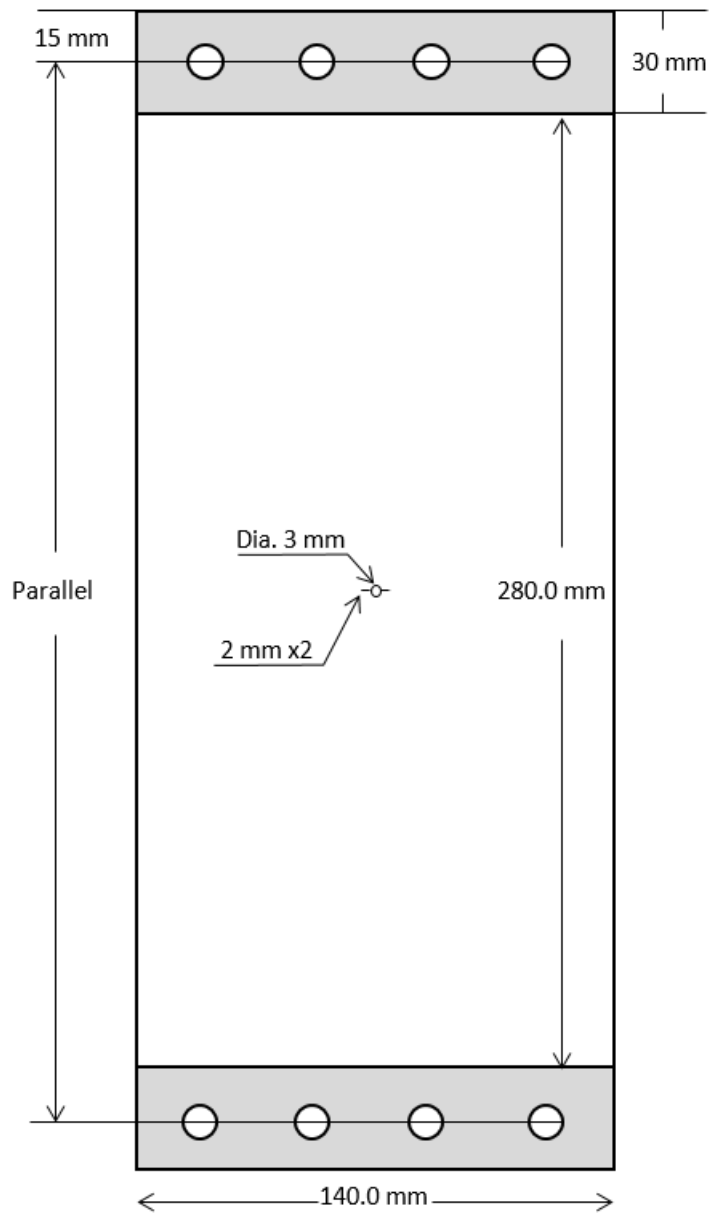


Figure 36: Fatigue specimen dimensions and tolerances.

Figure 37 shows the final product before testing.



Figure 37: Prepared fatigue specimen

### Fatigue Test Method

The fatigue specimens were attached to a Zwick 810 fatigue machine with a maximum load capacity of 100kN with the aid of mechanical clamps. Table 12 below is a matrix with the testing parameters.

Table 12: Fatigue Test Matrix

Specimen	$[Al_{0.3}/0/-45_g/90/Al_{0.3}]$	$[Al_{0.3}/0/-45_c/90/Al_{0.3}]$
Smax	120 MPa	120 MPa
R ratio	0.1	0.1
Fatigue rate	10 Hz	10 Hz
Measurement rate	1/2000 cycles	1/2000 cycles
Maximum cycles	300k	300k

Millimeter paper was attached to each specimen and after every 2000 cycles, the machine would pause at the maximum stress level (Smax) and take a picture of the front and back sides of the

specimen. Using the images taken, the crack lengths were measured and plotted to show the fatigue crack growth rate. Figure shows the fatigue machine with a fatigue specimen loaded and ready for testing.



Figure 38: Fatigue specimen loaded in a Zwick 810 100kN fatigue machine.

## Stiffness Results & Discussion

As discussed in the previous chapter, the post shear-buckled stiffness of the modified Glare3 materials are only expected to improve if the off-axis fibers are stiffer than standard Glare3. With the two specimens that were manufactured, one with off-axis glass fibers and the other with off-axis carbon fibers, only the latter is expected to show improvements. The raw data obtained from the shear tests came in the form of a force-deformation curve, which is shown in Figure 39.

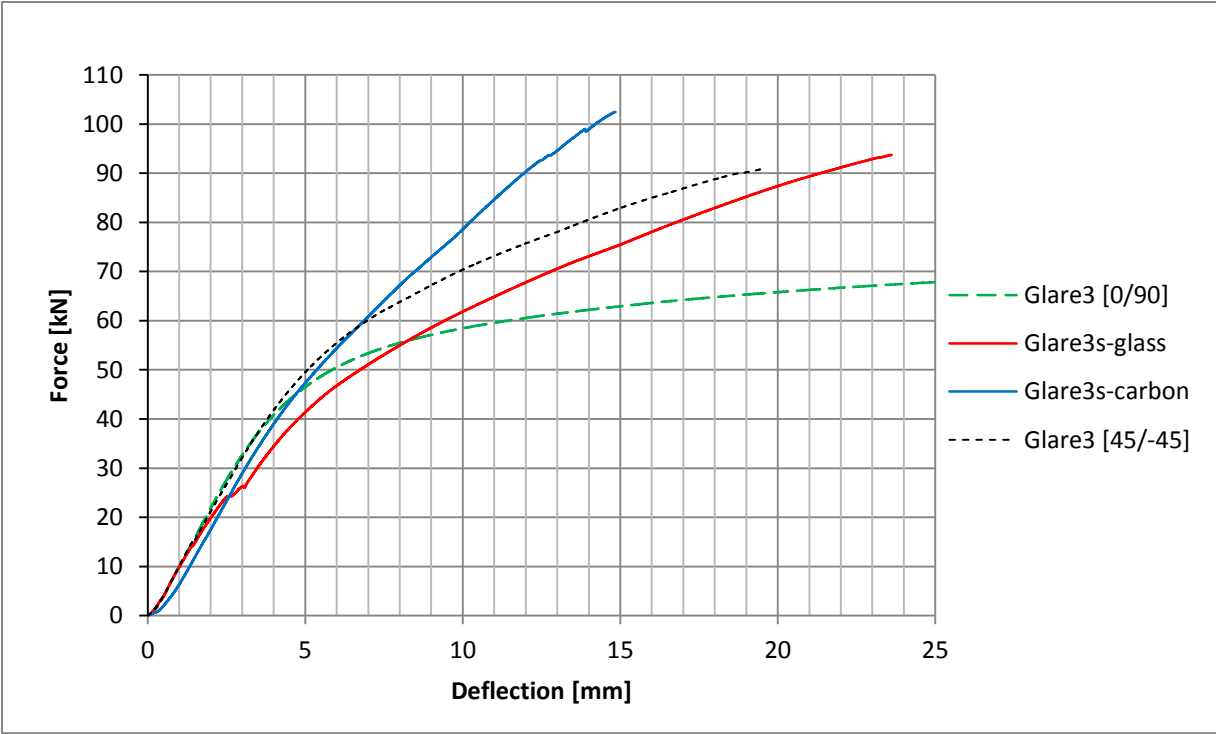


Figure 39: Force-deflection curves for standard and modified Glare3.

Force-deflection curves show the geometric stiffness of a material, which is independent of material thicknesses. Since the standard Glare3 specimens have a different thickness than the modified Glare3 specimens, force-deflection curves provide a good base for material comparisons. Figure 39 shows that the initial stiffness, up until about 40 kN is nearly the same for all specimens. During testing of the Glare3s-glass specimen, an audible pop sound occurred as the test past 26 kN. A noticeable divot in the curve in Figure 39, appears there. It is unknown what caused this popping noise, but afterward, the slope of the curve continued at the same rate. If the specimen had broken, there should have been an immediate decrease in stiffness. However, since that did not happen, this may indicate that the specimen slipped inside the grips. After the onset of yielding, the slope of the Glare3s-glass curve matched that of the Glare3 [45/-45] curve. Both specimens had two aluminum layers of the same thickness and a single glass ply oriented with the buckling angle.

The shear stress-shear strain data that was converted from the force-deflection data is plotted in Figure 40.

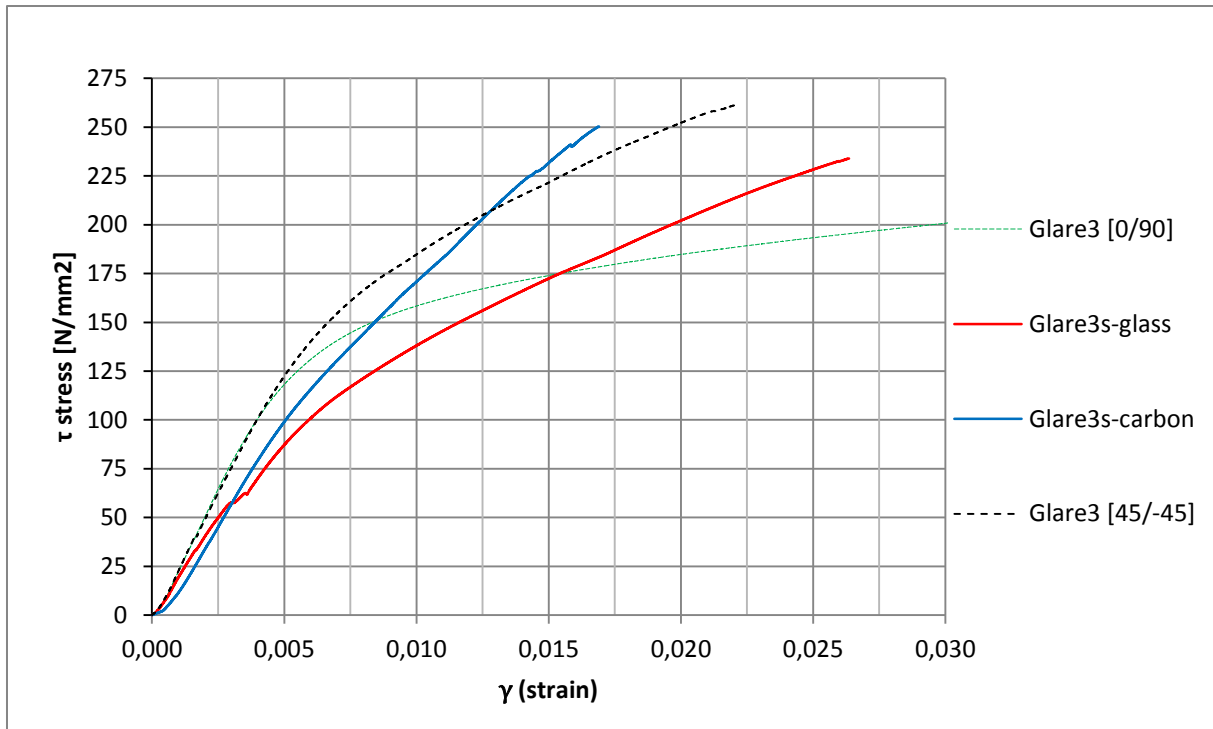


Figure 40: Shear stress-shear strain curves for standard and modified Glare3 layouts.

The Glare3s-carbon specimen shows a considerable increase in stiffness after yielding, which was expected. However, previous to yielding, the post shear-buckled stiffness of the specimen is less than those of standard Glare3. According to the predictions,  $G_{\alpha}$  should have been higher. Table 13 and Table 14 show the measured and predicted values of  $G_{\alpha}$  respectively.

Table 13: Measured  $G_{\alpha}$  Values for Standard and Modified Glare3 Layouts

Laminate	Fiber Layup	$\rho_{aerial}$ [kg/m <sup>2</sup> ]	MVF [%]	$G_{\alpha}$ [MPa]
Glare3-2/1-0.3	0/90	2.175	69.8%	27914
Glare3s-2/1-0.3	0/-45 <sub>g</sub> /90	2.429	60.6%	20917
Glare3s-2/1-0.3	0/-45 <sub>d</sub> /90	2.409	60.6%	23167

Table 14: Predicted  $G_{\alpha}$  Values for Standard and Modified Glare3 Layouts

Laminate	Fiber Layup	$\rho_{aerial}$ [kg/m <sup>2</sup> ]	MVF [%]	$G_{\alpha}$ [MPa]
Glare3-2/1-0.3	0/90	2.175	69.8%	27579
Glare3s-2/1-0.3	0/-45 <sub>g</sub> /90	2.429	60.6%	27168
Glare3s-2/1-0.3	0/-45 <sub>d</sub> /90	2.409	60.6%	34160

A comparison of the data in Table 13 and Table 14 reveals that  $G_{\alpha}$  of the Glare3s-glass and Glare3s-carbon specimens were respectively about 77% and 68% of what was predicted. Unfortunately,

without more testing, it is not known what the reasons are for these unexpected results. However, two theories which may explain the results are given below.

1. As a rule of thumb, a testing apparatus should be at least ten times stiffer than the test specimen. The picture frame used met this criterion, yet since no applicable ASTM standards for the picture frame shear test method are available, it is difficult to say whether the picture frame was indeed sufficient. If a picture frame test apparatus is not stiff enough to apply a uniform shear load on the specimens, stress concentrations in the specimen may build causing it to strain more and yield sooner. To some extent, this phenomenon already occurs due to the buckles in the material and (because only average stresses and strains are measured) the effect is a smoother transition in the stress-strain curve from pre- to post-yielding. This smoothing is already visible in the shear stress-shear strain figures given in this thesis. However, a non-uniform loading, caused by bending of the picture frame, would only cause this phenomenon to be made manifest in more abundance.
2. The analytical models used were not specifically designed to make predictions in the post shear-buckled regime, and most were not designed to accommodate Glare materials with off-axis fibers. It is known that in the post shear-buckled regime, both diagonal tension action and shear action are resisting the applied shear loads. Here it was assumed, due to the high buckling ratio, that vast majority of the applied loads would be resisted through diagonal tension action. This is what allowed the use of the CLT, ROM, and MVF methods for making post shear-buckled stiffness predictions.

As such, it is possible that the assumptions made in using the models may not have been appropriate for the analysis of modified Glare3 materials. However, part of the reason for the shear tests of standard Glare3 in chapter 3 was to determine whether the analytical models would be sufficient for a modified Glare3. From the study in chapter 3 the analytical results and test results for standard Glare 3 were close enough that it was decided that the analytical models could fare well enough with the modified Glare3 specimens.

As it seems with all the shear tests during this thesis, the best indicator as to the effectiveness of off-axis fibers in improving stiffness is in the post-yielding regime. Although that regime is beyond the scope of this thesis, it does provide some valuable insight. The stiffness of all the tested panels in that regime follow a logical pattern of increasing stiffness as fibers are oriented more toward the buckling angle and as the stiffness of the off-axis plies were increased by changing to carbon.

## **Fatigue Results & Discussion**

As discussed in the previous chapter, the fatigue crack growth rates of the modified Glare3 materials were expected to remain nearly the same compared to standard Glare3. Unlike the shear tests of modified Glare3 specimens, the fatigue test results from the two modified fatigue specimens do match up fairly well with the predictions. Figure 41 gives the fatigue crack growth curve for unrotated standard Glare3-2/1/0.3. Figure 42 and Figure 43 are the predicted fatigue crack growth curves for the two modified Glare3 specimens. Each figure was obtained from FMLGROW\_V2.0.

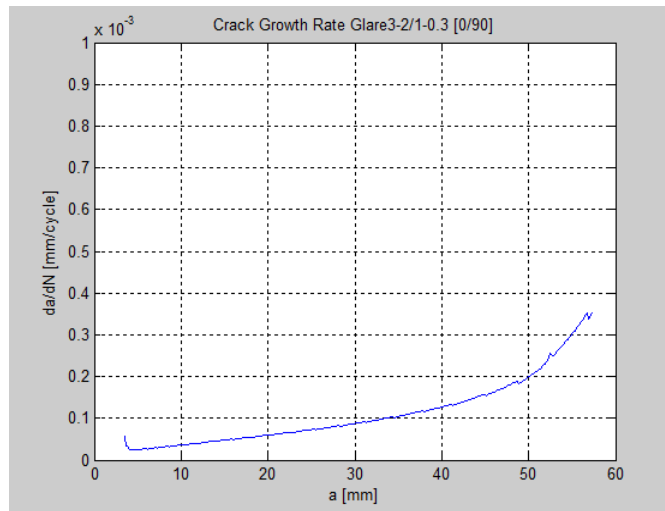


Figure 41: Crack growth life curve for Glare3-2/1-0.3 no rotation.

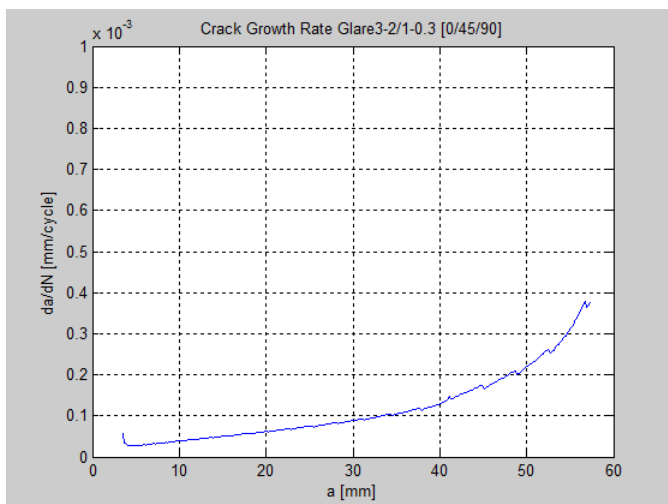


Figure 42: Crack growth life curve for Glare3s-2/1-0.3 (glass).

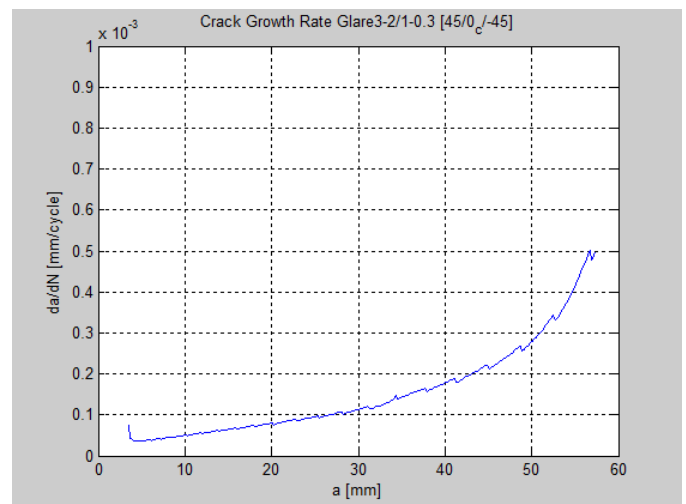


Figure 43: Crack growth life curve for Glare3s-2/1-0.3 (carbon).

Figure 41 and Figure 42 are nearly identical while Figure 43 shows a slightly higher fatigue crack growth rate. Figure 44 and Figure 45 show the results from testing together with their predictions.

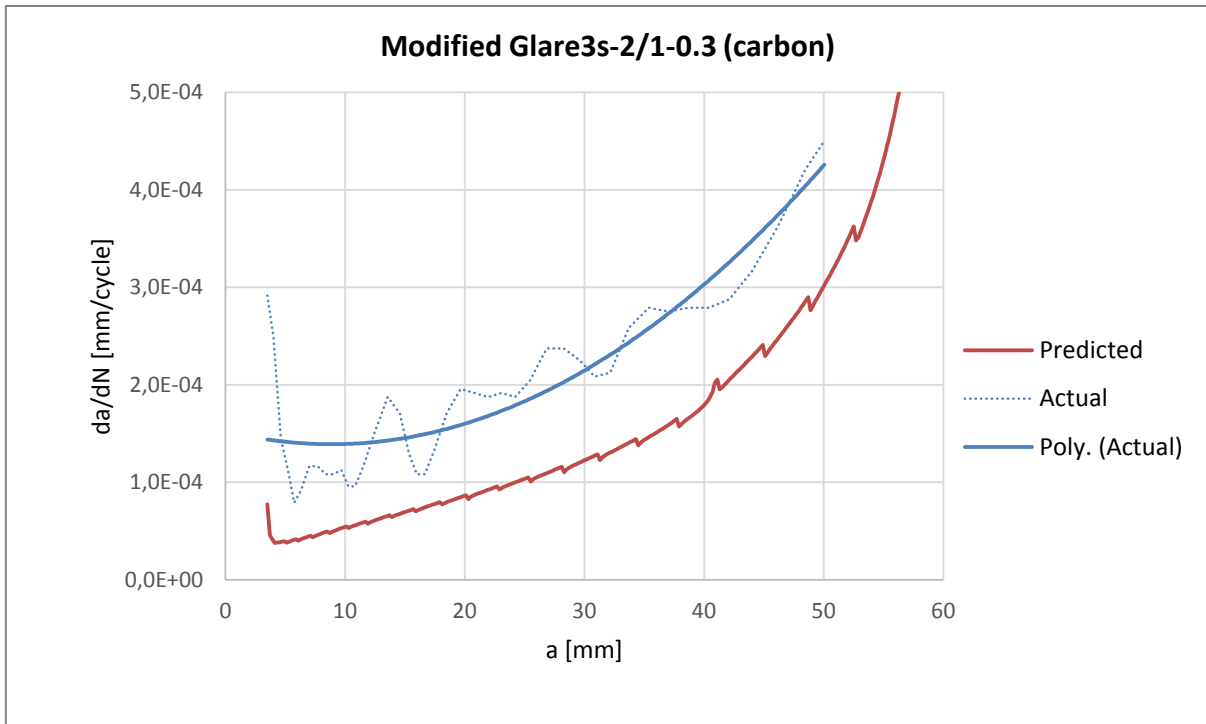


Figure 44: Fatigue crack growth curve for modified Glare3s-2/1-0.3 (carbon)

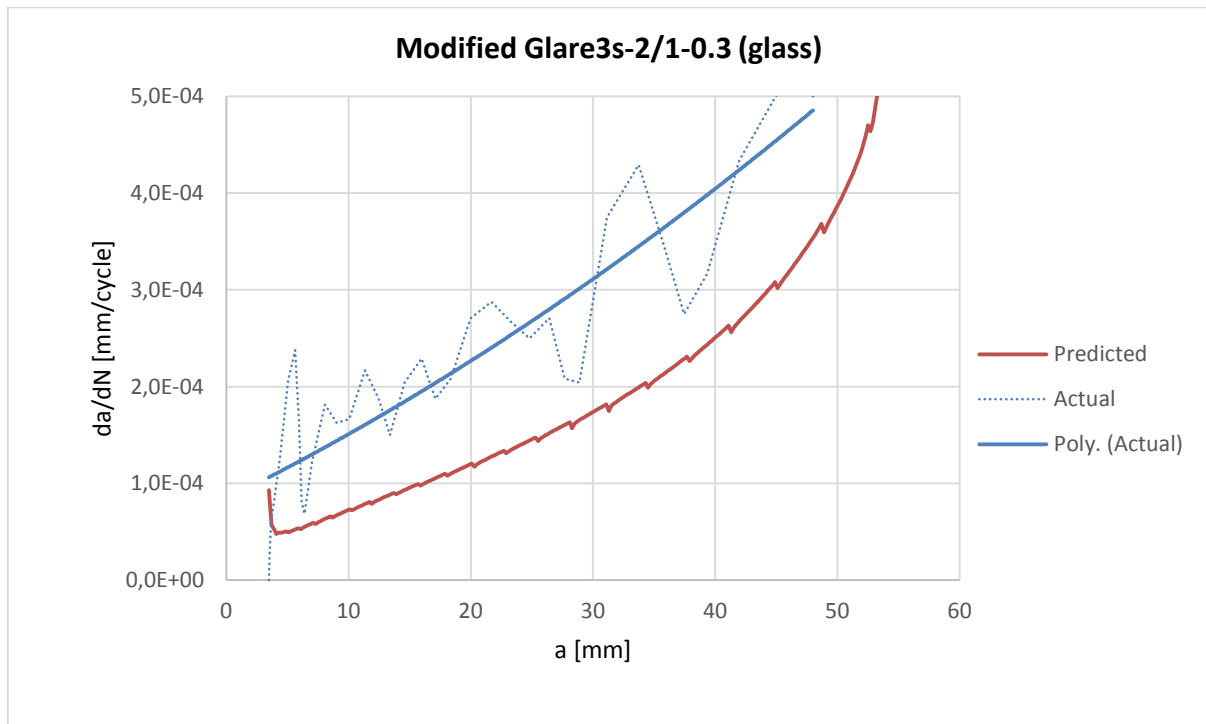


Figure 45: Fatigue crack growth curve for modified Glare3s-2/1-0.3 (glass)

As can be seen from Figure 44 and Figure 45, the fatigue crack growth curves are higher than expected. Based on the scale of the y axis, the difference average distance between the two curves is only about  $0.00012 \text{ mm/cycle}$ . However, at high cycles, this difference adds up quickly. For example, the Glare3s-2/1-0.3 (glass) specimen got to complete failure after the crack reached the

edge of the specimen (66.5 m) at 256.5k cycles. Had the fatigue crack growth rate been that of the predictions, the specimen is likely to have had a few millimeters left before reaching the edge.

Due to the off-axis fibers, the fatigue cracks grew at an angle. This happens when fatigue specimens are not loaded on the principle material axes. Figure 46 shows the fatigue cracking of the modified Glare3 with carbon fibers.

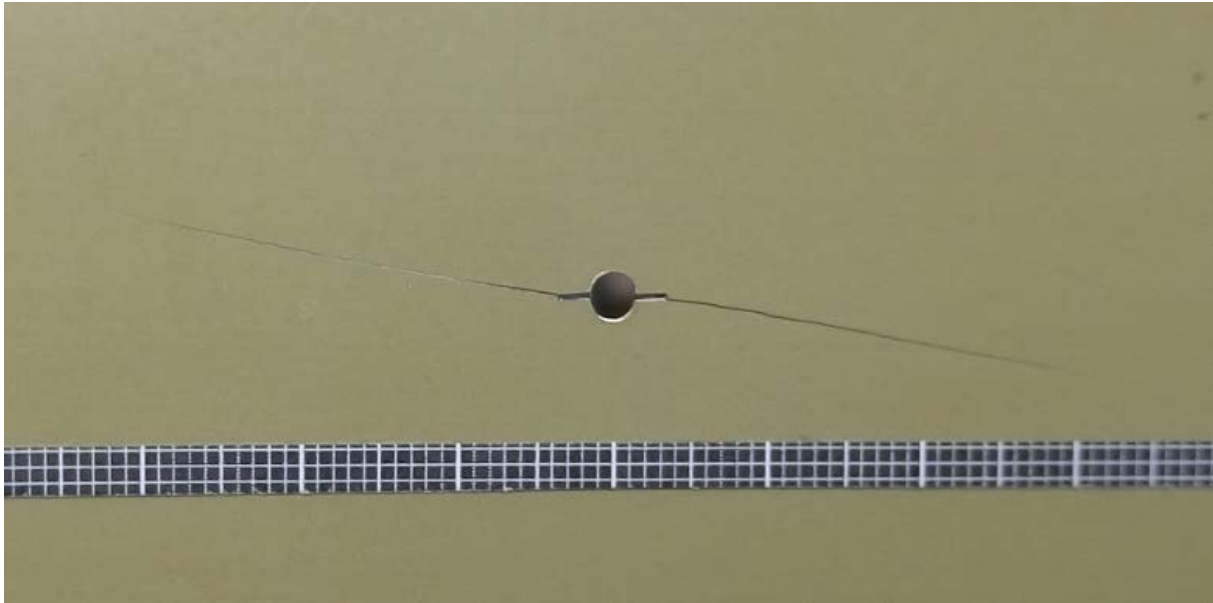


Figure 46: Fatigue crack turning in modified Glare3 (carbon).

Note: The fatigue crack growth rates were found to be the same on the left and right sides (as can be seen in Figure 46) as well as on the front and the back.

The crack turning is evidence that the off-axis fibers are causing a shear load to develop inside the specimen. This additional shear load could be responsible for the increased fatigue crack growth rates the modified Glare3 materials experienced. FMLGROW\_V2.0 is not capable of handling Glare materials with off-axis fibers, which explains why the predictions do not better match the test results. In an attempt to circumvent this problem as much as possible, the properties of all the fiber plies were added together and considered to be a single ply with the same properties. This works well for Glare materials with no off-axis fibers, but still comes relatively close if a single off-axis fiber is added.

Since FMLGROW\_V2.0 is not suited for calculating the fatigue crack growth rates in Glare materials with off-axis fibers, no firm conclusion can be made as to the performance of the modified Glare3 specimens. However, the specimens were made with appropriate dimensions, the initial crack was properly cut, and tests were carried out accurately. As such there is high amount of confidence that the test results are accurate. Thus, comparing the fatigue crack growth rates of the modified Glare3 specimens with that of the predictions of the standard Glare3 (for which FMLGROW\_V2.0 works very well), it can be concluded that the modified Glare3 materials have similar, yet slightly higher fatigue crack growth rates than does standard Glare3.

## Conclusion 4

It was demonstrated through testing that Glare3 which has been modified with off-axis fibers has an improved stiffness in the post-yielding regime. Due to uncertainty in the test results in the post shear-buckled regime, which displayed a much lower than expected stiffness, no firm conclusion can be made as the effects of off-axis fibers on the post shear-buckled stiffness,  $G_{\alpha}$ . However, the theory behind optimizing  $G_{\alpha}$  is good and further investigation is recommended. The modified Glare3 displays comparable fatigue crack growth rates with that of standard Glare3, although they are slightly higher due to the shear loads induced by the off-axis fibers.



## Conclusions

The information presented in this thesis was gathered through research and experimentation. It describes what effects off-axis fibers have on the post shear-buckled stiffness and damage tolerance of a modified Glare3 material. The background information includes a thorough investigation into the individual components of Glare, its history, and its development. Following the same design criteria, a new Glare grade was proposed which has an improved post shear-buckling performance for fuselage skin panels on narrow-bodied aircraft that experience relatively large shear forces. The experimental approach to determining the effects of the off-axis fibers involved testing material specimens in both shear and fatigue as well as analyzing a wide range of material options with analytical models. Results from the experiments were analyzed and interpreted to show that improving the post shear-buckled stiffness of Glare3 may be best achieved through the addition of off-axis carbon fibers. The conclusions below are repeated from the conclusions drawn in the body of the thesis.

### Conclusion 1

The post shear-buckled stiffness of standard Glare3 oriented at various angles, was tested in a picture frame shear apparatus, and compared against analytical models. The shear test results were inconclusive, but the analytical models predicted the post shear-buckled stiffness of Glare3 oriented at  $\pm 45^\circ$  would be seven percent higher than the un-rotated standard Glare3. They also demonstrated that in the axial directions, an increase in the fiber angles resulted in a steady decrease in the axial stiffness, while the fatigue crack growth rates increased. This leads to the conclusion that simply rotating Glare3 will have more disadvantages than benefits and attempts at improving the post shear-buckled stiffness of Glare3 should involve more than a simple rotation of the existing fiber layers.

### Conclusion 2

The aluminum in Glare materials is responsible for most of the material's stiffness, and is the main driving factor. Thus, increasing the metal volume fraction (MVF) of Glare3 will rapidly increase the post shear-buckled stiffness. However, a sharp increase in the MVF only yields a small increase in stiffness, and the aerial density goes up five times faster than the stiffness does. Also, the increased thickness of the aluminum layers decreases the damage tolerance. Thus, it is concluded that for purposes of this thesis, increasing the material's MVF will not yield desirable results and should be avoided.

### Conclusion 3

Modifying Glare3 to include off-axis fibers which are in-line with the shear buckling angle may increase or decrease the material's post shear-buckled stiffness depending upon the type of fibers used. Glass fibers are less stiff than Glare3 and using them as off-axis fibers will decrease the material's post shear-buckled stiffness. Carbon fibers are much stiffer than Glare3 and using them as off-axis fibers will increase the material's geometric stiffness and should also increase its post shear-buckled stiffness. However, the addition of a carbon fiber layer comes with the potential for galvanic corrosion, which requires additional measures to mitigate. In terms of increasing the post shear-buckled stiffness of Glare3-2/1-0.3, adding a single off-axis fiber layer appears to produce the largest benefits. This results in an optimized layup of  $[Al/0/45/90/Al]$ , when the off-axis layer is carbon fiber.

#### Conclusion 4

It was demonstrated through testing that Glare3 which has been modified with off-axis fibers has an improved stiffness in the post-yielding regime. Due to uncertainty in the test results in the post shear-buckled regime, which displayed a much lower than expected stiffness, no firm conclusion can be made as the effects of off-axis fibers on the post shear-buckled stiffness,  $G_{\alpha}$ . However, the theory behind optimizing  $G_{\alpha}$  is good and further investigation is recommended. The modified Glare3 displays comparable fatigue crack growth rates with that of standard Glare3, although they are slightly higher due to the shear loads induced by the off-axis fibers.

## Recommendations

- 1- Due to uncertainty associated with the picture frame apparatus, further research along the lines of this thesis should use a bigger picture frame.
- 2- Increasing the number of aluminum layers will increase the critical buckling load. This will prevent the specimen from buckling too soon and allow the shear modulus,  $G$ , and the critical buckling stress,  $\tau_{crit}$ , to be measured.
- 3- It has not been proven that the analytical models used in this thesis provided accurate predictions. As such, these models should be validated, or modified to improve their accuracy with FMLs in the post shear-buckled regime and/or where off-axis fibers are employed.
- 4- The effects of off-axis fibers on the post shear-buckled stiffness were not significantly manifested until after the aluminum began to yield. Future research may want to consider prestraining the material. This will reverse the sign of the residual stresses and may make the stiffness effects of off-axis fibers be expressed prior to yielding.

## References

1. Vlot, A.D. & Gunnink, J.W. (2001). *Fibre Metal Laminates an Introduction*. Dordrecht, NL: Kluwer Academic Publishers.
2. Vlot, A.D. (2001). *Glare - History of the Development of a New Aircraft Material*. Dordrecht, NL: Kluwer Academic Publishers.
3. Vogelesang, L. B., & Roebroeks, G. H. (1981). *U.S. Patent No. 5039571*. Washington, DC: U.S. Patent and Trademark Office.
4. Roebroeks, G. (1991). *Towards Glare - The development of a fatigue insensitive and damage tolerant aircraft material* (Ph,D). Delft University of Technology.
5. Vlot, A. (1991). *Low-velocity impact loading on fibre reinforced aluminium laminates (ARALL) and other aircraft sheet materials* (Ph.D). Delft University of Technology.
6. Schijve, J., & Vogelesang, L. B. (1985). *U.S. Patent No. 4500589*. Washington, DC: U.S. Patent and Trademark Office.
7. Van Lipzig, H. T. M., (1973). *Retardation of fatigue crack growth* (in Dutch). Thesis Dept. of Aerospace Eng., Delft, Netherlands.
8. Schijve, J., Van Lipzig, T., Van Gestel, G., & Hoeymakers, A. (1979). *Fatigue properties of adhesive-bonded laminated sheet material of aluminum alloys*. *Engineering Fracture Mechanics*, 12, 561-579.
9. Schijve, J. (2009). *Fatigue of structures and materials*. Berlin: Springer.
10. Schijve, J. (1993). *Development of fiber-metal laminates, ARALL and GLARE, new fatigue resistant materials*. Report LR-715, Delft University of Technology.
11. Roebroeks, G. (1991). *Towards Glare - The development of a fatigue insensitive and damage tolerant aircraft material*. TR diss 1996, Delft University of Technology.
12. Kock, G.H. (1979). *Crack propagation in multiply layer adhesive bonded material*. Proc. 10<sup>th</sup> ICAF Symposium, Brussels, 1979, paper 4.4.
13. Heiser, F. A., & Hertzberg, R. W. (1971). *Anisotropy of fatigue crack propagation* (Vol. 93). New York, NY: ASME.
14. Marissen, R. (1988). *Fatigue crack growth in ARALL, a hybrid aluminium-aramid composite material. Crack growth mechanisms and quantitative predictions of the crack growth rates*. TR diss 1636, Delft University of Technology.
15. Vogelesang, L., & Gunnink, J. (1986). *Materials and Design*, Vol.7, p289.
16. FM 94 adhesive film. (2015, September 8). Retrieved September 16, 2016, from <https://www.cytec.com/products/fm-94-0>

17. Airoidi, A., Lanzi, L., & Sala, G. (2006). *Shear post-buckling behavior of Glare modeling fiberglass damage*. 47th AIAA/ASME/ASCE/AHS/ASC Structures, Structural Dynamics, and Materials Conference.
18. Wittenberg, T.C., van Baten, T.J., & de Boer, A. (2001). *Design of fiber metal laminate shear panels for ultra-high capacity aircraft*. *Aircraft Design*, 4(2-3), 99-113.
19. Taheri, F., Moradi, S. (2000). *A robust methodology for the simulation of postbuckling response of composite plates*. *Computational Mechanics* 26, 295-301.
20. Farley, G. F., Baker, D. J. (1982). *In-plane Shear Test of Thin Panels*. Langley Research Center, Hampton, Va.
21. Kuhn, P., Peterson, J.P., & Levin, L.R. (1952). *A Summary of Diagonal Tension, Part I – Methods of Analysis*. (Technical Note 2661). Langely Field, VA: NACA
22. Kuhn, P. (1940). *Investigations on the Incompletely Developed Plane Diagonal-Tension Field*. (Report No. 697). Langely Field, VA: NACA
23. ESDU (1971). *ESDU 71005: Buckling of Flat Plates in Shear*. London: ESDU
24. Gerard, G., & Becker, J. (1957). *Handbook of Structural Stability, Part I – Buckling of Flat Plates*. (Technical Note 3781). Langely Field, VA: NACA
25. Kassapoglou, C. (2010). *Design and analysis of composite structures: With applications to aerospace structures*. United States: John Wiley & Sons.
26. Wittenberg, T.C., & van Baten, T.J. *Shear Buckling of Flat Rectangular Glare Plates Above the Elastic Limit*. ID-1500, Delft University of Technology.
27. Aldersliesten, R.A. (2005). *Fatigue Crack Propagation and Delamination Growth in Glare*. Ph.D. dissertation, Delft University of Technology.



## **APPENDIX: A**

This section contains the details on how the final laminate was selected for testing. It was initially written as a stand-alone document and has been kept largely the same to aid in reader coherence, although it has been modified with some references to the main body of the thesis. This document is referenced in the section

Modified Glare Design.

## Laminate Selection Criteria

As the goal is to ultimately increase the post shear-buckled stiffness of FMLs the first obvious thing to check is how the shear stiffness,  $G$ , changes as the various material parameters change. Comparisons of the results coupled with specific design criteria make it possible to narrow down the options to a few ideal layups. The material parameters and design criteria for the FML are listed below.

### Material Parameters

1. Laminates must have a  $0^\circ$  and  $90^\circ$  glass fiber plies
2. Laminates must have an angle ply (otherwise there is no change in the material)
3. Angle plies may be either glass fiber or carbon fiber
4. Metal layers must have a thickness within the acceptable range of  $0.2 \leq t_{Al} \leq 0.5$  [mm]
5. Total laminate thickness must not exceed 2 mm
6. Laminates must be within the valid range of  $0.45 < MVF < 0.85$

These material parameters allow the following 10 laminates to be considered:

2/1 layup of  $[Al/0/\theta/90/Al]$  with  $0.2 \leq t_{Al} \leq 0.5$  [mm]

2/1 layup of  $[Al/0/\theta/\theta/90/Al]$  with  $0.3 \leq t_{Al} \leq 0.5$  [mm]

3/2 layup of  $[Al/0/\theta/90/Al]$  with  $0.3 \leq t_{Al} \leq 0.4$  [mm]

3/2 layup of  $[Al/0/\theta/\theta/90/Al]$  with  $t_{Al} = 0.3$  [mm]

Where  $\theta$  is either glass or carbon fiber.

### Design Criteria

1. Laminates should have an increase in post shear-buckled stiffness
2. Laminates should have an increase in geometric stiffness
3. Laminates should either maintain or increase the damage tolerance (for fatigue crack growth)
4. (For specific design requirements) Laminate should have a minimum stiffness value

To determine the post shear-buckled stiffness, it is important to consider the stress state the buckled panel is in. Before shear buckling, the panel is in a state of pure shear with no applied axial stresses. Due to how thin the laminates are, buckling occurs readily at about 2.25 MPa. After this, any additional applied load is carried in incomplete diagonal tension as previously discussed in SECTION#. The direction in which the diagonal tension acts is in-line with the buckling angle. In this case, the buckling angle,  $\alpha$ , occurs at  $45^\circ$ . Thus, to find the post shear-buckled stiffness, which will be referred to as  $G_\alpha$ , the web stresses in the direction of  $\alpha$  need to be found.

Since the web stresses of interest are rotated in the direction of  $\alpha$ , an element rotated at that angle can be used to find the principal tensile and compressive stresses. An example of a shear stress element and its equivalent rotated principal stress element can be seen in Figure 47.

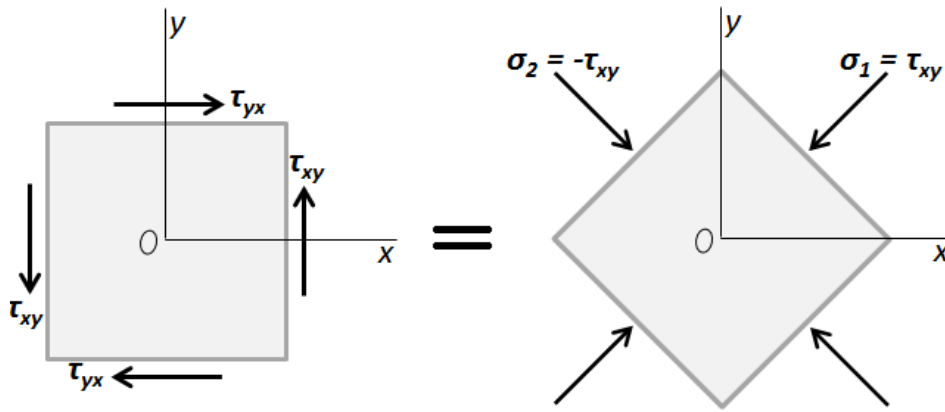


Figure 47: Shear stress element and an equivalent rotated principal stress element.

With the help of Mohr's circle the pre and post shear-buckling principal stresses in the web can be found. An example of this can be seen in Figure 48.

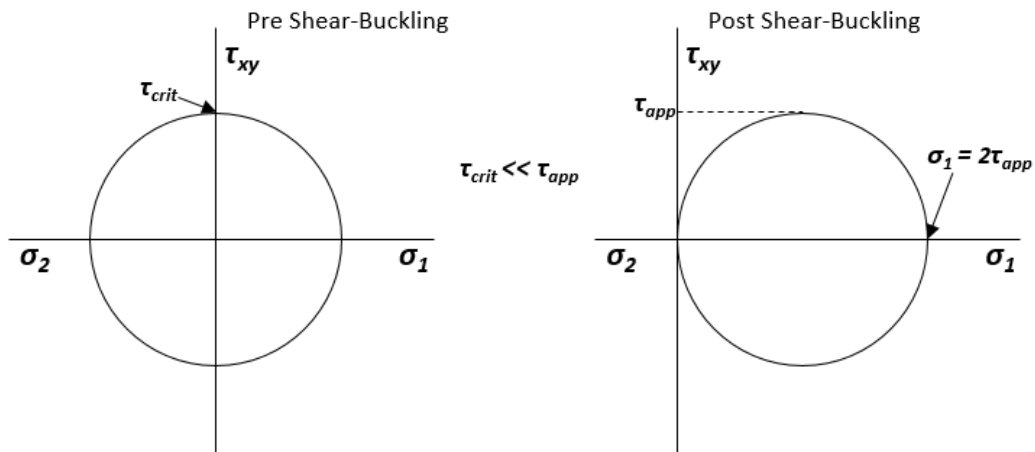


Figure 48: Mohr's circles depicting the pre and post shear-buckling stress states.

Mohr's circle shows that the principal stress,  $\sigma_1$ , is twice the value of the applied shear stress,  $\tau_{app}$ , after shear buckling has occurred. Since  $\tau_{app}$  is so much greater than the shear buckling load,  $\tau_{crit}$ , the compressive stresses in  $\sigma_2$  are negligible. Thus, the expression to find  $G_\alpha$  is:

Equation 15

$$G_\alpha = \frac{2\tau_{app}}{\gamma}$$

Using Equation 15,  $G_\alpha$  for all possible laminate layups can be found and compared against the first design criterion. However, a direct comparison of material stiffness wouldn't be accurate because each one is different. This is overcome by normalizing  $G_\alpha$  with the respective material's density (not aerial density as done in the body of the thesis) and finding the percent increase in  $G_\alpha$ . For convenience, these results can then be divided by  $G_\alpha$  of the base Glare3 laminate to show the overall change in  $G_\alpha$  for modified vs unmodified FML. These results for glass fibers can be seen in Figure 49

and Figure 50, where the circled areas contain the possible laminates identified from the material parameters.

Change in  $G_{\alpha}$  For Possible Laminates with Glass Fiber Angle Plies

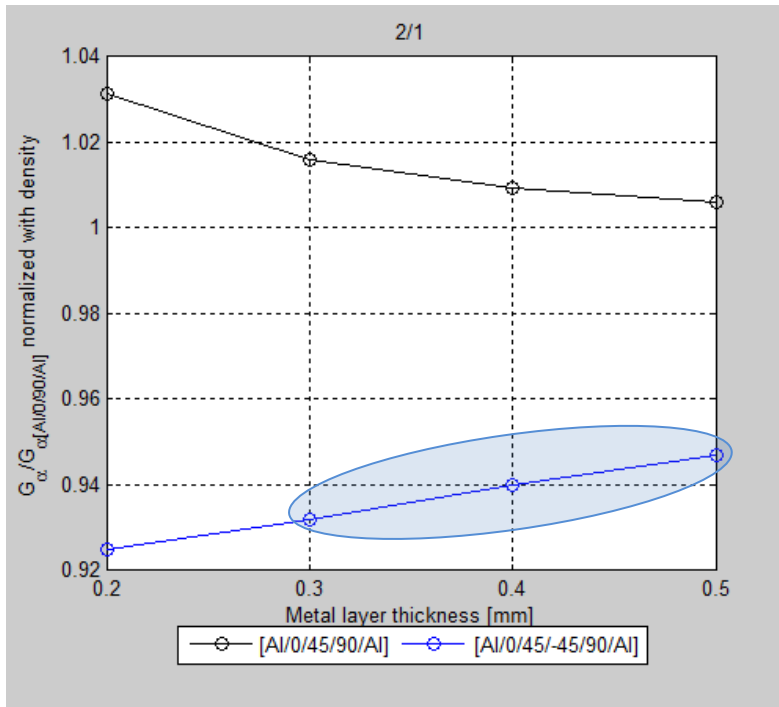


Figure 49:  $G_{\alpha} / G_{\alpha-Glare3}$  for possible 2/1 layups.

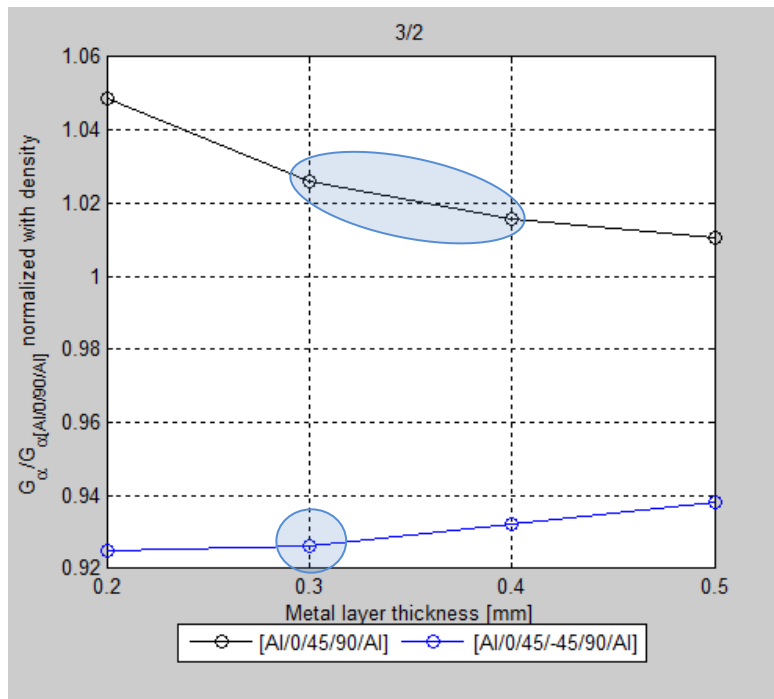


Figure 50:  $G_{\alpha} / G_{\alpha-Glare3}$  for possible 3/2 layups.

From Figure 49 and Figure 50 it is evident that the layout [Al/0/45/-45/90/Al] does not meet the first design criterion. This leaves the layout [Al/0/45/90/Al] as the only remaining option.

For the second design criterion, the geometric stiffness of the laminates need to be compared. This is accomplished by calculating the spring constants of the laminates. The following expressions in Equation 16 show how this is done and were derived using EQUATION# and solving for the relevant constants.

Equation 16

$$d = 2a \left( \sin(\alpha) - \sin \left( \arccos \left( \frac{(2 * \gamma + 1) \sin(\alpha)}{a} \right) \right) \right)$$

$$F_{\tau} = \tau_{app} * t * a$$

$$K = \frac{F_{\tau}}{d}$$

- Where  $a$  is the laminate width,
- $d$  is the deformation of the laminate,
- $F_{\tau}$  is the applied shear force,
- $K$  is the spring constant.

By taking the spring constant when the angle plies are at 45° and dividing it by the spring constant of the base Glare3 laminate the result shows the percent increase between the two. Comparing the percent increase in geometric stiffness between the various laminates show which are more greatly improved. These results for glass fibers can be seen in Figure 51 and Figure 52, where the circled areas contain the six remaining possible laminates identified from the material parameters and the first design criterion. All results for glass and carbon fibers can be seen in APPENDIX#.

K/K<sub>Glare3</sub> For Possible Laminates with Glass Fiber Angle Plies

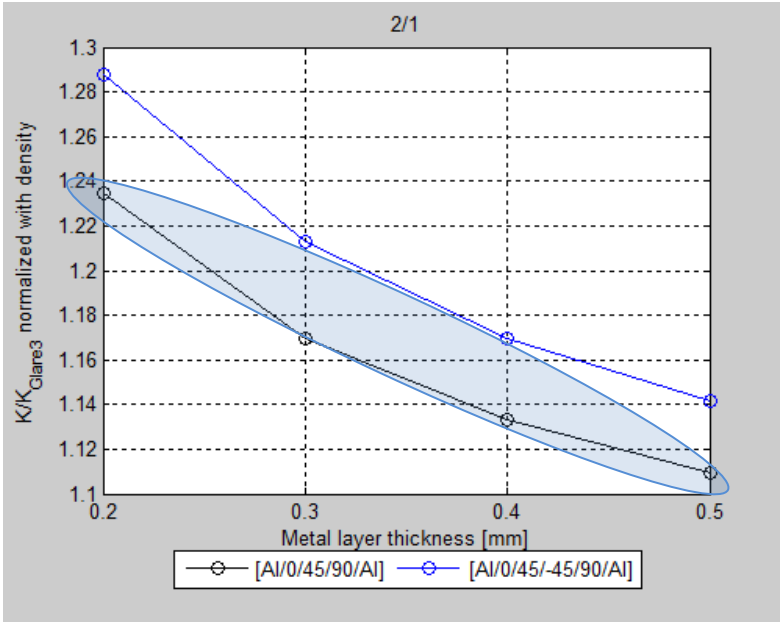


Figure 51: K/K<sub>Glare3</sub> for possible 2/1 layups.

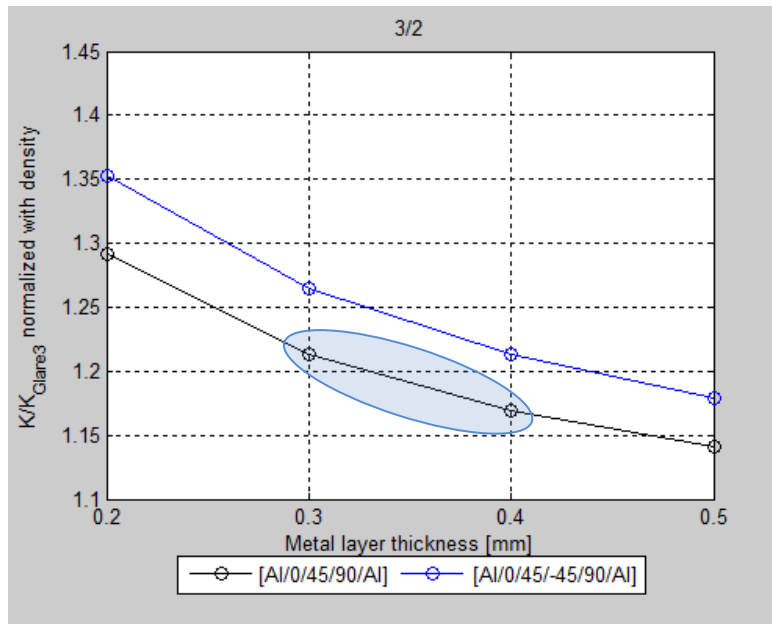


Figure 52:  $K/K_{Glare3}$  for possible 3/2 layups.

With both forms of stiffness presented, the laminates can be placed in order from highest improvement in stiffness to lowest. These are as follows:

1. 2/1 layup with  $t_{Al} = 0.2$
2. 3/2 layup with  $t_{Al} = 0.3$
3. 2/1 layup with  $t_{Al} = 0.3$  or 3/2 layup with  $t_{Al} = 0.4$  [mm] (these have the same MVF)
4. 2/1 layup with  $t_{Al} = 0.4$
5. 2/1 layup with  $t_{Al} = 0.5$

The third design criterion requires as high of a damage tolerance as possible. For FMLs, this most likely means that the best designs would have as many aluminum layers as possible with the smallest thickness possible. Due to this, the laminates with the two thickest metal layers can easily be discarded. Between the remaining three laminates, the 2/1 layup with  $t_{Al} = 0.3$  can also be discarded, because it has thicker metal layers than the first option. At last, only two options remain.

1. 2/1 layup with  $t_{Al} = 0.2$
2. 3/2 layup with  $t_{Al} = 0.3$

It is too hard to tell between these two which will perform better in fatigue crack growth without using an analytical model. However, there are limited materials for use in the lab at TU Delft and only aluminum sheets with  $t_{Al} = 0.3$  are available. In addition, the picture frame apparatus is rather small, and can only accommodate very thin laminates. As a result, the best laminate that can be made and tested at TU Delft is 2/1 layup  $[Al_{0.3}/0/45/90/Al_{0.3}]$ .

Even though a final laminate design has already been determined, fatigue crack growth curves for the top two materials still yield valuable insights. After all, Glare is a compromise between stiffness and damage tolerance. If the stiffness is increased, but the damage tolerance drops too much, then the new material will likely not be more beneficial than current grades of Glare. The damage tolerance of the proposed materials was determined using FMLGROW\_V2.0, which is an analytical model for fatigue crack growth rates in FMLs developed in-house at TU Delft.

Figure 53 and Figure 54 show the fatigue crack growth rate estimates for Glare3-2/1-0.2 and Glare3-3/2-0.3 respectively. These may be compared with Figure 55 and Figure 56, which show the fatigue crack growth rate estimates for  $[Al_{0.2}/0/45/90/Al_{0.2}]$  and  $[Al_{0.3}/0/45/90/Al_{0.3}/0/45/90/Al_{0.3}]$  respectively. The differences between each of them are very small, which means that the damage tolerance of the modified Glare material is largely unaffected. This indicates that with an increase in shear stiffness and no change in the damage tolerance, the proposed material may in fact be an improvement upon Glare3 in the post shear-buckling regime. However, FMLGROW\_V2.0 was developed for use with fibers in the  $0^\circ$  and  $90^\circ$  orientations only. To get around this, the material properties of the off-axis ply were rotated and added to the  $0^\circ$  and  $90^\circ$  plies. It has not been tested or verified that this method will yield valid results using FMLGROW\_V2.0, but it may help give an initial idea of what test results may show.

### Crack growth rates for Glare3

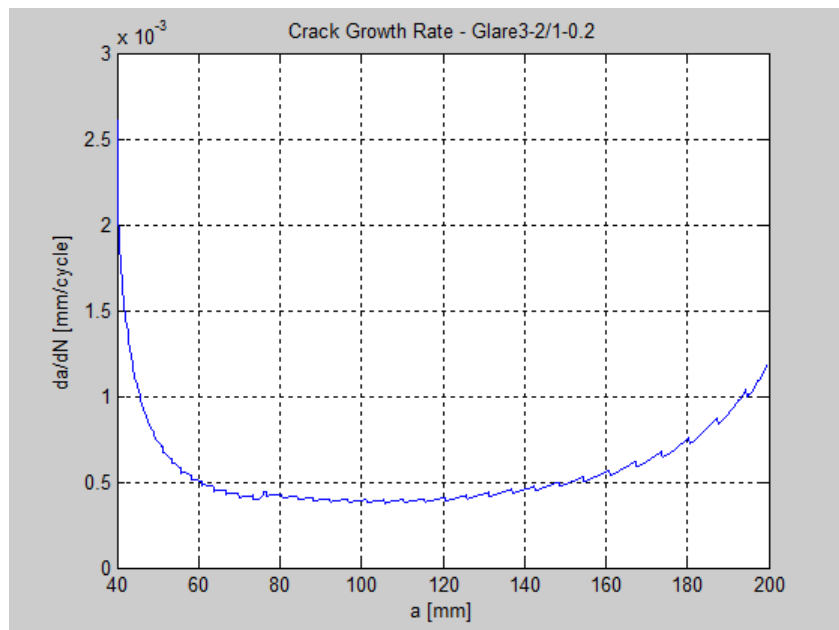


Figure 53:Crack growth rate for Glare3-2/1-0.2

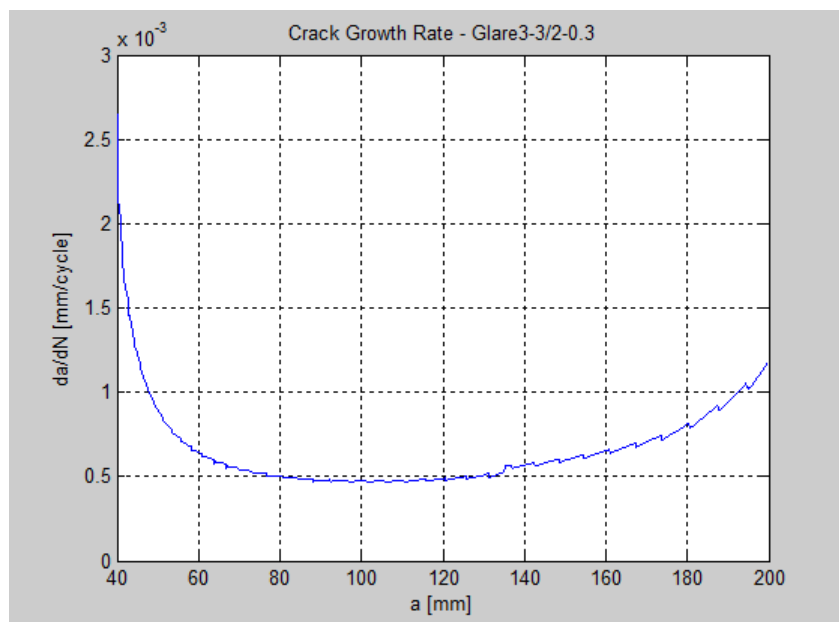


Figure 54:Crack growth rate for Glare3-3/2-0.3

### Crack growth rates for modified FML

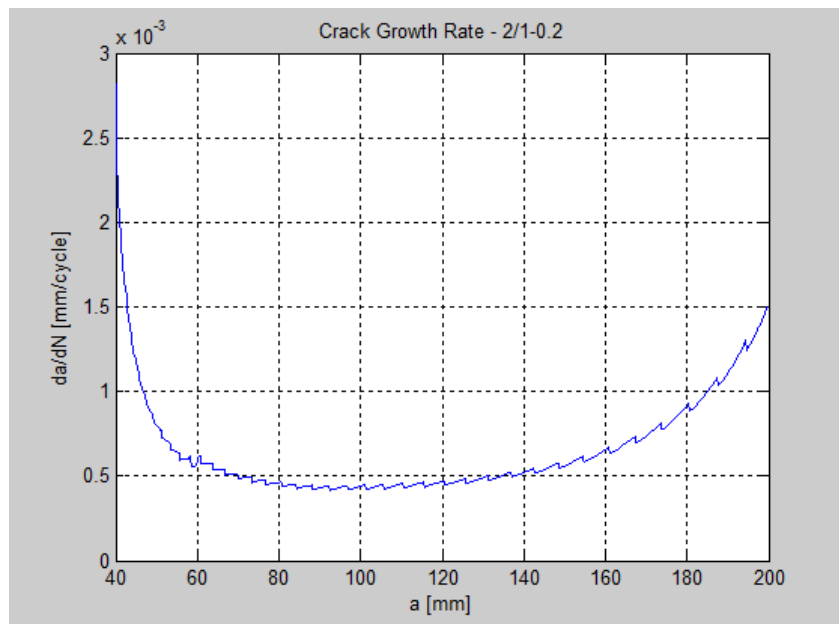


Figure 55: Crack growth rate for  $[Al_{0.2}/0/45/90/Al_{0.2}]$

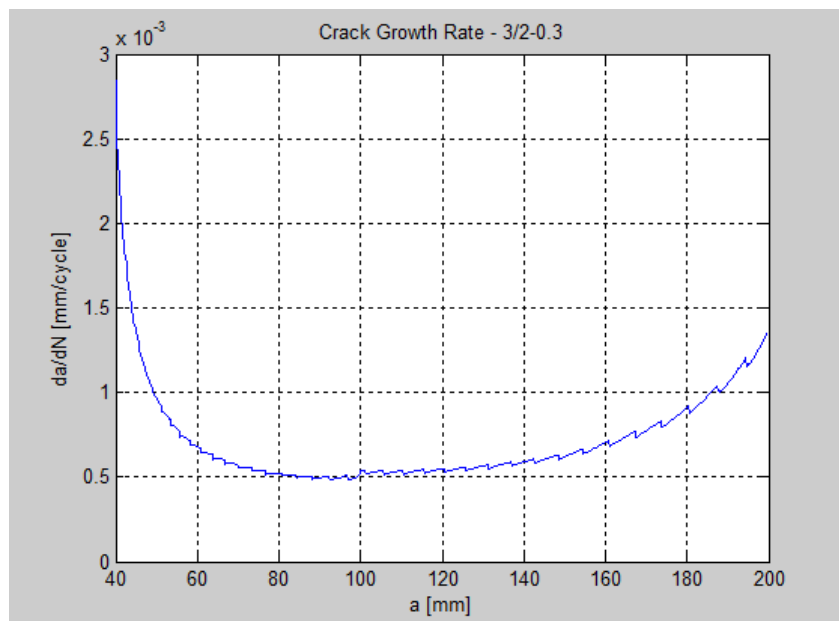


Figure 56: Crack growth rate for  $[Al_{0.3}/0/45/90/Al_{0.3}/0/45/90/Al_{0.3}]$

When replacing the glass fiber angle ply with a carbon fiber angle ply, the trends exactly mimic those of the glass fibers, yielding the same conclusions of which laminate is best. The figures for the carbon fiber angle plies are presented below in Figure 57 to Figure 60.

Change in  $G_{\alpha}$  For Possible Laminates with Carbon Fiber Angle Plies

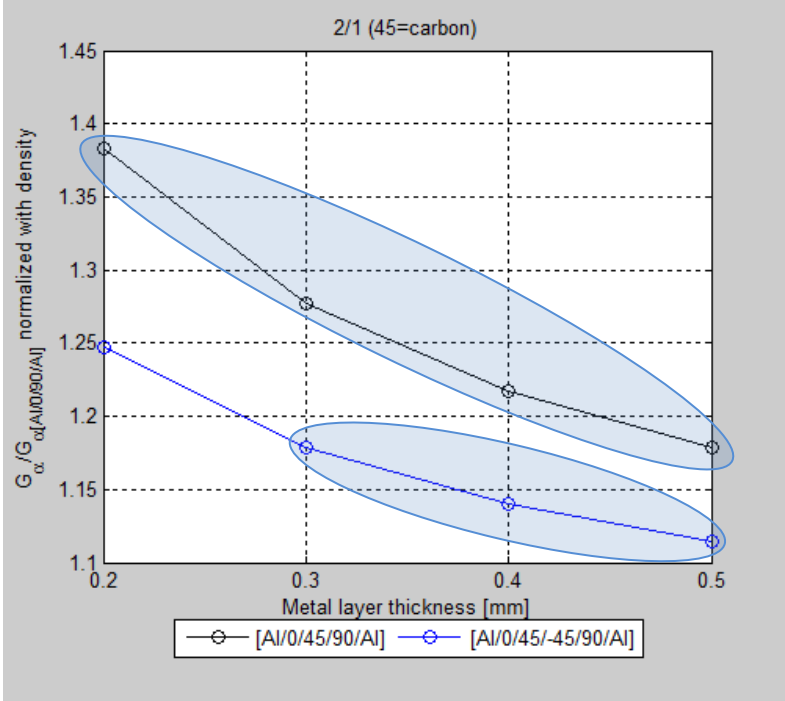


Figure 57:  $G_{\alpha}/G_{\alpha-Alare3}$  for possible 2/1 layups.

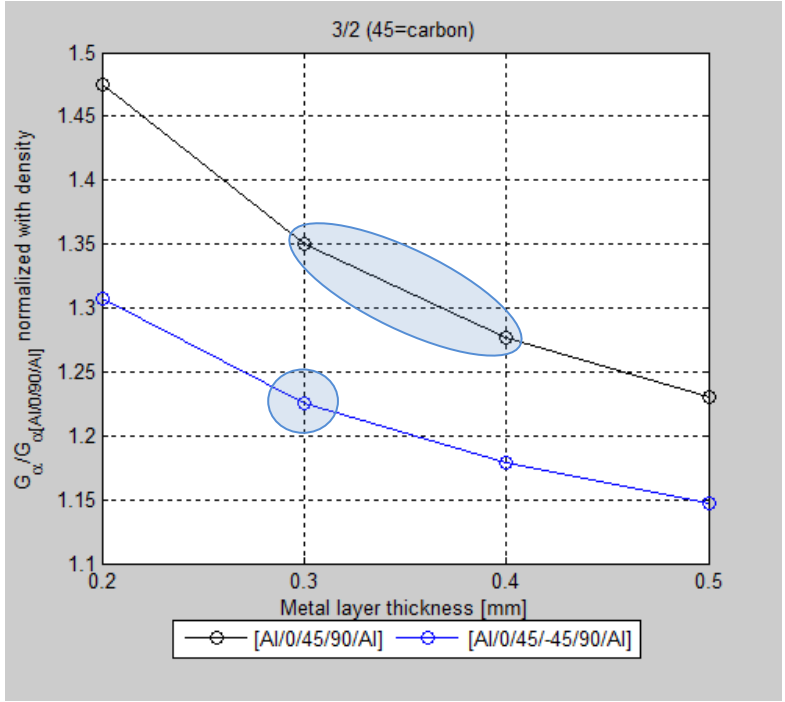


Figure 58:  $G_{\alpha}/G_{\alpha-Alare3}$  for possible 3/2 layups.

$K/K_{Glare3}$  For Possible Laminates with Carbon Fiber Angle Plies

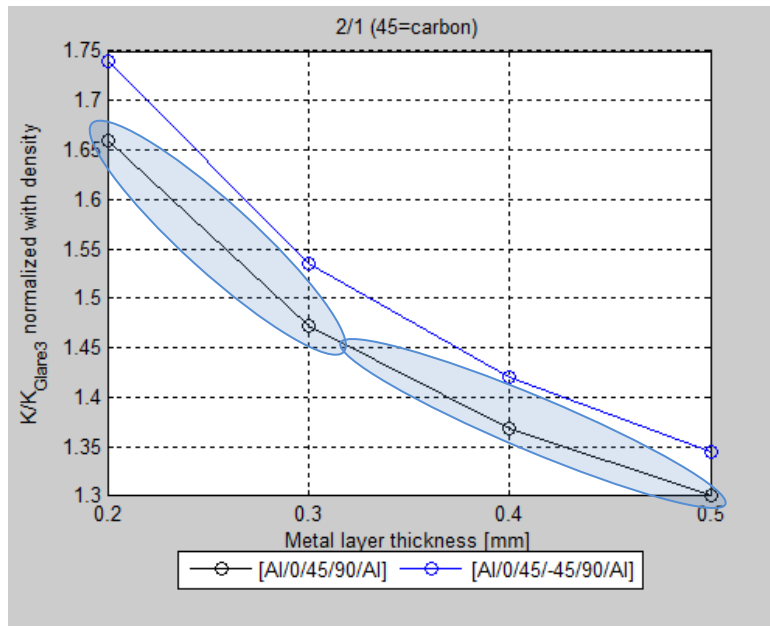


Figure 59:  $K/K_{Glare3}$  for possible 2/1 layups.

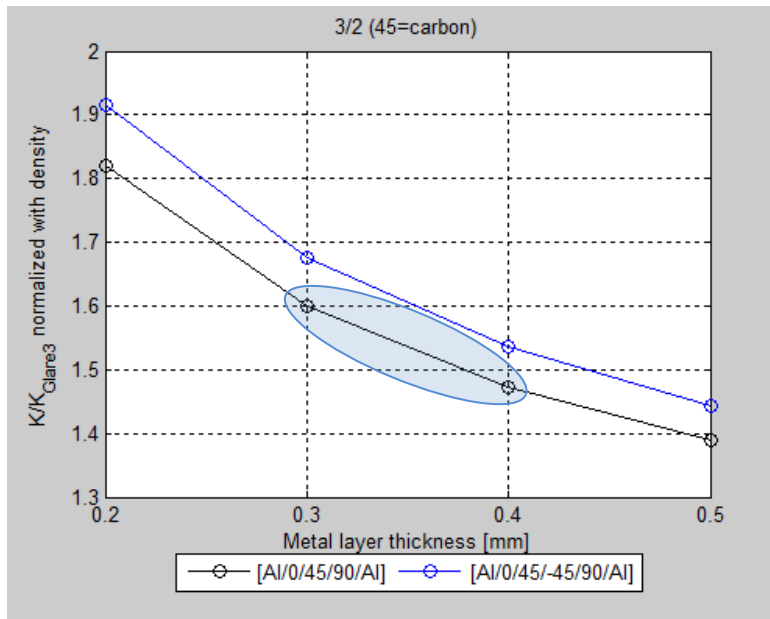


Figure 60:  $K/K_{Glare3}$  for possible 3/2 layups.



# APPENDIX: B

## Analytical Models

### Classical Laminate Theory (CLT)

The results from CLT were calculated in MatLab using Equation 2 through Equation 4. They were compared with a CLT calculator written in Excel by a professor at TU Delft to verify that the MatLab code was written correctly. CLT was used to obtain the properties  $E_x$ ,  $G_{xy}$ , and  $E_\alpha$  (modulus of elasticity in the buckling angle direction). The ABD matrices for each laminate are not shown. In Table 15 are the results from the un-modified Glare 3 panels, which were tested at the orientations stated. Table 16 gives the results from three modified Glare3 panels.

Table 15: Glare3 Elastic and Shear Moduli from CLT

Laminate	Fiber Orientation	$E_x$ [MPa]	$G_{xy}$ [MPa]	$E_\alpha$ [MPa]
Glare3-2/1-0.3	0/90	59024	20547	55158
Glare3-2/1-0.3	15/-75	58052	21103	56150
Glare3-2/1-0.3	30/-60	56150	22214	58052
Glare3-2/1-0.3	45/-45	55158	22769	59024

Table 16: Modified Glare3 Elastic and Shear Moduli from CLT

Laminate	Fiber Orientation	$E_x$ [MPa]	$G_{xy}$ [MPa]	$E_\alpha$ [MPa]
Glare3s-2/1-0.2	0/45/90	48719	17630	49860
Glare3s-3/2-0.3	0/45/90	50111	18192	51179
Glare3s-2/1-0.3	0/45/90	53439	19536	54336

### Rayleigh-Ritz

The Rayleigh-Ritz method, as described previously, uses the  $ABD$  matrices obtained from CLT. It is used to calculate the critical shear buckling load,  $N_{xy_{crit}}$ , in thin shear webs. Table 17 gives the critical shear buckling loads and Table 5 gives the critical shear buckling stresses for various Glare layups, where  $t$  is the thickness of the aluminum layers.

Table 17: Critical Running Shear Loads for Shear Buckling of Various Glare Layups

Laminate	Fiber Orientation	$N_{xy_{crit}}$ [kN/m]			
		t=0.2 [mm]	t=0.3 [mm]	t=0.4 [mm]	t=0.5 [mm]
Glare3-2/1	0/90	0.719	1.627	3.073	5.181
	15/-75	0.717	1.625	3.072	5.180
	30/-60	0.716	1.624	3.070	5.179
	45/-45	0.715	1.623	3.069	5.177
Glare3s-2/1	0/45/90	1.181	2.426	4.288	6.894
Glare3s-3/2	0/45/90	6.022	11.530	19.398	30.055

Table 18: Critical Shear Stresses for Shear Buckling of Various Glare Layups

Laminate	Fiber Orientation	$\tau_{crit}$ [MPa]			
		t=0.2 [mm]	t=0.2 [mm]	t=0.2 [mm]	t=0.2 [mm]
Glare3-2/1	0/90	1.089	1.089	1.089	1.089
	15/-75	1.087	1.087	1.087	1.087
	30/-60	1.085	1.085	1.085	1.085
	45/-45	1.083	1.083	1.083	1.083
Glare3s-2/1	0/45/90	1.495	1.495	1.495	1.495
Glare3s-3/2	0/45/90	4.364	4.364	4.364	4.364

### Kuhn Method

At the center of the Kuhn method is the assumption that "...the nominal applied shear stress is split into a pure shear part,  $\tau_s$ , and a part carried by diagonal tension action of the skin,  $\tau_{DT}$ ..." [1]. The values of  $\sigma_1$ ,  $\sigma_2$ ,  $\tau_{DT}$ , and  $\tau_s$  are all dependent upon the applied shear stress,  $\tau_{app}$ . In the shear test data for Glare3, the linear portion of the shear stress-shear strain curve in Figure 20 ranges between a  $\tau_{app}$  of roughly 10 MPa – 120 MPa, and lies between the shear buckling and yielding points. Table 19 shows the results of the calculations of the Kuhn method that were obtained for  $\tau_{app} = 100$  MPa.

**Table 19: Principal Stresses and Percentages of Applied Shear Stresses Resisted by Diagonal Tension and Shear**

Laminate	$t_{Al}$ [mm]	Fiber Orientation	$\sigma_1$ [MPa]	$\sigma_2$ [MPa]	$\tau_{DT}$ [%]	$\tau_S$ [%]
Glare3-2/1	0.2	0/90	167.642	-32.358	67.6%	32.4%
Glare3-2/1	0.3	0/90	159.952	-40.048	60.0%	40.0%
Glare3-2/1	0.3	15/-75	160.176	-39.824	60.2%	39.8%
Glare3-2/1	0.3	30/-60	160.642	-39.358	60.6%	39.4%
Glare3-2/1	0.3	45/-45	160.886	-39.114	60.9%	39.1%
Glare3-2/1	0.4	0/90	153.185	-46.815	53.2%	46.8%
Glare3-2/1	0.5	0/90	147.136	-52.864	47.1%	52.9%
Glare3s-2/1	0.2	0/45/90	164.747	-35.253	64.7%	35.3%
Glare3s-2/1	0.3	0/45/90	157.359	-42.641	57.4%	42.6%
Glare3s-2/1	0.4	0/45/90	150.841	-49.159	50.8%	49.2%
Glare3s-2/1	0.5	0/45/90	145.003	-54.997	45.0%	55.0%
Glare3s-3/2	0.3	0/45/90	141.127	-58.873	41.1%	58.9%

### Rule of Mixtures

This method was used to support the results obtained for  $E_\alpha$  from CLT. Table 20 gives the materials and their elastic modulus ( $E_x$ ) that were used. Table 21 gives the results of the Rule of Mixtures method for  $E_\alpha$ .

**Table 20: Elastic Moduli for Aluminum and Fiber Glass Plies at Various Orientations**

Material	Orientation	$E_x$ [MPa]
Al 2024-T3	0	72000
S2 Glass	0	48900
S2 Glass	15	42702
S2 Glass	30	28116
S2 Glass	45	16006

**Table 21: Elastic Moduli for Glare3 in the Direction of the Buckling Angle**

Laminate	$t_{Al}$ [mm]	Fiber Orientation	$E_\alpha$ [MPa]
Glare3-2/1	0.3	0/90	55072
Glare3-2/1	0.3	15/-75	55904
Glare3-2/1	0.3	30/-60	57651
Glare3-2/1	0.3	45/-45	58456

A comparison of these results with those of CLT demonstrates that they vary between 0.16% and 0.96%. This shows that this method can be reasonably used for making quick estimates of  $E_\alpha$  for analyzing Glare3. Since these results are so similar to those of CLT, it was decided that this method would not be used further.

### Metal Volume Fraction (MVF)

The MVF method, is used for determining the tensile strength, compression strength, and shear strength of Glare materials. Here, MVF was used to determine  $E_{\alpha}$ . Though  $E_{\alpha}$  is technically not included in the list of approved properties, the results below show that they differ from CLT results by  $\leq 0.2\%$ . That is even better than the Rule of Mixtures method. In Table 22, the  $E_{\alpha}$  obtained from the MVF method and the corresponding density ( $\rho$ ) and  $G_{\alpha}$  of various Glare layups are given.

Table 22: MVF Method Results for  $E_{\alpha}$  and  $G_{\alpha}$  of Various Glare Layups

Laminate	$t_{Al}$ [mm]	Fiber Orientation	$\rho_{aerial}$ [kg/m <sup>2</sup> ]	MVF [%]	$E_{\alpha}$ [MPa]	$G_{\alpha}$ [MPa]
Glare3-2/1	0.2	0/90	1.619	60.6%	49942	24971
	0.3	0/90	2.175	69.8%	55072	27536
	0.4	0/90	2.731	75.5%	58266	29133
	0.5	0/90	3.287	79.4%	60446	30223
Glare3s-2/1	0.2	0/45/90	1.873	50.6%	49783	24892
Glare3s-2/1	0.3	0/45/90	2.429	60.6%	54271	27136
Glare3s-3/2	0.3	0/45/90	4.023	53.6%	51105	25553

### FMLGROW\_V2.0

Results for the fatigue crack growth rates of nine different Glare materials using FMLGROW\_V2.0 are shown here. These results are used in the discussion of DISCUSSION2,3,5. Figure 61 through Figure 64 shows the Crack growth life curves for Glare3-2/1 with aluminum thicknesses varying from 0.2 mm – 0.5 mm.

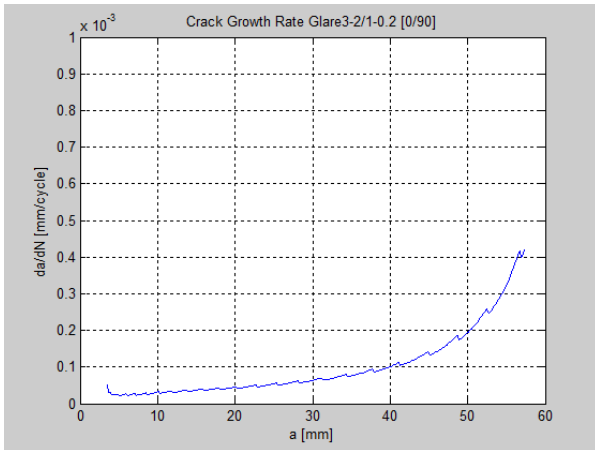


Figure 61: Crack growth life curve for Glare3-2/1-0.2

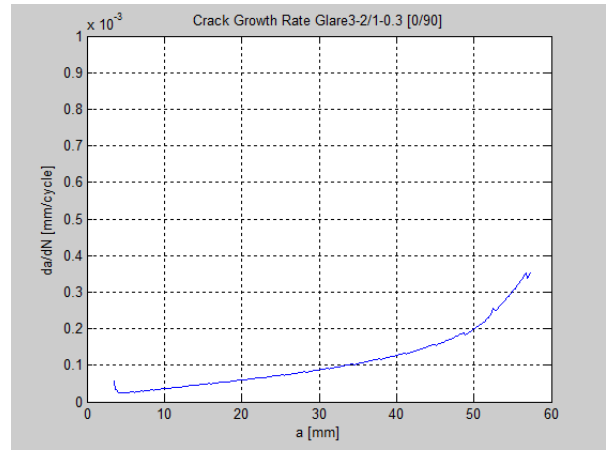


Figure 62: Crack growth life curve for Glare3-2/1-0.3

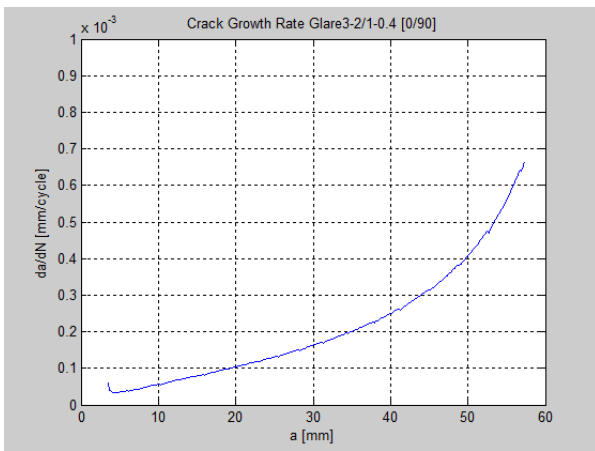


Figure 63: Crack growth life curve for Glare3-2/1-0.4

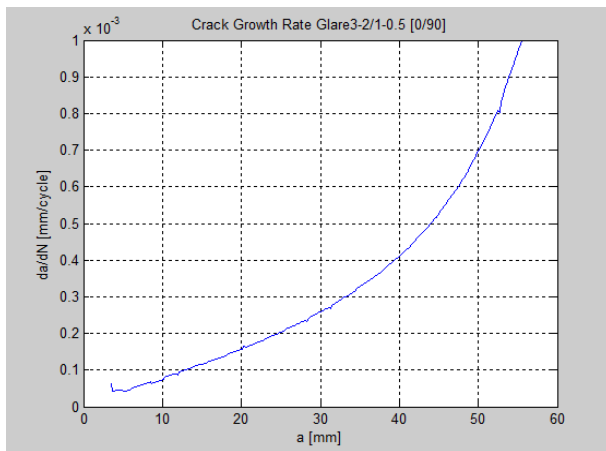


Figure 64: Crack growth life curve for Glare3-2/1-0.5

Figure 65 through Figure 68 shows the Crack growth life curves for Glare3-2/1 with constant aluminum thicknesses and the material rotated from 0° to 45°.

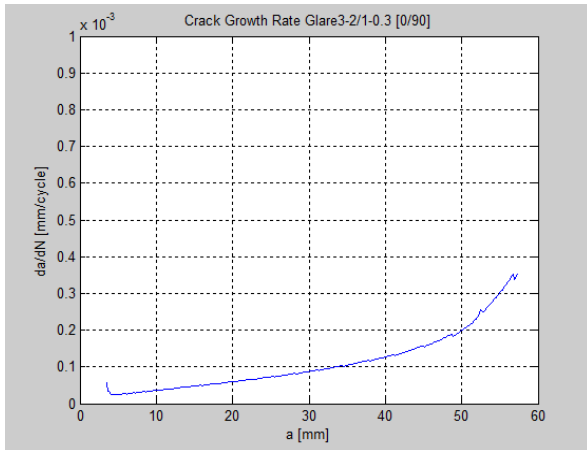


Figure 65: Crack growth life curve for Glare3-2/1-0.3 no rotation.

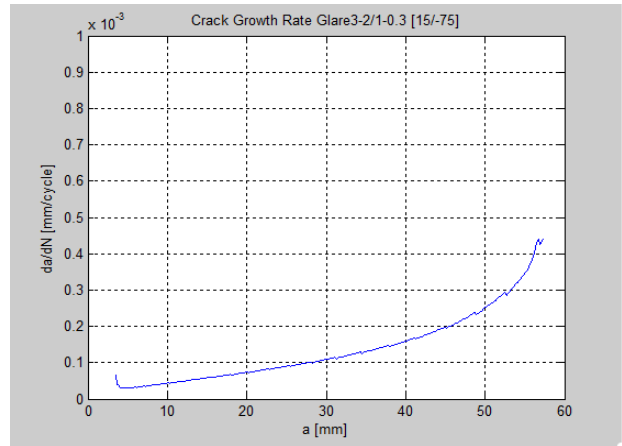


Figure 66: Crack growth life curve for Glare3-2/1-0.3 rotated 15 deg.

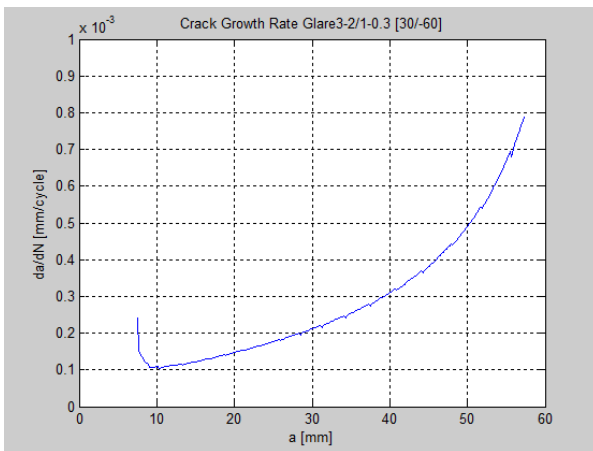


Figure 67: Crack growth life curve for Glare3-2/1-0.3 rotated 30 deg.

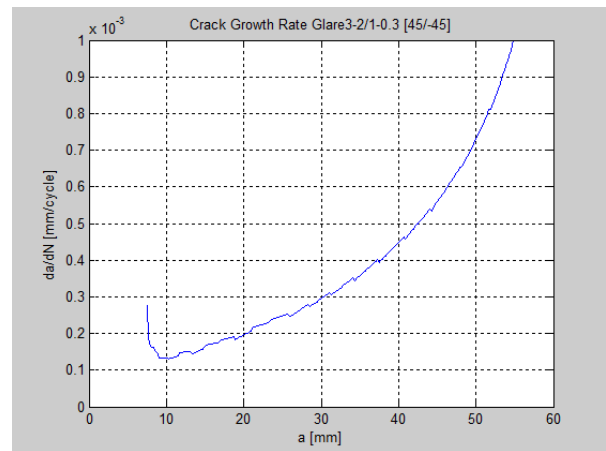


Figure 68: Crack growth life curve for Glare3-2/1-0.3 rotated 45 deg.

Figure 69 shows the Crack growth life curve for the modified material, Glare3s-2/1-0.3.

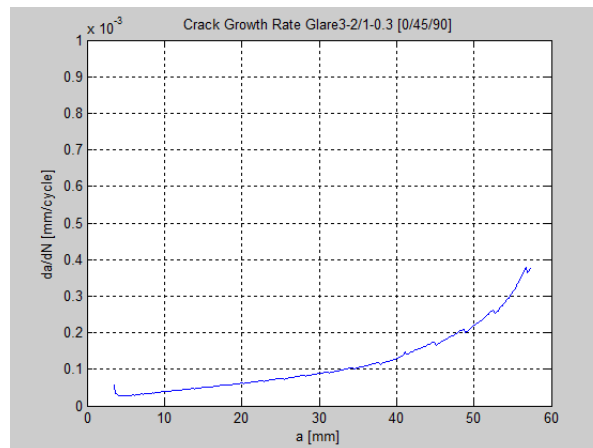


Figure 69: Crack growth life curve for Glare3s-2/1-0.3

### Stiffness Calculations

The  $G_\alpha$  stiffness calculations were done using  $E_\alpha$  obtained from CLT. Table 23 gives the results for various Glare layups. Calculating the spring constant,  $K$ , for the same Glare layups required the use of  $G_\alpha$  from Table 23 to obtain the displacement,  $d$ , for Equation 12. Table 24 gives the results for  $K$ .

Table 23:  $G_\alpha$  Results for Various Glare Layups with Glass Fiber Angle Plies

Laminate	$t_{Al}$ [mm]	Fiber Orientation	$E_\alpha$ [MPa]	$G_\alpha$ [MPa]
Glare3-2/1	0.2	0/90	50049	25025
	0.3	0/90	55158	27579
	0.3	15/-75	56150	28075
	0.3	30/-60	58082	29041
	0.3	45/-45	59024	29512
	0.4	0/90	58337	29169
	0.5	0/90	60507	30254
Glare3s-2/1	0.2	0/45/90	49860	24930
Glare3s-2/1	0.3	0/45/90	54336	27168
Glare3s-2/1	0.4	0/45/90	57306	28653
Glare3s-2/1	0.5	0/45/90	59421	29711
Glare3s-3/2	0.3	0/45/90	51179	25590

Table 24: Spring Constant,  $K$ , Results for Various Glare Layups with Glass Fiber Angle Plies

Laminate	$t_{Al}$ [mm]	Fiber Orientation	$K$ [kN/mm]
Glare3-2/1	0.3	0/90	8.31
	0.3	15/-75	8.44
	0.3	30/-60	8.70
	0.3	45/-45	8.83
	0.4	0/90	10.84
	0.5	0/90	13.38
Glare3s-2/1	0.2	0/45/90	6.90
Glare3s-2/1	0.3	0/45/90	9.43
Glare3s-2/1	0.4	0/45/90	11.96
Glare3s-2/1	0.5	0/45/90	14.49
Glare3s-3/2	0.3	0/45/90	15.06

Table 25:  $G_\alpha$  and  $K$  Results for Various Glare Layups with Carbon Fiber Angle Plies

Laminate	$t_{Al}$ [mm]	Fiber Orientation	$\rho_{aerial}$ [kg/m <sup>2</sup> ]	$MVF$ [%]	$E_\alpha$ [MPa]	$G_\alpha$ [MPa]	$K$ [kN/mm]
Glare3s-2/1	0.2	0/45/90	1.853	50.6%	63699	31850	8.822
Glare3s-2/1	0.3	0/45/90	2.409	60.6%	65380	32690	11.354
Glare3s-2/1	0.4	0/45/90	2.965	67.2%	66494	33247	13.885
Glare3s-2/1	0.5	0/45/90	3.521	71.9%	67287	33644	16.416
Glare3s-3/2	0.3	0/45/90	3.984	53.6%	64195	32098	18.910